SGP-TR-131

Reservoir and Injection Technology and Heat Extraction Project Fifth Annual Report

Principal Investigators:
R.N. Horne, H.J. Ramey, Jr., F.G. Miller
W.E. Brigham, Paul Kruger

December, 1989

Department of Energy Contract Number
DE-AS07-84ID12529
For the Period
January 1,1989 through December 31,1989

TABLE OF CONTENTS

INTRODUCTION

The Stanford Geothermal Program in the fiscal year 1989 was divided into several task areas, as defined by the: Department of Energy contract No. AS07-84ID12529. One of tasks is carried out in the .Department of Civil Engineering and rest at the Department of Petroleum Engineering.

The task areas include predictive modeling of reservoir behavior and tracer test interpretation and testing.

Predictive modeling of reservoir behavior consists of a multi-pronged approach to well test analysis under a variety of conditions. The efforts have been directed to designing and anayzing well tests in

- naturally fractured reservoirs
- fractured. wells
- complex reservoir geometries
- gas reservoirs including inertial and other effects

The analytical solutions for naturally fractured reservoirs are determined using a fracture size distribution. In the study of fractured wells, an elliptical coordinate system is used to obtain semi-analytical solutions to finite conductivity fractures. Effort has also been directed to the modeling and creation of a user friendly computer program for steam/gas reservoirs including wellbore storage, skin and non-Darcy flow effects. This work has a complementary effort on modeling high flow rate wells including inertial effects in the wellbore and fractures. In addition, work on gravity drainage systems is being continued.

The task on the use of Boundary Element Method for a variety of reservoir characteristics and configurations has been succesfully completed. This project shows the possibility of solving accurately for complex reservoir shapes including composite and piecewise homogeneous reservoirs.

The other task area consisting of tracer test interpretation and testing has been focussed towards monitoring both the tracer flow and thermal transients during reinjection. The work on mass and thermal transport in well-to-well, recirculating and injection-backflow tracer tests has been completed. Testing of the reinjection optimization algorithm is continuing and is

currently being applied to the Palinpinon field in the Phillipines. Stanford personnel also cooperated in a multilab tracer test in the Dixie Valley, Nevada.

International cooperative research is continuing at Stanford. Efforts are directed to cooperative work with Mexico and Italy. Laboratory studies of water adsorption in vapor-dominated geothermal reservoir continues to be a research topic of much interest for joint study by ENEL engineers and members of the Stanford Geothermal Program. At present, members of both the ENEL and Stanford research groups are seeking an extension of their proposal on joint adsorption research. The major plans for the following year include the acquisition of a state of the art equipment for steam adsorption work. Also, starting is the work on determining two-phase relative permeability of fractures. The equipment is set up currently and is hooked to a computerized data acquisition system.

The 14*th* Stanford Geothermal Workshop was held in Stanford in January 1989. 130 participants attended the meeting spread over three days. This workshop serves as a forum for exchange of ideas between the academic and industry personnel.

SECTION 1 : RESERVOIR TECHNOLOGY

Section 11 : Modeling Pressure Transient Behavior of Sectionally Homogeneous Reservoirs bv the Boundarv Element Method

Jitendra Kikani

Overview

Heterogeneities in petroleum and geothermal reservoirs complicate pressure transient testing. Conventional analytic techniques can only be used for fairly simple geometries. More complex situations usually require numerical simulation. This paper demonstrates a new approach using the Boundary Element Method (BEM) to solve for pressure transient behavior in complex reservoirs.

A Laplace space boundary element solution is proposed to determine the pressure solution in a piecewise homogeneous reservoir with arbitrary geometry of each region. Any number of such regions with different rock and fluid properties can be included in the solution procedure. This formulation can solve fluid injection problems which show composite behavior (as in water injection in geothermal reservoirs). In addition, impermeable barriers of any shape and orientation as well as large pressure support sources (aquifers) can be included. Both pressure and pressure derivative behavior for such systems is presented. Any number of line source wells can be included. Example solutions are verified against known analytical solutions.

At the same time as pressure transients are calculated, the method also determines fluid velocities. Injection fluid front velocity is therefore calculated as part of the solution and thus the fronts can be tracked accurately. The analytic aspects of this procedure are discussed.

BEM solutions are more accurate than other numerical methods such as finite element and finite differeince techniques because the method retains the free space Green's function of the governing differential operator as a global weighting function in the integral equation.

Introduction

Large scale features in reservoirs such as finite length faults, permeability barriers or different properties in front of and behind a flood zone significantly affect pressure transient response in well!;. Detection of such features or design of tests to include for their presence could be important in computing long term performance. The parameters obtained by the analysis may also serve as a front end input to a reservoir simulator. With better geological description of reservoirs becoming available, it is of relevance to be able to model the features in the flow field which may significantly affect the reservoir performance. In other words, the enhancement of predictive tools is desirable.

Two different types of problems are addressed in this paper. The Boundary Element method has been used to solve both of the problems. The first category of problems consists of wells producing from reservoirs which have permeability barriers and/or constant pressure "holes" of arbitrary size, shape and orientation. Permeability barriers occur as shale lenses or as structural features in the reservoir. These can also be artificially created due to the injection of low mobility and compressibility fluids. Constant pressure subregions ("holes") may occur in reservoirs as gas caps or limited extent recharge zones. Gas injection for a number of EOR schemes could create a similar effect.

These problems have received limited treatment because of the difficulty of handling them analytically. The simplest manifestation of heterogeneity is idealized as sealing boundaries in the flow field. Detailed literature review is presented in *Kikani* ***(1989).***

With the boundary element method outlined in this paper, any number of such sectional-heterogeneities can be present in the flow field consisting of a number of line source wells (injectors/producers).

The second category consists of fluid injection problems which create mobility and storativity contrasts in the reservoir. Injection/Falloff tests performed in wells show distinct characteristics of both the injection and in-situ fluid provided the test is run long enough and that wellbore storage does not dominate the early time pressure behavior. Such systems are treated as radial or elliptical composite reservoirs with different properties in the inner and outer regions. The interface between the two regions is assumed to be fixed in time and space. The radial composite models are used extensively to analyze well tests in water injection, steam injection, in-situ combustion and CO_2 injection projects. Extensive work has been done for such problems assuming both the inner and outer regions are perfectly radial and one well produces from the center of the reservoir. Analysis methods based on the pressure derivative have

been shown to provide accurate results. A survey of the literature on this subject is given in *Ambastha (1988)*.

In reality, the injection fronts are never truly radial due to a variety of reasons. Background drift caused by injection and production wells nearby can strongly affect the geometry of the propagating front and so can the outer boundary effects. Also, fractured injection wells could cause the fluid front to move in an elliptical or a rectangular fashion for a certain distance in the reservoir before the effect of inner boundary geometry is dissipated and the front becomes approximately radial.

The two categories of problems mentioned above are solved by the Boundary Element Method. This method holds promise for pressure transient type applications. The advantage of using this method to solve complex reservoir geometry problems in lieu of numerical methods stems from the fact that the analytical character of the solution is preserved in terms of the fundamental solution to the governing equations.

Boundary Element Method

Developed in the realm of potential theory, this method is now being used in a variety of engineering applications. The advantages of using this method for pressure transient type problems are :

- The accuracy of the method
- The reduction in the dimensionality of the problem, which leads to smaller size of mamx equations
- Flexibility of handling complex reservoir configurations and production schemes.

Applications of this method to reservoir engineering problems is recent. *Numbere and Tiab (1988)* and *Masukawa and Horne (1988)* looked at steady state problems for streamline generation. Transient problems have been investigated in the field of heat transfer *(Pina, 1984)* and groundwater flow *(Liggett and Liu, 1983)*, in addition to reservoir engineering. *Kikani and Horne (1988a,b)* discuss the development of this method in other disciplines and also showed the accuracy of solutions for transient problems in homogeneous systems. Two techniques were presented. One was the solution in real space which involved dealing with the history dependent nature of the integrals and the other was a Laplace transform solution. The use of this method in streamline generation and well testing with some field type examples has been presented *(Kikani and Horne, 1989)*.

Mathematical Considerations

Sectionally Heterogeneous Reservoirs

Figure 1.1.1 shows a schematic of a reservoir with small scale features. These features tend to alter the flow characteristics of the fluids and consequently the pressure behavior. Examples of this could be impermeable barriers or small recharge zones acting as constant pressure boundaries, or local concentration of injected gas near a wellbore. The constant pressure boundary is shown in Fig. 1.1.1 as a checkered region.

Mathematically, the problem domain is a multiply connected surface, the flow through which is governed by the diffusivity equation for single phase flow.

For the simply connected region (as in homogeneous reservoirs) the diffusivity equation is cast in an integral form in Laplace space. The boundary surface is discretized in a number of linear segments such that the boundary geometry is reasonably well represented. The linear segments, better known as boundary elements, are numbered such that on traversing the boundary in clockwise direction the domain is always to the right. Clockwise numbering of nodes is not essential but a consistent scheme should be used. The procedure for solving the diffusivity equation on a multiply connected surface follows the same concept except that the integrals have to be performed on the internal surfaces too. The interior sub-regions are numbered in a counter-clockwise direction to preserve the sense of the outward normal. The path integration scheme for one impermeable barrier in an otherwise homogeneous reservoir is shown in Fig. 1.1.2. It represents the fact that the reservoir on which the flow problem is solved is the annular region between the two surfaces. Both the internal sub-regions and the outer boundary are discretized in a number of boundary elements. The number of nodes on a boundary (Γ_i) is N_i.

The integral equation for the pressure at any point within the reservoir (excluding the interiors of the sub-regions) in Laplace space is given by

$$\theta\, \bar{p}_D(x_D, y_D; s) = \int_{\Gamma_1 + \Gamma_2} \left(\bar{G}\frac{\partial \bar{p}_D}{\partial n} - \bar{p}_D \frac{\partial \bar{G}}{\partial n}\right) d\Gamma + \sum_{i=1}^{n_w} \bar{G}_i\, Q_{D_i} \qquad (1.1.1)$$

$$\theta = 2\pi \qquad \text{if } (x_D, y_D) \in \Omega \qquad (1.1.2a)$$

$$\theta = \theta \qquad \text{if } (x_D, y_D) \in \Gamma_1 \qquad (1.1.2b)$$

$$\theta = 2\pi - \theta \qquad \text{if } (x_D, y_D) \in \Gamma_2 \qquad (1.1.2c)$$

where θ is the internal angle between two adjacent boundary elements. Equation (1.1.2c) implies that the exterior angles between adjacent boundary elements should be considered for

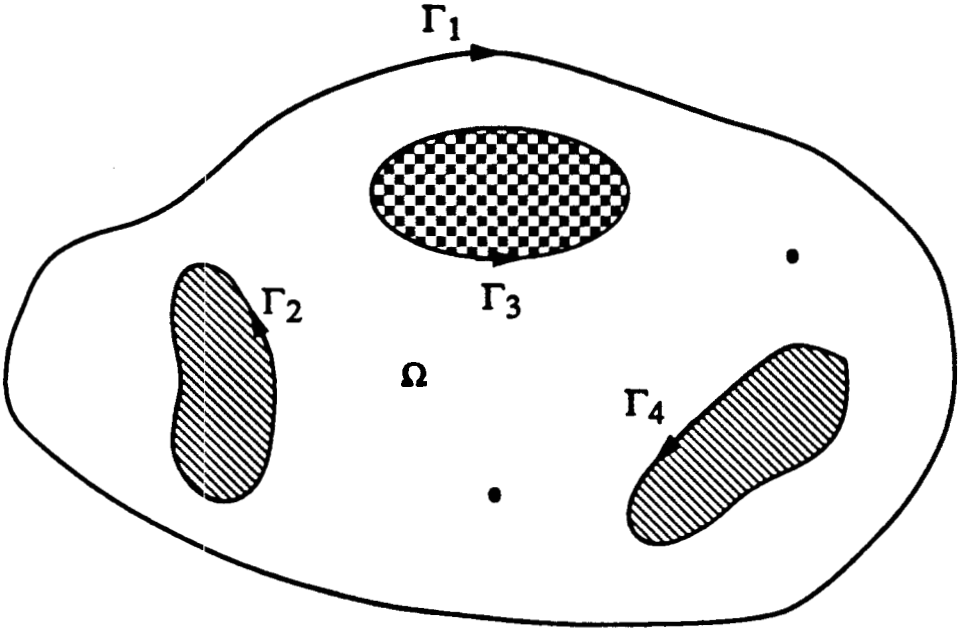

Figure 1.1.1: Schematic of a reservoir with heterogeneities

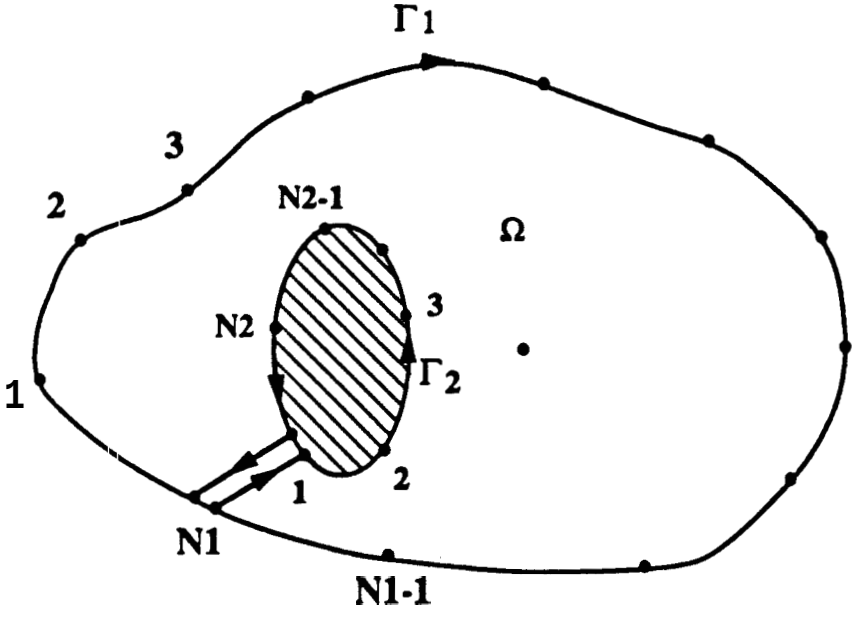

Figure 1.1.2 : Path integration scheme for a barrier in the reservoir

interior sub-regions.

$\bar{G}$ in Eq. (1.1.1) corresponds to the free space Green's function in Laplace space. A two-dimensional free space Green's function is defined [*Carslaw and Jaegar, 1959*] as the pressure response at (x_D, y_D) at a time t_D due to an instantaneous line source of strength unity generated at coordinates (ξ, ζ) at the time τ. The medium is initially at zero pressure and infinite in extent, $\bar{G}$ is given by

$$\bar{G}(x_D, y_D, \xi, \zeta; s) = -K_0(|r_D|\sqrt{s}) \tag{1.1.3}$$

where K_0 is the modified Bessel function of the second kind and order zero and r_D is given by

$$r_D^2 = (x_D - \xi)^2 + (y_D - \zeta)^2 \tag{1.1.4}$$

The integral Eq. (1.1.1) is solved in a discrete form by assuming a fictitious or Green's function source to be placed at each nodal point on the boundary, in turn. The resulting contribution of each of the nodes is compiled to give $N_1 + N_2$ equations in as many unknowns. The solution in Laplace space is sampled a number of times and inverted to real space by the use of *Stehfest algorithm (1970)* which is usually robust for diffusion type operators. With a few modifications the algorithm for solving the diffusivity equation in homogeneous reservoirs can be used for sectionally homogeneous reservoirs.

Two Region Composite Reservoir

Figure 1.1.3 shows the schematic of a composite reservoir. The properties of the inner and outer regions are different. The interface between the two-regions is assumed stationary. This assumption can be relaxed in an approximate sense and will be discussed later. There are three parameters which govern the system behavior. These are mobility ratio *(M)*, storativity ratio (F_s) and the distance to the discontinuity (R_D). The storativity ratio is defined as

$$F_s = \frac{M}{\eta} \tag{1.1.5}$$

where, η is the diffusivity ratio between the inner and outer regions.
The two regions can assume an arbitrary shape and consist of multiple injection and production wells. The non-dimensionalized governing equations and boundary conditions are as follows.

Inner Region

$$\frac{\partial^2 p_{D1}}{\partial x_D^2} + \frac{\partial^2 p_{D1}}{\partial y_D^2} = \frac{\partial p_{D1}}{\partial t_{DA}} +$$

$$\sum_{i=1}^{n_{w1}} Q_{D1_i}\, \delta(x_D - x_{D_i})\, \delta(y_D - y_{D_i}) \qquad [\,(x_D^2 + y_D^2 < R_D^2)\,] \tag{1.1.6}$$

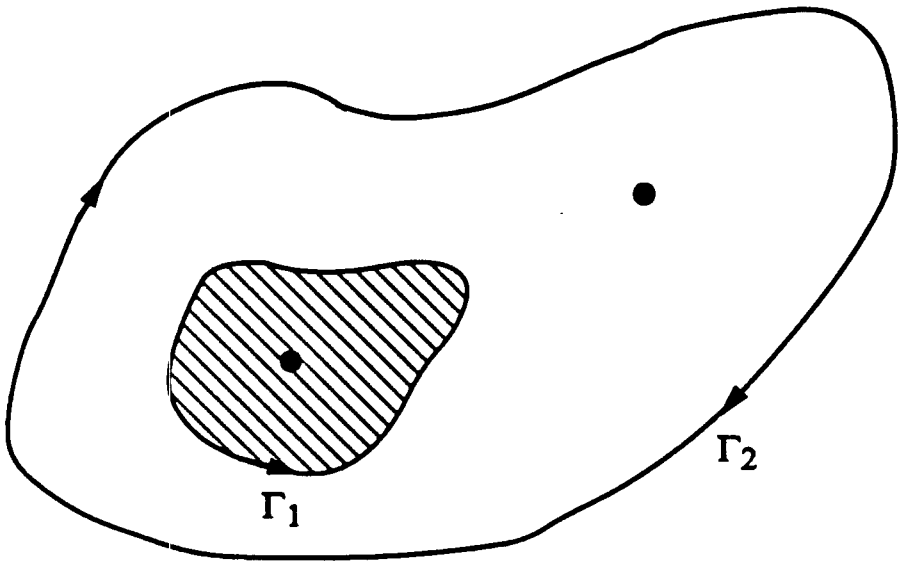

Figure 1.1.3 : Schematic of a composite reservoir

Outer Region

$$\frac{\partial^2 p_{D2}}{\partial x_D^2} + \frac{\partial^2 p_{D2}}{\partial y_D^2} = \frac{M}{F_s}\frac{\partial p_{D2}}{\partial t_{DA}} +$$

$$M\sum_{j=1}^{n_{w2}} Q_{D2_j}\,\delta(x_D - x_{D_j})\,\delta(y_D - y_{D_j}) \qquad [\,(R_D^2 < x_D^2 + y_D^2 < R_{eD}^2)\,] \qquad (1.1.7)$$

Initial Condition

$$p_{D1}(t_{DA} = 0) = p_{D2}(t_{DA} = 0) = 0 \qquad (1.1.8)$$

Interface Conditions

$$p_{D1}\,(\,x_{D1}^2 + y_{D1}^2 = R_D^2\,) = p_{D2}\,(\,x_{D2}^2 + y_{D2}^2 = R_D^2\,) \qquad (1.1.9)$$

$$\frac{\partial p_{D1}(R_D)}{\partial n} = -M\frac{\partial p_{D2}(R_D)}{\partial n} \qquad (1.1.10)$$

The negative sign in ***Eq.*** (1.1.10) accounts for the opposite sense of the outward normal in the two regions.

Exterior **Boundary** ndi

$$p_{D2}(R_{eD}, t_{DA}) = p_e \qquad (1.1.1\ 1)$$

$$\frac{\partial p_{D2}}{\partial n}(R_{eD}, t_{DA}) = q_e \qquad (1.1.12)$$

$$\alpha\, p_{D2} + \beta\frac{\partial p_{D2}}{\partial n} = \gamma_e \qquad (1.1.13)$$

The non-dimensional variables in the above equations are defined as follows

$$p_{D1} = \frac{P1 - P0}{\bar{p}} \qquad p_{D2} = \frac{P_2 - P0}{\bar{p}} \qquad (1.1.14)$$

$$x_D = \frac{x}{\sqrt{A_I}} \qquad y_D = \frac{y}{\sqrt{A_I}} \qquad (1.1.15)$$

$$t_{DA} = \frac{\eta_1 t}{A_I} \qquad Q_{Di} = \frac{Q_i \mu_1}{k_1 \rho \bar{p}} \qquad (1.1.16)$$

A_I in Eqs. (1.1.15) and (1.1.16) is the area of the inner region. The above equations can be normalized, alternatively, with respect to the exterior drainage area. $\bar{p}$ is a reference normalization pressure and p_0 is the initial reservoir pressure.

Transforming Eqs. **(1.1.16)** through **(1.1.13)** to Laplace space and casting them into a boundary integral., we obtain the following integral equations

$$\theta_1 \bar{p}_{D1}(x_D, y_D; s) = \int_{\Gamma_1} \left(\bar{G}_1 \frac{\partial \bar{p}_{D1}}{\partial n} - \bar{p}_D \frac{\partial \bar{G}_1}{\partial n} \right) dS + \frac{1}{s} \sum_{i=1}^{n_{w1}} \bar{G}_{1i} Q_{D_{1i}} \qquad (1.1.17)$$

$$\theta_2 \bar{p}_{D2}(x_D, y_D; s) = \int_{\Gamma_1 + \Gamma_2} \left(\bar{G}_2 \frac{\partial \bar{p}_{D2}}{\partial n} - \bar{p}_D \frac{\partial \bar{G}_2}{\partial n} \right) dS + \frac{1}{s} \sum_{i=1}^{n_{w2}} \bar{G}_{2i} Q_{D_{2i}} \qquad (1.1.18)$$

where θ_i has the same meaning as in **Eq. (1.1.1).** The $\bar{G}_i$ in Eqs. **(1.1.17)** and **(1.1.18)** denote the contributions of injector/producer wells at the Green's function source location. The details of the derivation for each of the the Eqs. (1.1.17) and **(1.1.18)** are similar to the single region homogeneous reservoir and is given in ***Kikani*** (1989). Consequently, it will not be discussed here.

The weighting functions or kernel functions (Green's functions) in the integral equations of **Eqs. (1.1.17)** and **(1.1.18)** are denoted by $\bar{G}_1$ and $\bar{G}_2$. The Green's function for the inner region is given by **Eq. (1.1.3).** The Green's function for the outer region is given by

$$\bar{G}_2(x_D, y_D, \xi, \zeta; s) = -K_0\left(|r_D| \sqrt{s \frac{M}{F_s}} \right) \qquad (1.1.19)$$

where $K_0(z)$ is the modified Bessel function of second kind of order zero, and r_D is given in **Eq. (1.1.4).**

Implementation

The integral equations obtained in the previous section are solved discretely on the boundaries in a collocation **type** scheme. For this, behavior of the pressure and fluxes have to be prescribed over each element. Linear interpolation functions have been used in this **work. A** comparison of oonstant and linear elements suggested that the use of linear elements gives accurate results with fewer elements. Higher order elements can be used if deemed necessary. The pressure and the normal derivative of pressure at any point on the element is expressed in terms of the nodal values **as** follows

$$p_D = \left[(p_{D_{j+1}} - p_{D_j})\,\xi + (\xi_{j+1} p_{D_j} - \xi_j p_{D_{j+1}}) \right] / (\xi_{j+1} - \xi_j) \qquad \xi_j < \xi < \xi_{j+1} \qquad (1.1.20)$$

$$\left(\frac{\partial p_D}{\partial n}\right) = \left\{ \left[\left(\frac{\partial p_D}{\partial n}\right)_{j+1} - \left(\frac{\partial p_D}{\partial n}\right)_j \right] \xi + \left[\xi_{j+1} \left(\frac{\partial p_D}{\partial n}\right)_j - \xi_j \left(\frac{\partial p_D}{\partial n}\right)_{j+1} \right] \right\} / (\xi_{j+1} - \xi_j) \qquad \xi_j < \xi < \xi_{j+1} \qquad (1.1.21)$$

where ξ is the local coordinate varying along the element. Once the interpolation functions are defined, the integral equations are discretized in a local coordinate system in order to reduce the integrals in two-dimensions to a one-dimensional contour integral. Figure **1.1.4** shows the local coordinate system. The point 'i' is the fictitious source point and ξ_j and ξ_{j+1} are the nodal locations for the element, on which the contribution of the source is evaluated. The fictitious source point is moved, in turn, to all the nodes and the respective contributions at all nodal locations are calculated. The discrete form of the integral Eqs. **(1.1.1), (1.1.17)** or **(1.1.18)** is then, given symbolically as

$$0 = \sum_{j=1}^{N} \int_{\xi_j}^{\xi_{j+1}} d\xi \left[\bar{p}_{D_{j+1}} f_1(\xi, \zeta_i; s) + (1 - 2\theta_i \delta_{ij}) \bar{p}_{D_j} f_2(\xi, \zeta_i; s) + \bar{p}_{Dn_j} g_1(\xi, \zeta_i; s) + \bar{p}_{Dn_j} g_2(\xi, \zeta_i; s) \right] \qquad i = 1, N \qquad (1.1.22)$$

The integrals in **Eq. (1.1.22)** consisting of functions f_1, f_2, g_1, and g_2 are evaluated either analytically or numerically. Rewriting **Eq. (1.1.22)** in a matrix form we obtain

$$\sum_{j=1}^{N} a_{ij} \bar{p}_{D_j} + b_{ij} \bar{p}_{Dn_j} = 0 \qquad i = 1, N \qquad (1.1.23)$$

where, a_{ij} and b_{ij} are the elements of the augmented coefficient matrix. Equation **(1.1.23)** is then sorted for the unknowns. The resultant matrix equation for the unknown boundary conditions is given by

$$\sum_{j=1}^{N} H_{ij} u_j = G_j \qquad i = 1, N \qquad (1.1.24)$$

where, u is the solution vector and G_j the right hand side vector. Solution of **Eq. (1.1.24)** gives the nodal values of the unknown at the boundaries. The solutions in the interior are obtained by using the same discretized integral equation again for an internal point.

The implementation of the integral equation for sectionally heterogeneous reservoirs is similar to that for homogeneous reservoirs and has been discussed in detail in *Kikani* (1989). The only difference between the two is in the numbering of the nodes. For the multiply connected surface, the sub-domains have to be considered.

For two region composite reservoirs, Eqs. **(1.1.17)** and **(1.1.18)** must be solved separately and coupled through the interface conditions. The boundary of the inner zone is divided into N_1 nodes and the exterior boundary is divided in N_2 nodes. Figure **1.1.5** shows the partition of the boundaries in the two regions. Region I consists of the fluid interface and the domain

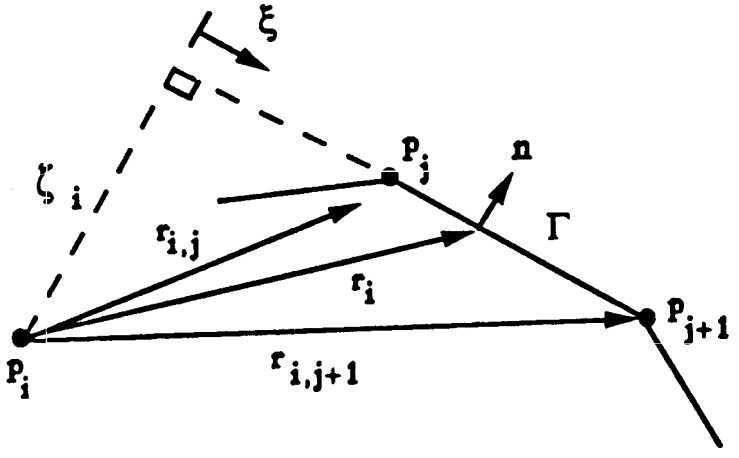

Figure 1.1.4: Local **coordinate system**

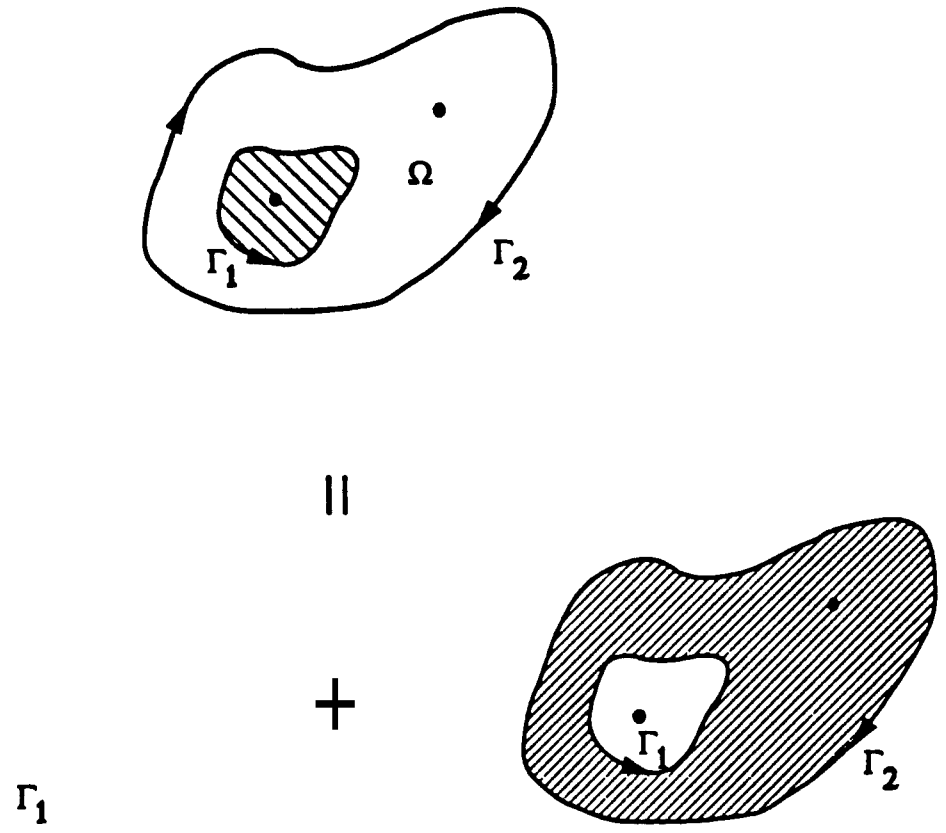

Figure 1.1.5: Partition of reservoir boundary into two regions

internal to it. Region II includes both the external boundary and the internal surface (interface). In other words region II is the annular region between the interface and the outer boundary.

Discretized equations as in Eq. (1.1.22) are written for both regions. The inner region is a simply connected surface. The fictitious or the Green's function source is placed at each of the nodal points and the contribution at all the other nodes are calculated in turn. This gives N_1 equations in $2N_1$ unknowns. There are more unknowns than equations because the boundary of inner region is the fluid interface or the discontinuity and neither pressures nor the fluxes are known apriori on this surface.

Meanwhile, the outer region of the composite reservoir consists of a multiply connected surface. The node numbering for the inner sub-region in this case follows the sectionally heterogeneous reservoir case. The number of nodes in this region are $N_1 + N_2$. Thus, $N_1 + N_2$ equations in $N_2 + 2N_1$ unknowns are obtained. In Fig. 1.1.5 this is shown as the region on the extreme right. Once the coefficient matrix for this region is compiled, the interface conditions are forced to be satisfied pointwise. Figure 1.1.6 shows the matrix structure resulting from constraining the solution to the interface conditions. The two rectangular sub-matrices are the coefficient matrices obtained from the boundary integral equations. These are completely filled. The other sub-matrices relate to the interface constraints and are diagonal. The blank spaces correspond to zero elements. These constraints could be eliminated in terms of common interface variables, reducing the matrix size. The structure of the reduced matrix is shown in Fig. 1.1.7. The bottom left hand corner sub-matrix is a null matrix. On solving the matrix, the boundary unknowns both on the inner and outer regions are known. This implies that both the pressure and the velocity of the fluid interface is known, pointwise. This provides a way to move the front in time. In other words, the front can be tracked in time in an Eulerian sense. Of course this is an approximation because the injection problem truly is a moving boundary problem and belongs to a class of problems known as Stefan's problem.

Once the boundary solutions are known, the pressures can be calculated at any well or interference location, be it in the inner or outer region. This is done by re-solving the integral Eqs. (1.1.17) or (1.1.18), depending on where the well is located. Since the boundary information on both pressure and fluxes is known, the problem reduces to quadratures.

Results and Discussion

The boundary element solution for both internal boundaries and composite reservoirs are verified against known analytical solutions. Figure 1.1.8 is a schematic of a well producing external to a circular boundary such as a flow barrier or a constant pressure "hole". The dimensionless parameters governing the system behavior are F, the ratio of the size of the

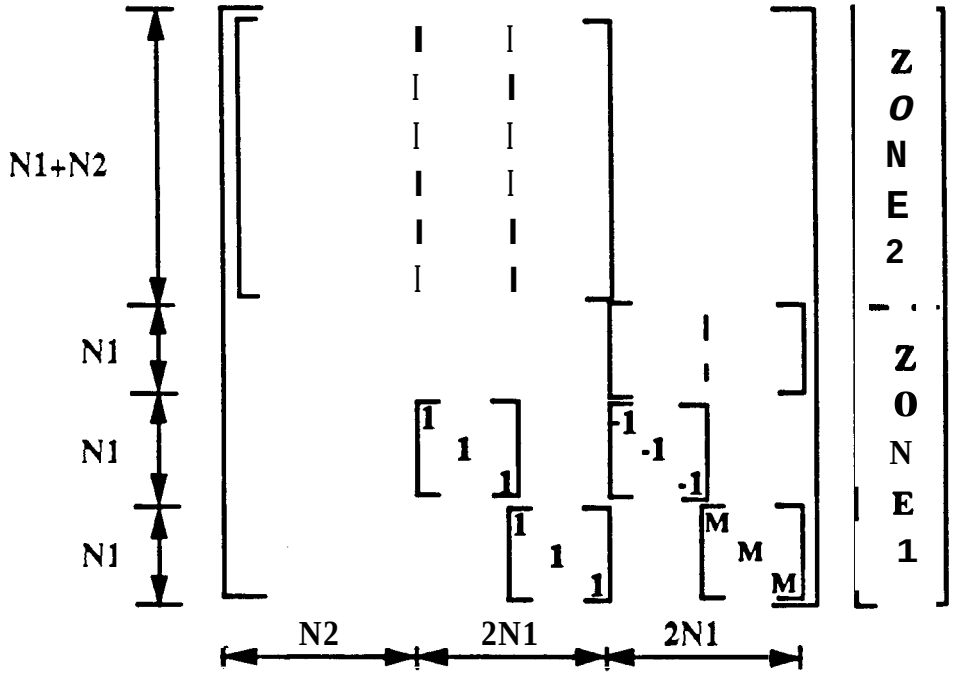

Figure 1.1.6 : Matrix structure for the composite reservoir

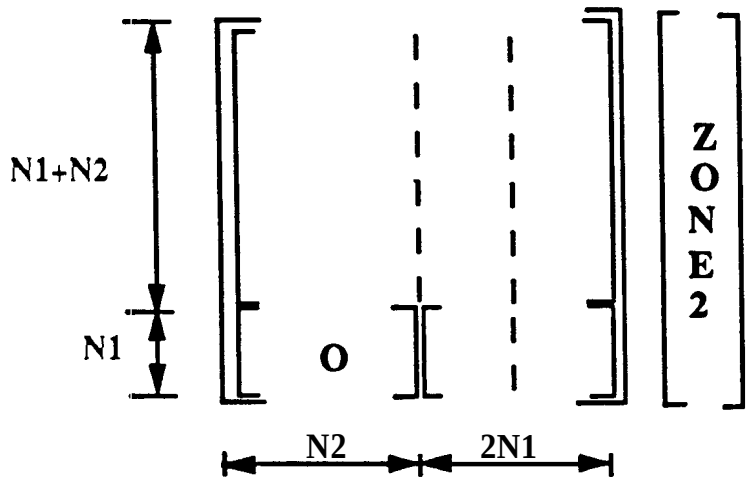

Figure 1.1.7 : Reduced **matrix** structure **on removing** the **constraint equations**

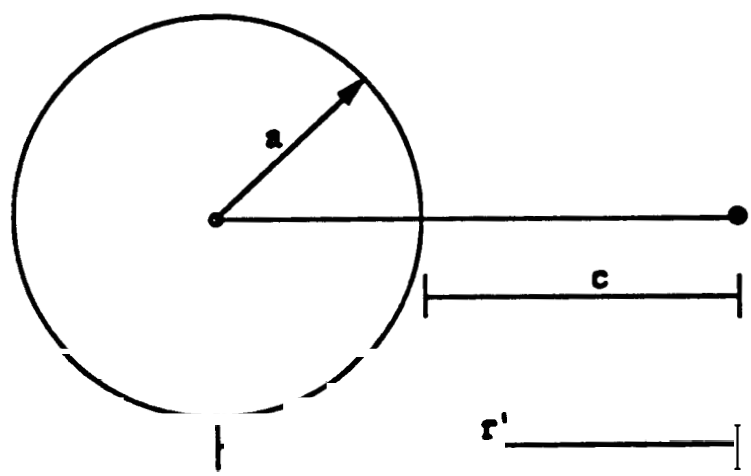

Figure 1.1.8 : Well producing external to an internal circular boundary

internal circular lboundary to its distance from the well, and c which is the distance from the well to the closest part of the internal boundary. Figure 1.1.9 shows a semi-log plot of dimensionless pressure vs. time for c = 250 and values of F ranging from 0.3 to 0.9. In the limit when F = 0, the system behaves like a line source solution. On the other extreme, F = 1 shows the behavior of well near a linear fault. Both closed and constant pressure internal boundaries are considered. The analytic solution was given by ***Sageev and Horne (1983).*** The analytic solution is composed of infinite series of modified Bessel functions [$I_n(x), K_n(x)$] of all integer orders. Table I.1.1 compares the boundary element solution with the analytic solution for F = 0.5 and c = 250. The results are within 0.5 % for $t_D \leq 8 \times 10^5$. Log-linear instead of linear interpolation between the computed values to obtain pressures at the times shown in the table, would show even smaller errors.

Figure 1.1.10 is a log-log plot of dimensionless semi-log pressure derivative vs. time corresponding to Fig. 1.1.9. It is quite instructive to look at the derivative plot. At early times, the derivative group shows infinite acting behavior given by a slope of 0.5. As the presence of the internal boundary is felt, the derivative group deviates from the infinite acting behavior for a short time before the system realizes that it is not a depletion system and more fluid is present. This results in another infinite acting behavior. The pressure derivative at late time becomes a constant and the value depends on the size and distance of the boundary from the active well. If the internal boundary is at constant pressure, then the derivative group dips below the infinite acting behavior when it feels the presence of the pressure support.

Figure 1.1.11 is a schematic of a well producing external to impermeable elliptic internal boundaries of various sizes. The major axis and the minor axis are labeled a_D and b_D respectively. The minimum distance from the well to the internal boundary is shown as $r_{D,\min}$. Figure 1.1.12 shows a semi-log plot of dimensionless pressure vs. time for a constant value of the ratio $\frac{b_D}{a_D} = 0.25$. $r_{D,\min}$ is chosen to be 100. The sizes of the ellipses are shown in Fig. 1.1.11. ***Britto and Grader (1988)*** used an iterative procedure as described earlier to generate pressure transient solutions for an elliptical internal boundary. Their solutions are represented as open circles in Fig. 1.1.12. At late times, the two solutions do not match very well. This may be due to several reasons and the exact cause could not be isolated due to lack of detailed information about the errors associated with ***Britto and*** Grader's ***solution.***

Composite Reservoirs

Figure 1.1.13 shows the effect of mobility (M) and storativity (F_s) ratios on the semi-log pressure derivative behavior of an infinite circular composite reservoir. The storativity ratios chosen cover a spectrum of values that are usually seen. The time axis is scaled by the front

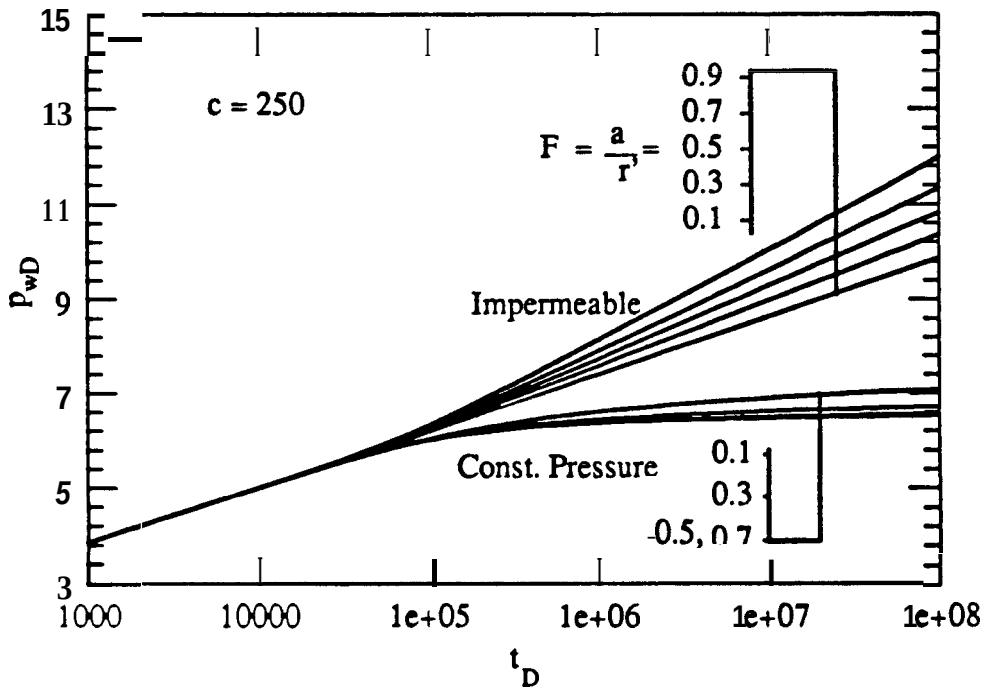

Figure 1.1.9: Pressure response at a well producing external to a circular sub-region

Table 1.1.1. Comparison with Analytical Solution (Circular Impermeable Barrier)

Dimensionless Time (t_D)	Analytical (Sageev[7])	Boundary Element (16 nodes)	Abs. Percent Error
4.0e+0	1.1283	1.1289	+ 0.053
8.0e+0	1.4597	1.4590	- 0.048
4.0e+1	2.2520	2.2527	+ 0.031
8.0e+1	2.5970	2.5963	- 0.027
4.0e+2	3.4005	3.40 12	+ 0.021
8.0e+2	3.7469	3.7462	- 0.019
4.0e+3	4.55 15	4.55 10	- 0.011
8.0e+3	4.8981	4.8974	- 0.014
4.0e+4	5.7288	5.7257	- 0.054
8.0e+4	6.1299	6.1246	- 0.086
4.0e+5	7.092 1	7.0400	- 0.738
8.0e+5	7.4739	7.4578	- 0.215

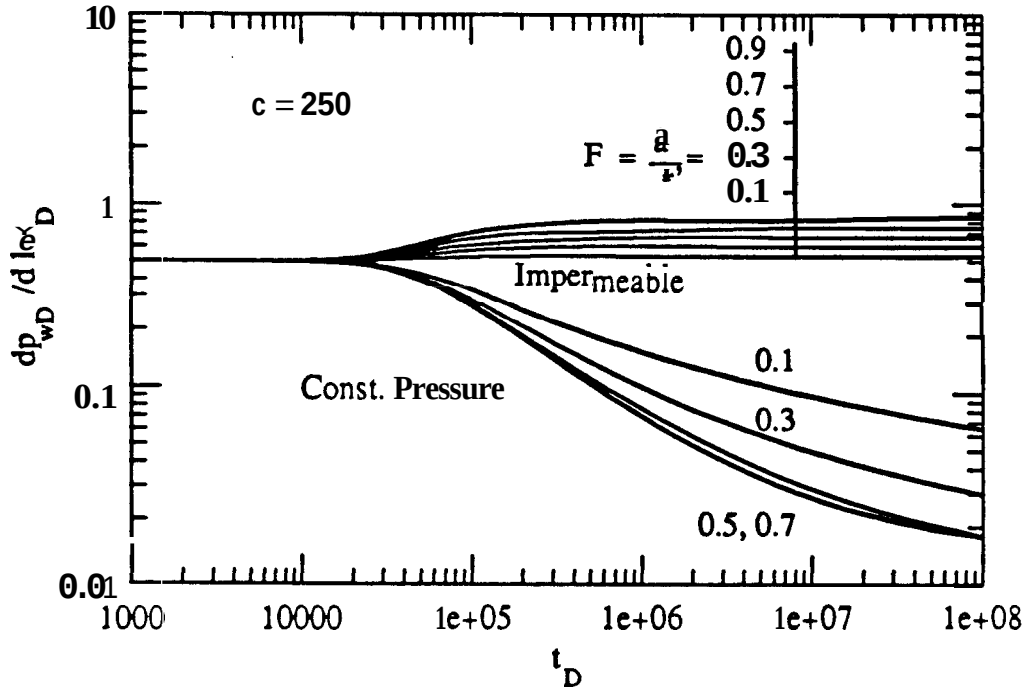

Figure 1.1.10: Pressure derivative behavior at a well producing external to a circular **sub-region**

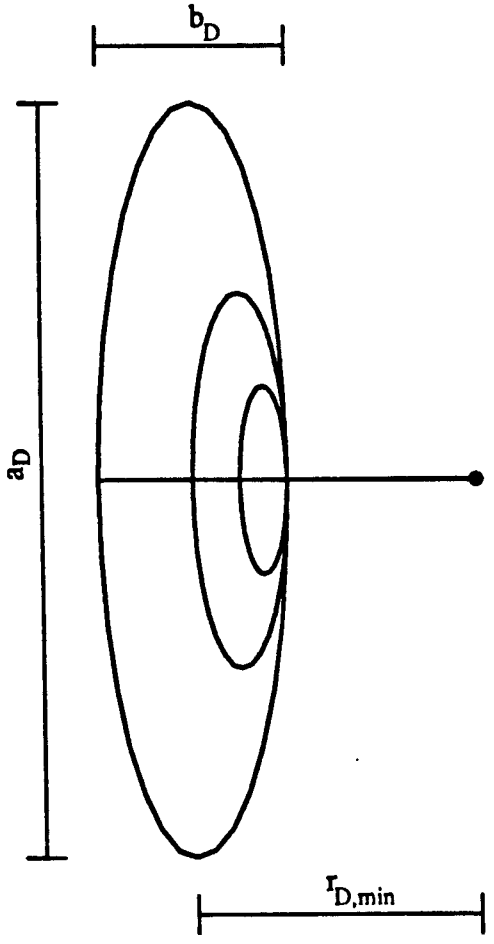

Figure 1.1.11: Schematic of a well external to impermeable elliptical sub-regions of different sizes

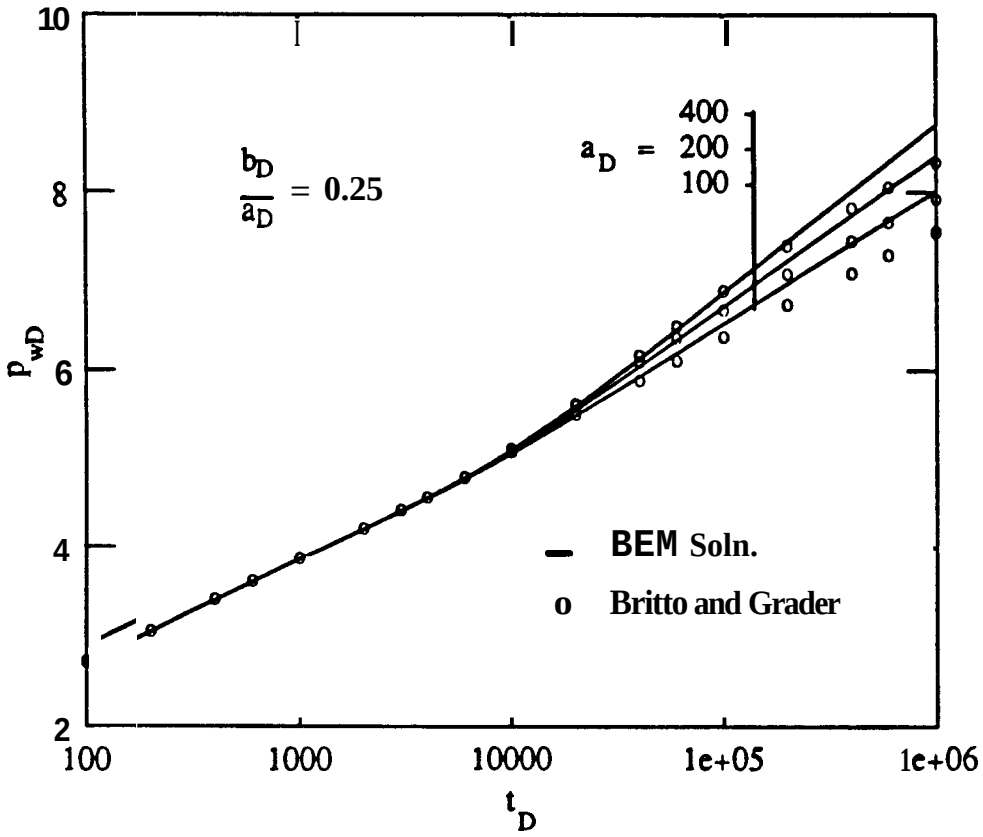

Figure 1.1.12 : Pressure response at a well producing external to an impermeable elliptic sub-region

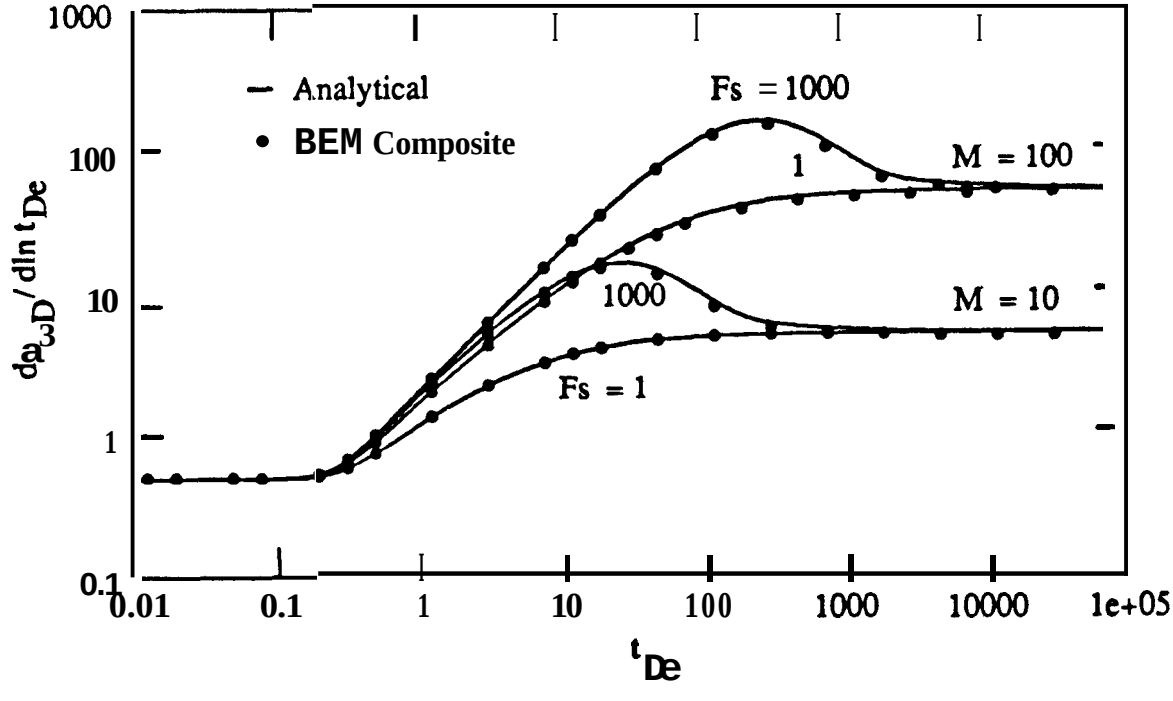

Figure 1.1.13: Effect of mobility and storativity ratio on the derivative response of a radial composite reservoir

radius

$$t_{De} = t_D/R_D^2 \qquad (1.1.25)$$

Early time radial infinite acting behavior corresponding to the inner region is seen as a constant value 0.5 on the pressure derivative plot. Depending on the value of storativity ratio, the pressure derivative deviates from the infinite acting behavior. The derivative passes through a maximum and goes to another radial infinite acting behavior, corresponding to the external region. The pressure derivative group is given by a value of M/2, where M is the mobility ratio of inner to the outer region. The solid lines in Fig. 1.1.13 are the analytical solution and the circles are the boundary element solution. Figure 1.1.14 shows the effects of a closed external boundary on the pressure transient response of a two-zone circular composite reservoir with a mobility ratio of 10 and storativity ratio of 1000. The composite reservoir effects are not seen if the ratio R_{eD}/R_D is $\leq$ 10. For R_{eD}/R_D at 1000, the infinite acting behavior due to the outer region can be seen before pseudo-steady state begins, which appears as a unit slope straight line on the derivative plot.

Field data suggest that there are thermal injection wells which are intercepted by a vertical fracture. In such cases, the dislacement front will move in a direction normal to the plane of the fracture at early times. The swept region at early times can be idealized as a low width to length ratio rectangle. Figure 1.1.15 shows the dimensionless pressure vs. time based on the length of the inner zone, for various width to length ratios of the inner swept region. The mobility and storativity ratios used were 200 and 16.67 respectively. *Teng (1984)* studied a similar problem for gas injection in a vertically fractured well with a finite difference simulator. The nonlinearities caused by the gas flow were included in the study. The solution matches qualitatively with Teng's results.

Computational Effort

The computations for composite reservoirs are quite intense and substantial computing effort is required. This is due to the fact that at every time step a fairly large mamx is inverted 6 to 8 times, depending on the number of sampling points in Laplace space. In addition, the geometry of the inner region must be represented quite accurately. For example, for a radial composite reservoir the phase discontinuity is a circle. If this circle is represented by a hexagon (6 nodes) then the pressure behavior is affected at late times significantly, because the isopotential lines are configured so that they are hexagons instead of circles.

No effort has been made to optimize the code for speedup. But, considerable improvement can be obtained by eliminating repetitive calculations, which are numerous, in favor of increased storage. Optimum number of nodes required varies from problem to problem. For a

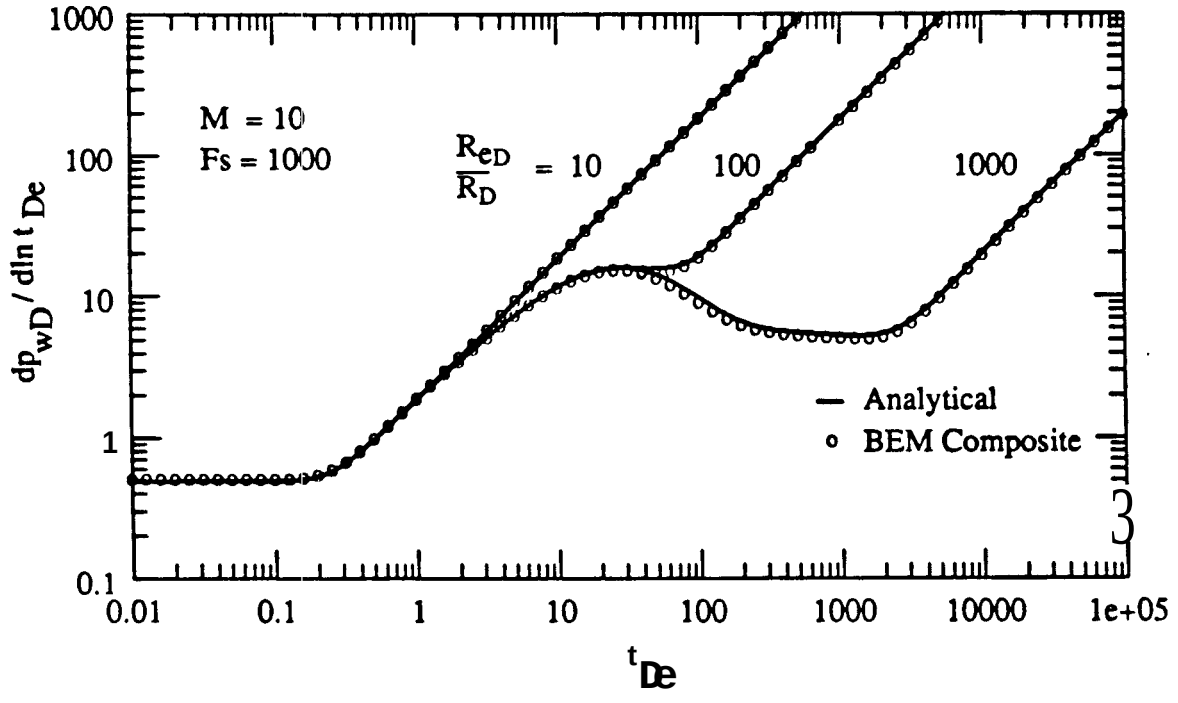

Figure I. 1.14 : Effect of external boundary on the derivative behavior of a radial composite reservoir

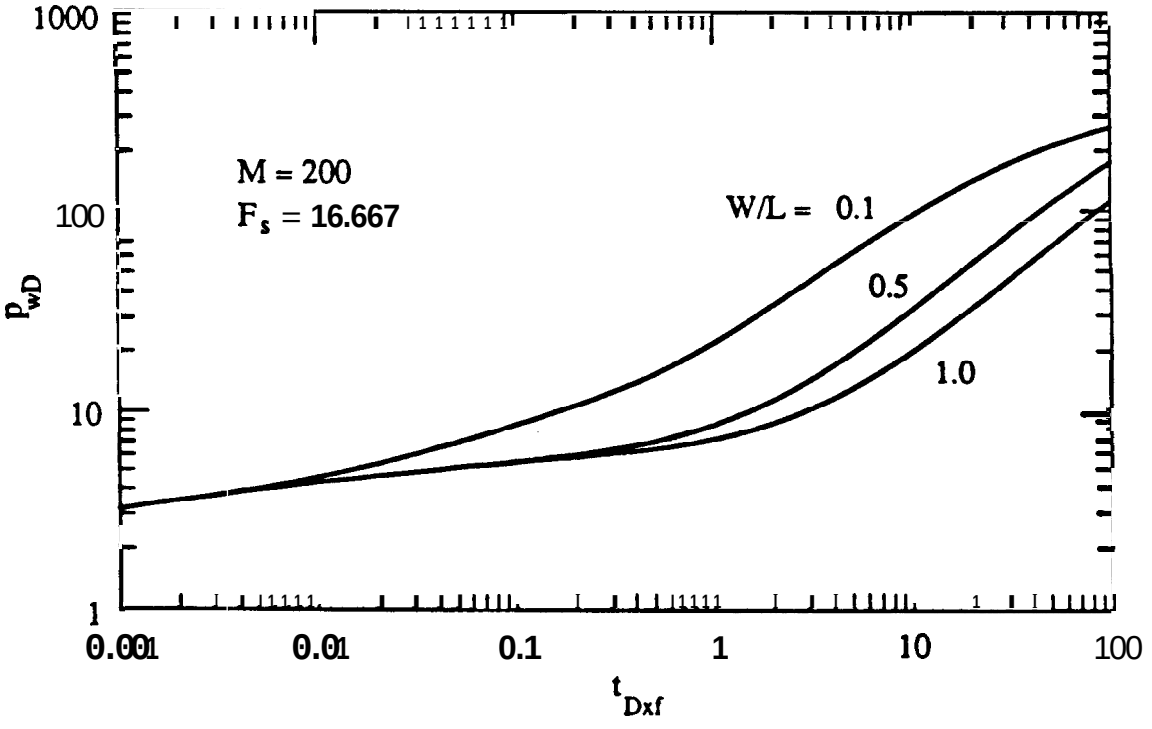

Figure 1.1.15: Effect of W/L ratio on the **pressure** response of **a** rectangular composite reservoir

homogeneous reservoir, it was found that good results were obtained with 16 nodes on a circular boundary. Whereas, for a composite reservoir a circular phase discontinuity must be represented by 32 points in order to obtain accurate results, although representing an outer boundary by 16 points does not degrade the results.

Conclusions

A new technique for simulating pressure transient response in arbitrarily shaped reservoirs with internal boundaries and in two-zone composite reservoirs is presented. The Boundary element method has been used for this purpose. The advantages of using the boundary element method are its accuracy, generality of use, and boundary only character. The boundary only character requires one to discretize only the surface of the problem domain.

The internal boundaries can be of any shape, size and orientation. These types of boundaries significantly modify the flow field and show its signature on the pressure response. The two-zone composite reservoir problems arise in a host of injection situations. Drift effects due to nearby wells cause the injection fronts to deviate from being radial. This can be accounted for by the solution method proposed. An approximate method for tracking the injection fluid front is shown, although no results have been presented at this time. The extension of the analysis to more than two composite zones is straightforward, and requires only some extra bookkeeping.

Section 1.2 : Comparison of Pressure Transient Response in Intensely and Sparsely Fractured Reservoirs

R.T. Johns and Y. Jalali-Yazdi

A compreheruive analytical model is presented to study the pressure transient behavior of a naturally fractured reservoir with a continuous matrix block size distribution. Geologically realistic probability density functions for matrix block size are used to represent reservoirs of varying fracture intensity and uniformity. Transient interporosity flow is assumed and interporosity skin is incorporated.

Drawdown and interference pressure transient tests are investigated. The results show differences in the pressure response from intensely and sparsely fractured reservoirs in the absence of interporosity skin. Also, uniformly and nonuniformly fractured reservoirs exhibit different responses, irrespective of the degree of fracture intensity. The pressure response of a nonuniformly fractured reservoir with large block size variability approaches a nonfractured (homogeneous) reservoir response. Type curves are developed to estimate matrix block size variability and the degree of fracture intensity from drawdown and interference well tests.

Introduction

The ***Warren and Root*** model (1963) and other pressure transient models for naturally fractured reservoirs assume fracture intensity is constant throughout the reservoir, i.e., they assume fracturing is uniform and matrix block size is constant. Geological and geomechanical studies of fractured reservoirs and outcrops, however, commonly report occurrences of nonuniform fracture patterns due to variability in lithology, bed thickness, degree of diagenesis, and stress environment ***(Pollard and Aydin, 1988; Segall, 1981).*** For reservoir engineering purposes, fracture patterns can be represented by simple geometric shapes or designs shown in Fig. 1.2.1. Skewed fracture patterns can also result due to variability in matrix block size and intersection angle. Some fractures are calcite cemented or mineral filled, which can restrict flow from the matrix blocks to the fractures. This phenomenon is termed interporosity skin ***(Cinco-Ley et al., 1985; Moench, 1984).***

The distribution of fracture lengths commonly observed in outcrops are exponentially decaying (i.e. there are many short joint lengths and few large joint lengths). Figure 1.2.2 illustrates a probability density function constructed from an outcrop in the Mt. Abott quadrangle of the central Sierra Nevadas (***Segall, 1981).***

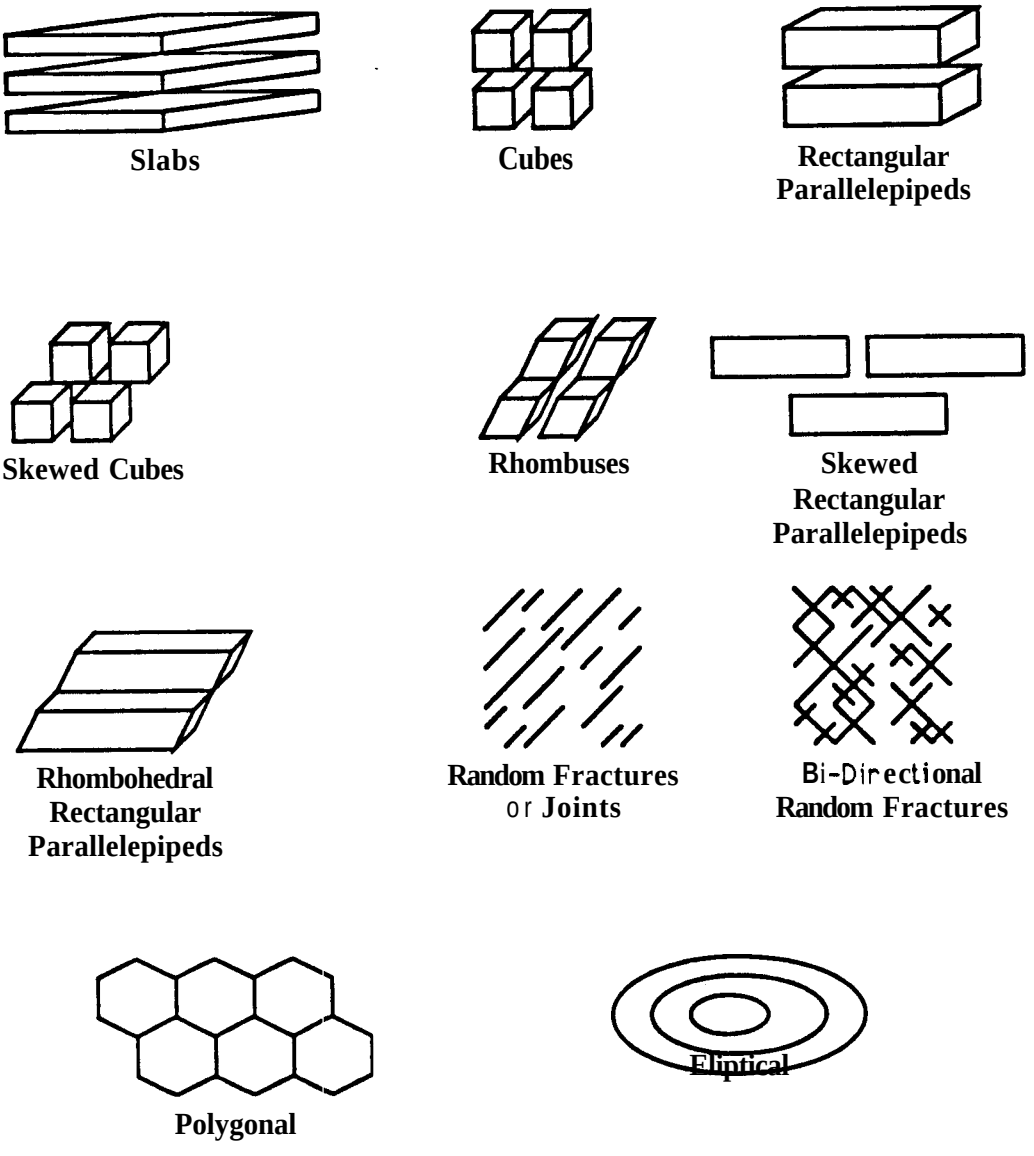

Figure 1.2.1: Idealizations of Typical Fracture Patterns seen in Nature.

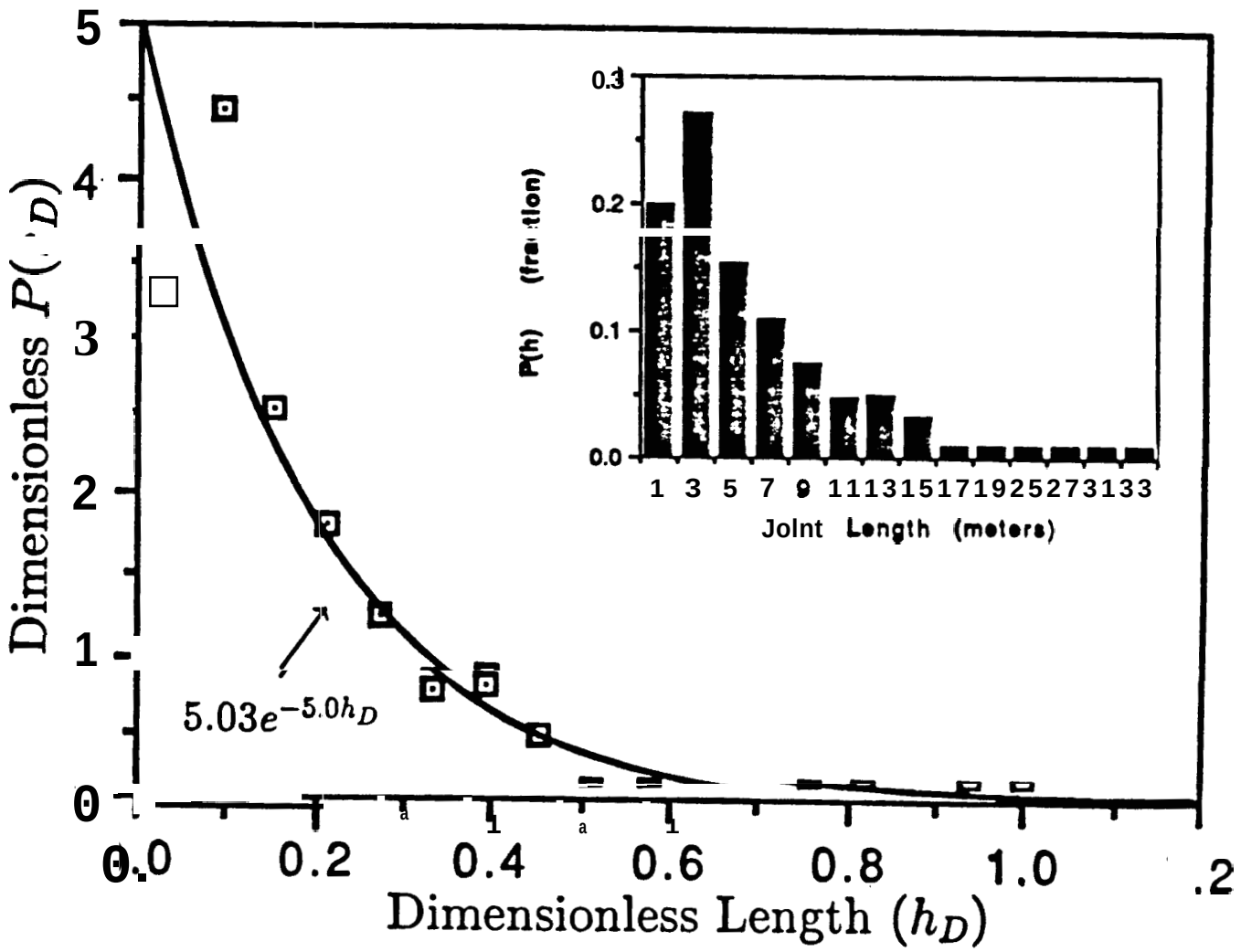

Figure 1.2.2: Construction of Probability Density Function from Outcrop, Central Sierra Nevadas. (Segall, 1981)

In well testing literature, the variability of matrix block size is generally not considered and a pseudosteady state (PSS) interporosity flow assumption is commonly used. Cinco-Ley *et al* (1985), however, used a discrete model of up to five different block sizes and demonstrated the transition zone is affected significantly while the late and early time responses are not. Both ***Cinco-Ley et al*** , and ***Moench*** (1984) presented a realistic explanation for the observance of the PSS behavior by introducing an interporosity skin factor. ***Belani and Jalali-Yazdi*** (1988), extended the discrete formulation of Cinco-Ley ***et al*** to continuous probability density functions of matrix block size. They considered three probability density functions: Dirac delta, rectangular, and bimodal. With an increase in the variance of the matrix block size distribution, they found features of a fractured reservoir response become less pronounced,

In this paper, a continuous probability density function of matrix block sizes is used. The objective is to show that drawdown and interference **well** testing can provide an indication of the degree of fracture intensity and the degree of uniformity of fracturing.

Theory and Solution

The diffusivity equation for a double porosity reservoir can be modified to include a probability distribution of matrix block size by introducing a source integral ***(Belani and Jalali-Yazdi,*** 1988; ***Johns,*** 1989; ***Johns and Jalali-Yazdi,*** 1989)

$$\frac{k_f}{\mu}\nabla^2 P_f = \phi_f c_f \frac{\partial P_f}{\partial t} + \int_{h_{min}}^{h_{max}} Q(h)P(h)\,dh\,. \tag{1.2.1}$$

The source integral in Eq. 1.2.1 accounts **for** the flow contribution of the matrix to the fracture. It is assumed that fluid travels from the matrix to the fractures and to the wellbore. P(h) is the probability density function (PDF) describing the likelihood of a certain matrix block size to exist and Q(h) is the flow contribution from that matrix block to the fracture. For transient interporosity flow and slab geometry:

$$Q(h) = -\frac{k_m}{\mu h}\nabla p_m\,|_{interface}\,. \tag{1.2.2}$$

Q(h), therefore, takes into consideration the mode of interporosity flow and also the geometry of the matrix blocks.

For a well producing at constant rate in an infinite reservoir, the interference solution in Laplace space is:

$$\bar{P}_{D_f} = \frac{K_0(xr_D)}{s[C_D s(K_0(x) + S_D x K_1(x)) + xK_1(x)]}, \tag{1.2.3}$$

and for drawdown:

$$\overline{P}_{D_w} = \frac{K_0(x) + S_D x K_1(x)}{s[C_D s(K_0(x) + S_D x K_1(x)) + x K_1(x)]}. \quad \textbf{(1.2.4)}$$

Parameter s is the Laplace variable related to dimensionless time (t_D) and the Bessel function argument is:

$$x = \sqrt{sf(s)}. \quad (1.2.5)$$

The function f(s) embodies the reservoir parameters including the matrix block size distribution. **For** transient interporosity flow in the presence of interporosity shin:

$$f(s) = \omega_f + \omega_m \int_{h_{ratio}}^{1} \frac{\sqrt{\frac{\lambda}{\omega_m s}} \tanh(\sqrt{\frac{\omega_m s}{\lambda}}) P(h_D)}{1 + S_{ID}\sqrt{\frac{\omega_m s}{\lambda}} tanh(\sqrt{\frac{\omega_m s}{\lambda}})} dh_D, \quad (1.2.6)$$

where,

$$hratio = \frac{h_{min}}{h_{max}}, \quad (1.2.7)$$

$$S_{ID} = \frac{k_m h_s}{k_s h}. \quad (1.2.8)$$

The interporosity skin factor (S_{ID}) is a function of matrix block size distribution and, hence is constant if $\frac{h_s}{h}$ is constant. An alternate assumption is that the depth of skin damage (h_s) is constant for all matrix blocks, and hence, S_{ID} is a variable:

$$S_{ID} = S_{ID_{min}} \sqrt{\frac{\lambda}{\lambda_{min}}}, \quad (1.2.9)$$

where,

$$S_{ID_{min}} = \frac{k_m h_s}{k_s h_{max}}, \quad (1.2.10)$$

and now:

$$f(s) = \omega_f + \omega_m \int_{h_{ratio}}^{1} \frac{\sqrt{\frac{\lambda}{\omega_m s}} \tanh(\sqrt{\frac{\omega_m s}{\lambda}}) P(h_D)}{1 + S_{ID_{min}}\sqrt{\frac{\omega_m s}{\lambda_{min}}} tanh(\sqrt{\frac{\omega_m s}{\lambda}})} dh_D \quad (1.2.11)$$

Probability Density Functions

Prediction of the pressure response requires the type of matrix block size distribution be known or assumed. When the PDF is selected, fracture intensity can be inferred from pressure transient data. **Two** types of probability density functions are used to represent

the variability of matrix block size. These types, exponential and linear (Fig. **1.2.3),** occur in outcrops **as** indicated in the geological literature ***(Pollard and Aydin*, 1988; Segall, 1981).** The Dirac delta and rectangular distribution are each subsets of the exponential and linear distributions.

The mean of a distribution is a measure of fracture intensity, while the variance is a measure of the degree of fracture uniformity. **As** fracture intensity increases, mean block size decreases and P(h) becomes skewed toward smaller block sizes. **As** fracture intensity decreases, P(h) becomes skewed toward large block sizes. When fracturing becomes uniform, h_{ratio} approaches unity and P(h) becomes 'narrow'. When fracturing becomes nonuniform, h_{ratio} approaches zero and P(h) becomes 'wide'.

The exponential PDF is given by:

$$P(h_D) = \frac{a(exp^{-ah_D})}{exp^{-(ah_{ratio})} - exp^{-a}}, \tag{1.2.12}$$

where 'a' is the exponential constant. The linear distribution function is:

$$P(h_D) = \frac{mh_D + b}{.5m(1 - h_{ratio}^2) + b(1 - h_{ratio})}, \tag{1.2.13}$$

where 'm' is the slope and 'b' is the vertical intercept of the Cartesian plot of $P(h_D)$ versus h_D. Because a probability function must be positive, the slope must be in the range:

$$\frac{-2}{(1 - h_{ratio})^2} \leq m \leq \frac{2}{(1 - h_{ratio})^2}. \tag{1.2.14}$$

The intercept 'b' is given by:

$$b = \frac{1 - .5m + .5h_{ratio}^2}{1 - hratio} \tag{1.2.15}$$

When 'm' is zero (linear) or 'a' is zero (exponential), both probability density functions reduce to the rectangular distribution:

$$P(h_D) = \frac{1}{1 - h_{ratio}}, \tag{1.2.16}$$

and when 'm' or 'a' approach infinity, the distributions reduce to the Dirac delta function:

$$P(h_D) = \delta(h_D - 1) = \begin{cases} 0 & \text{for } h_D \neq 1 \\ 1 & \text{for } h_D = 1 \end{cases}. \tag{1.2.17}$$

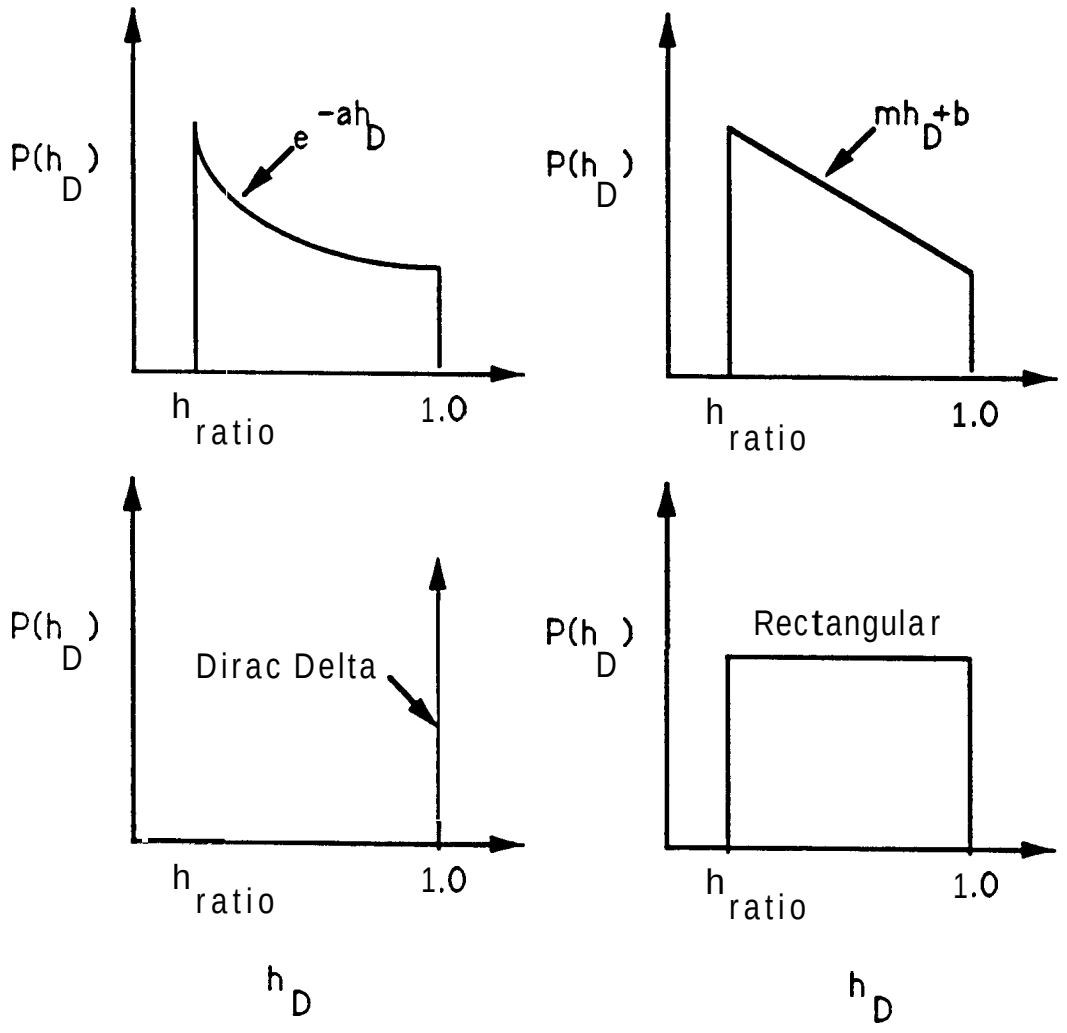

Figure 1.2.3: Probability Density Functions.

The Dirac delta distribution describes fractures that are perfectly ordered as in the Warren and Root model. The rectangular distribution, however, represents fractures that are perfectly disordered with a continuum of block sizes that are equally probable from the smallest (h_{min}) to the largest (h_{max}). In general, the rectangular distribution should be used if the distribution type is unknown.

Upon specifying the type of PDF, Eq. **1.2.11** can be solved for f(s). Table **1.2.1** lists the solutions of f(s) for the particular PDF.

Discussion-Drawdown Testing

Equation **1.2.4** in the absence of wellbore storage and **skin** reduces to:

$$\overline{P}_{D_w} = \frac{K_0(\sqrt{sf(s)})}{s^{3/2}\sqrt{f(s)}K_1(\sqrt{sf(s)})}. \qquad \textbf{(1.2.18)}$$

Equation **1.2.18** is numerically evaluated using the Stehfest algorithm for the exponential PDF listed in Table **1.2.1.** Figure **1.2.4** illustrates the response for varying values of 'a' holding h_{ratio} constant. For positively increasing values of 'a', fracture intensity increases and the response approaches the Dirac delta response for a uniform matrix block size h_{min} (i.e. the response occurs earlier in time). **For** negatively increasing values of 'a', fracture intensity decreases and the response approaches the Dirac delta response for a uniform matrix block size h_{max} (i.e. the response occurs later in time). Thus, fracture intensity determines the temporal position of the pressure response. Fracture uniformity, however, affects the shape of the pressure response. From Fig. **1.2.4,** it is evident the derivative profile shows a substantial degree of asymmetry with respect to the time axis as 'a' increases or decreases to large absolute values. The response for the rectangular matrix block size distribution

(i.e. a=0), however, is nearly symmetric. Therefore, asymmetry increases as fracturing becomes more uniform, and the shape of the derivative profile can be used as a qualitative indicator of the degree of matrix block size variability or nonuniformity.

In addition, parameter h_{ratio} provides an estimate of matrix block size variability. An h_{ratio} approaching one indicates perfectly uniform fracturing, while h_{ratio} approaching zero indicates perfectly nonuniform fracturing. Figure **1.2.5** illustrates the pressure response for varying values of h_{ratio} with 'a' held constant. For h_{ratio} approaching zero, the response approaches a homogenous reservoir response. This occurs because there is an incessant gradual contribution from the matrix to the fractures. As long as fracturing is extremely nonuniform, the response will not exhibit the classical profile of a distinct transition zone separating early and late time semilog straight lines.

PDF	f(s), where $\xi = \sqrt{\lambda_{min}}$
Exponential	$\omega_f + \frac{a\omega_m}{\xi(e^{-ah_{ratio}} - e^{-a})} \int_{\xi h_{ratio}}^{\xi} \frac{e^{\frac{-ay}{\xi}} tanh(y)}{y[1 + S_{ID_{min}} \xi \, tanh(y)]} dy$
Linear	$\omega_f + \frac{\omega_m}{\xi[.5m(1 - h_{ratio}^2) + b(1 - h_{ratio})]} \int_{\xi h_{ratio}}^{\xi} \frac{[\frac{m}{\xi} + \frac{b}{y}] tanh(y)}{1 + S_{ID_{min}} \xi \, tanh(y)} dy$
Rectangular	$\omega_f + \frac{\omega_m}{\xi(1 - h_{ratio})} \int_{\xi h_{ratio}}^{\xi} \frac{tanh(y)}{y[1 + S_{ID_{min}} \xi \, tanh(y)]} dy$
Dirac delta	$\omega_f + \frac{\omega_m tanh(\xi)}{\xi[1 + S_{ID} \xi tanh(\xi)]}$, where $\lambda_{min} = \lambda_{max} = \lambda$

Table 1.2.1: Functions f(s) for various PDF's.

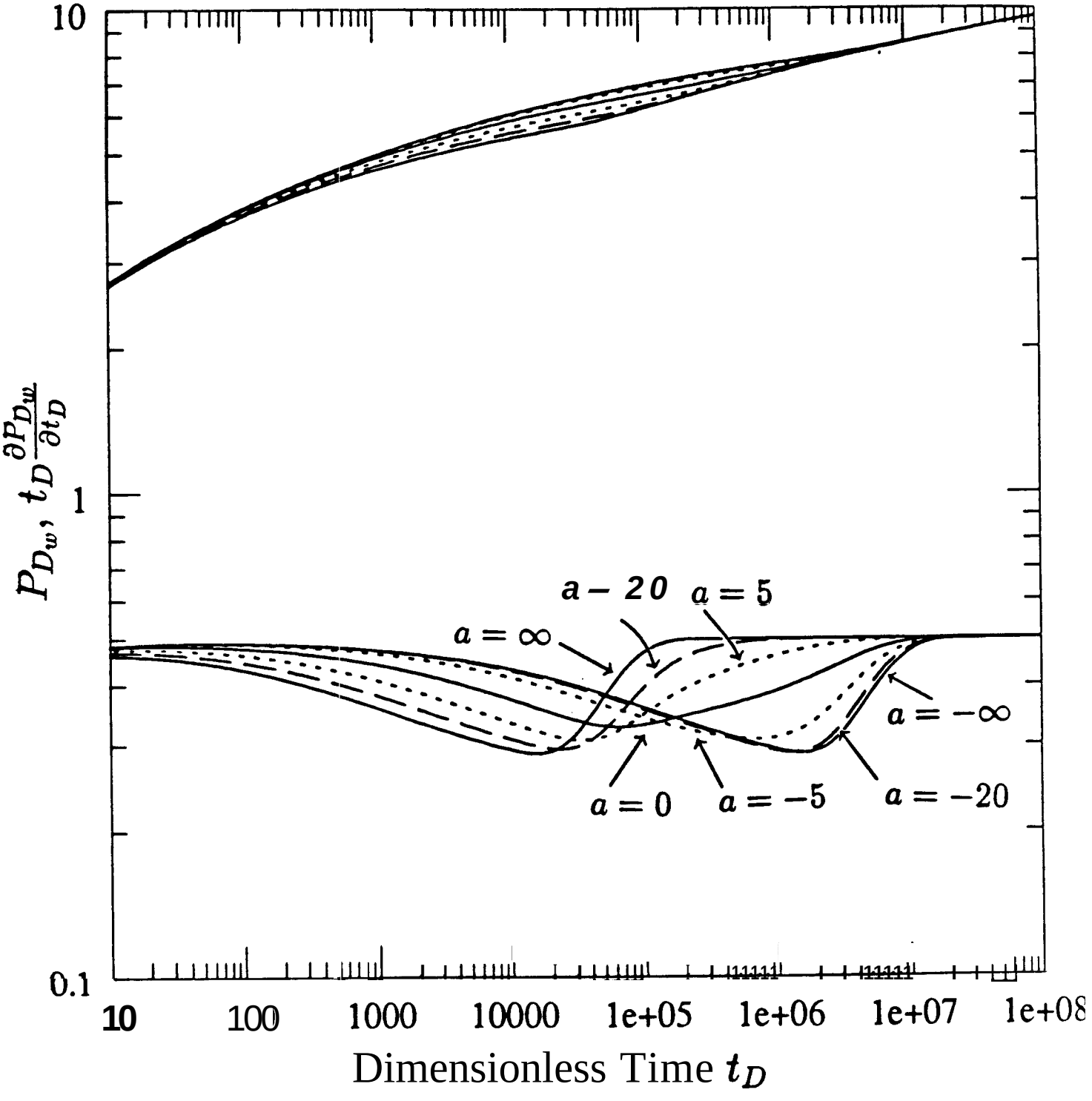

Figure 1.2.4: Exponential PDF: Varying 'a' with $h_{ratio} = .1$, $\lambda_{min} = 10^{-7}$, $\omega_m = .9$.

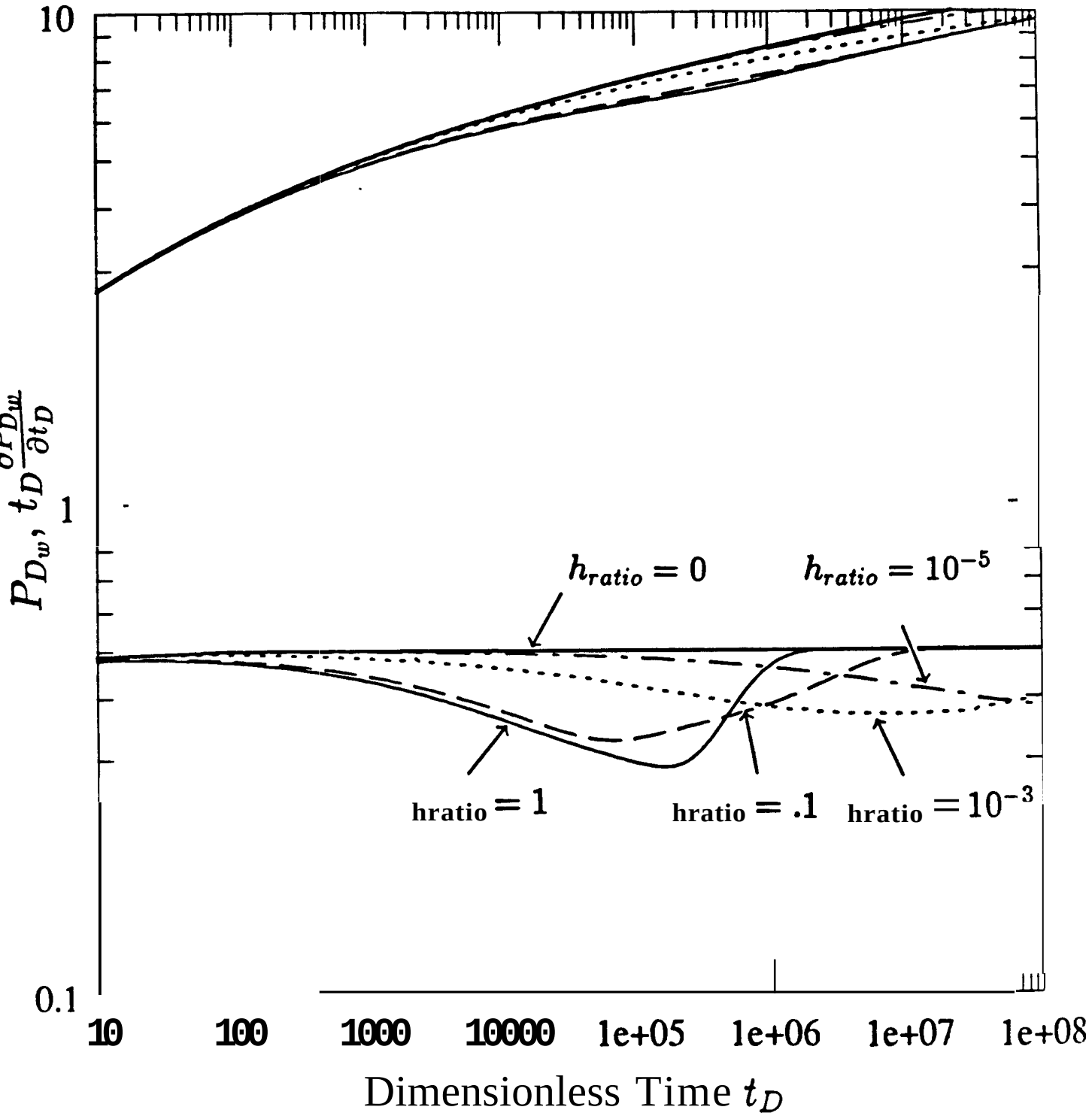

Figure 1.2.5: **Rectangular PDF: Varying h_{ratio} for Geometric** Mean $\lambda = 10^{-6}, \omega_m = .9$.

For the rectangular PDF, a type curve can be developed for estimation of ω_m, λ_{min}, and h_{ratio}. The type curve is based on the following time domain solution of the wellbore pressure response:

$$P_{D_w} = \frac{1}{2}[ln(\frac{t_D}{F(t_D)r_D^2}) + .80907], \quad \textbf{(1.2.19)}$$

where $F(t_D)$ is the time-dependent reservoir storativity:

$$F(t_D) = \omega_f + \omega_m \int_{h_{ratio}}^{1} \sqrt{\frac{t_D}{\tau}} tanh(\sqrt{\frac{\tau}{t_D}}) P(h_D)\, dh_D, \quad \textbf{(1.2.20)}$$

and τ is the matrix response time coefficient:

$$\tau = \frac{\omega_m}{\gamma\lambda}. \quad \textbf{(1.2.21)}$$

Equations **1.2.19** and **1.2.20** are obtained by applying the inversion technique of *Najurieta* **(1980)** and *Schapery* **(1961).** For the rectangular PDF, Eq. **1.2.20** becomes:

$$F(\frac{t_D}{\tau_{max}}) = \omega_f + \frac{\omega_m}{(1-h_{ratio})}\sqrt{\frac{t_D}{\tau_{max}}} \int_{h_{ratio}\sqrt{\frac{\tau_{max}}{t_D}}}^{\sqrt{\frac{\tau_{max}}{t_D}}} \frac{tanh(y)}{y}\, dy, \quad \textbf{(1.2.22)}$$

where y is the variable of integration and τ_{max} is the response time coefficient of the most dormant (or largest) matrix block:

$$\tau_{max} = \frac{\omega_m}{\gamma\lambda_{min}}. \quad \textbf{(1.2.23)}$$

In general, the time domain approximation gives remarkably good results (Fig. **1.2.6).** Using the difference between the extrapolated late time pressure response and the observed pressure, one obtains:

$$\mathbf{\Delta P} = P_{D_w} - P_{D_{w_{late}}} = -\frac{1}{2} lnF(\frac{t_D}{\tau_{max}}). \quad \textbf{(1.2.24)}$$

The type curve (Fig. **1.2.7)** is generated for the rectangular PDF by plotting the pressure difference ΔP versus $\frac{t_D}{\tau_{max}}$ for a range of h_{ratio} and ω_m values. The time match yields τ_{max} (and hence, λ_{min}), and the pressure match yields ω_m. Fracture permeability, k_f, can be calculated from the slope of the semilog straight line. Given reliable estimates of matrix permeability (i.e. from core analysis), one can calculate h_{max} from the definition of λ_{min}. From the shape of the curve, h_{ratio} is estimated, and hence, h_{min} is determined. The arithmetic mean of h_{min} and h_{max} is a measure of fracture intensity or sparsity.

The type curve demonstrates two key ideas. First, as matrix storativity predominates (increasing ω_m), h_{ratio} affects the pressure response more significantly. Conversely, as *w,*

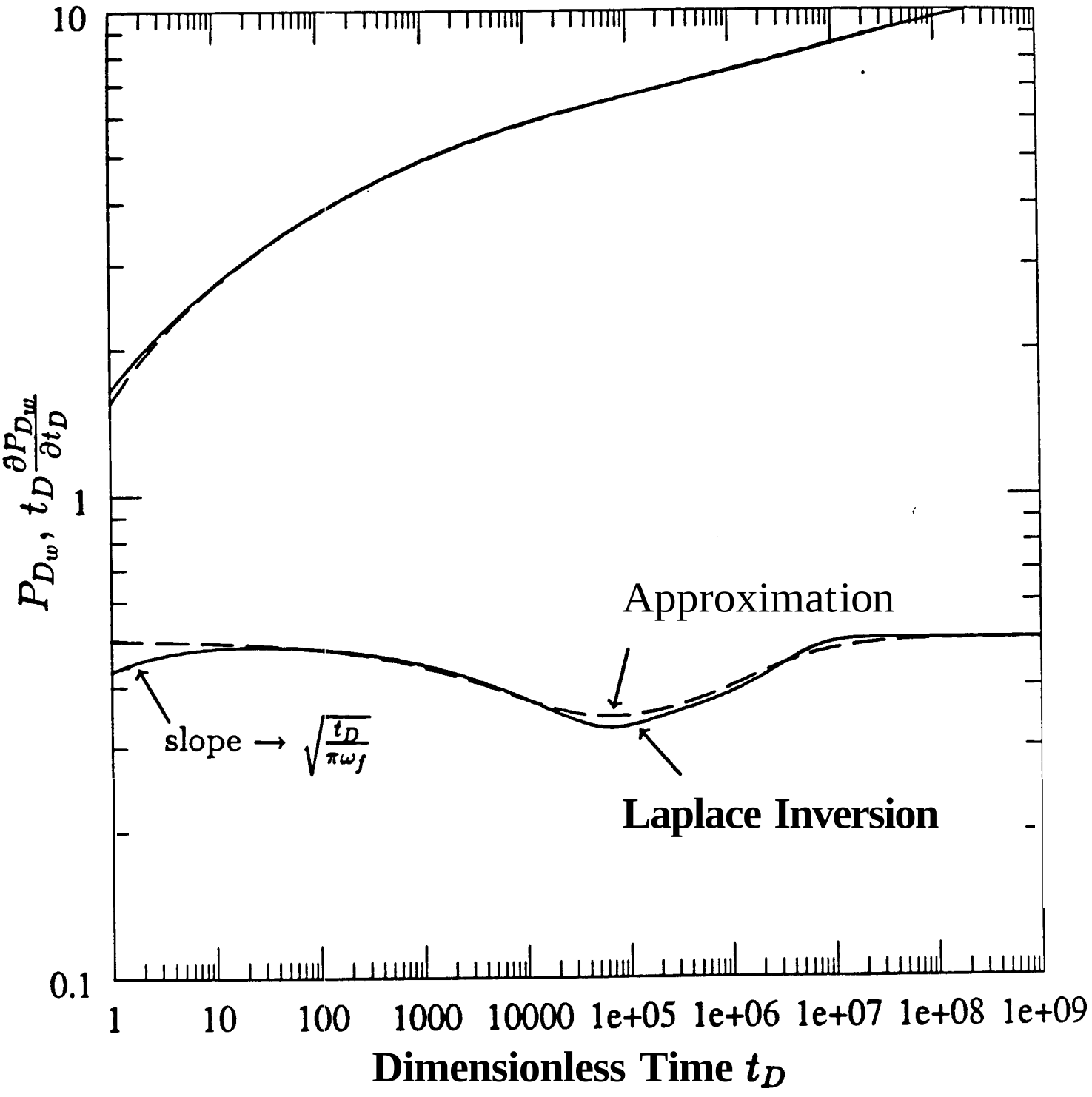

Figure 1.2.6: Rectangular PDF: Solution by Stehfest Inversion versus Time Domain Approximation, $h_{ratio} = .1$, $\lambda_{min} = 10^{-7}$, $\omega_m = .9$.

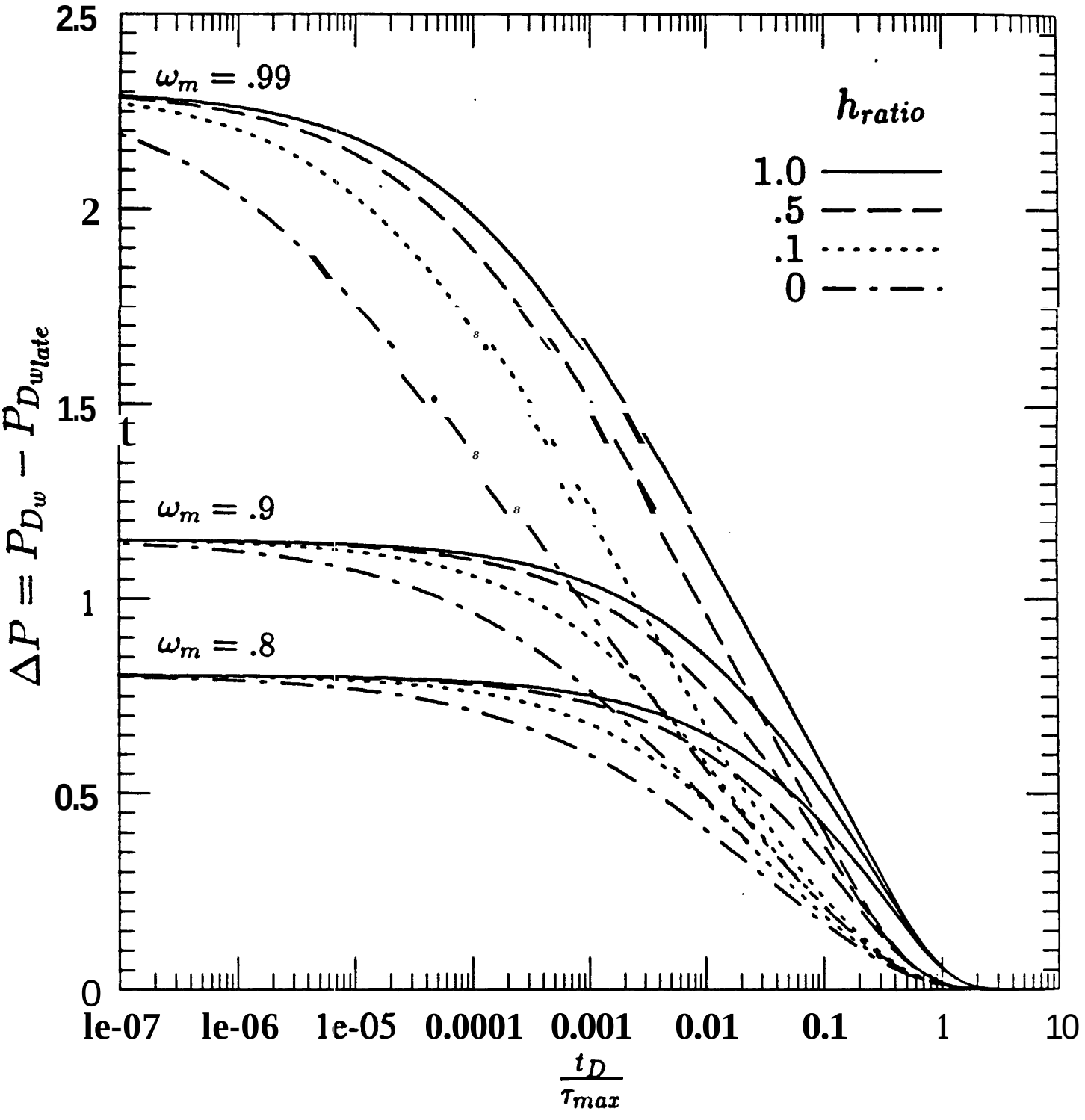

Figure 1.2.7 : Rectirngular PDF: Drawdown Type Curve for Varying h_{ratio}, λ_{min}, ω_m. Accurate for $t_D > 100$ and $\lambda_{min} < 10^{-4}$.

decreases, the effect of matrix block size variability becomes less significant. Second, the effect of h_{ratio} on the pressure response is greatest for lower values of h_{ratio} (e.g. the pressure response changes more significantly for h_{ratio} values from 0.1 to **0.5** than from 0.5 to **1.0).** This indicates that block size variability affects the pressure response significantly if h_{min} and h_{max} differ by at least one order of magnitude. Block size variability less than half an order of magnitude does not affect the pressure response significantly.

An example of the effect of interporosity skin $(S_{ID_{min}})$ on the pressure transient response is shown in Fig. **1.2.8. A** significant change in the pressure derivative is seen for small changes in $S_{ID_{min}}$, and thus, the effect of the matrix block size distribution is masked. The derivative profile becomes symmetric and more pronounced which is typical of the PSS response of Warren and Root. A symmetric PSS type response develops even if the no skin profile is asymmetric. **As** interporosity skin increases, the derivative profile shifts in time, giving apparent λ values that are too small (more dormant matrix). Thus, if interporosity skin exists, interpretation of pressure transient tests by the Warren and Root model underestimates λ and fracture intensity.

Discussion-Interference Testing

Braester (1984) demonstrated that drawdown (or buildup) tests in naturally fractured reservoirs may not be influenced by matrix blocks significantly away from the wellbore. Interference testing, therefore, is preferred because the response is affected by matrix blocks between the active and observation wells. **A** simplified solution for interference testing in the absence of storage and wellbore skin is the line source solution:

$$\overline{P}_{D_f} = \frac{K_0(r_D\sqrt{sf(s)})}{s} \qquad \textbf{(1.2.25)}$$

For any PDF distribution, it can be shown that $\theta = \lambda_{min} r_D^2$ is a correlating parameter ***Deruyck* et *al* (1982). For** instance, using the rectangular PDF:

$$f(sr_D^2) = \omega_f + \frac{\omega_m}{1-h_{ratio}}\sqrt{\frac{\theta}{\omega_m sr_D^2}}\int_{h_{ratio}\sqrt{\frac{\omega_m sr_D^2}{\theta}}}^{\sqrt{\frac{\omega_m sr_D^2}{\theta}}} \frac{tanh(y)}{y}\,dy. \qquad \textbf{(1.2.26)}$$

Equation **1.2.25** can then be evaluated using the inverse Laplace transform relation:

$$\mathcal{L}^{-1}[\overline{P}_{D_f}(sr_D^2)] = \frac{1}{r_D^2}P_{D_f}\left(\frac{t_D}{r_D^2}\right). \qquad \textbf{(1.2.27)}$$

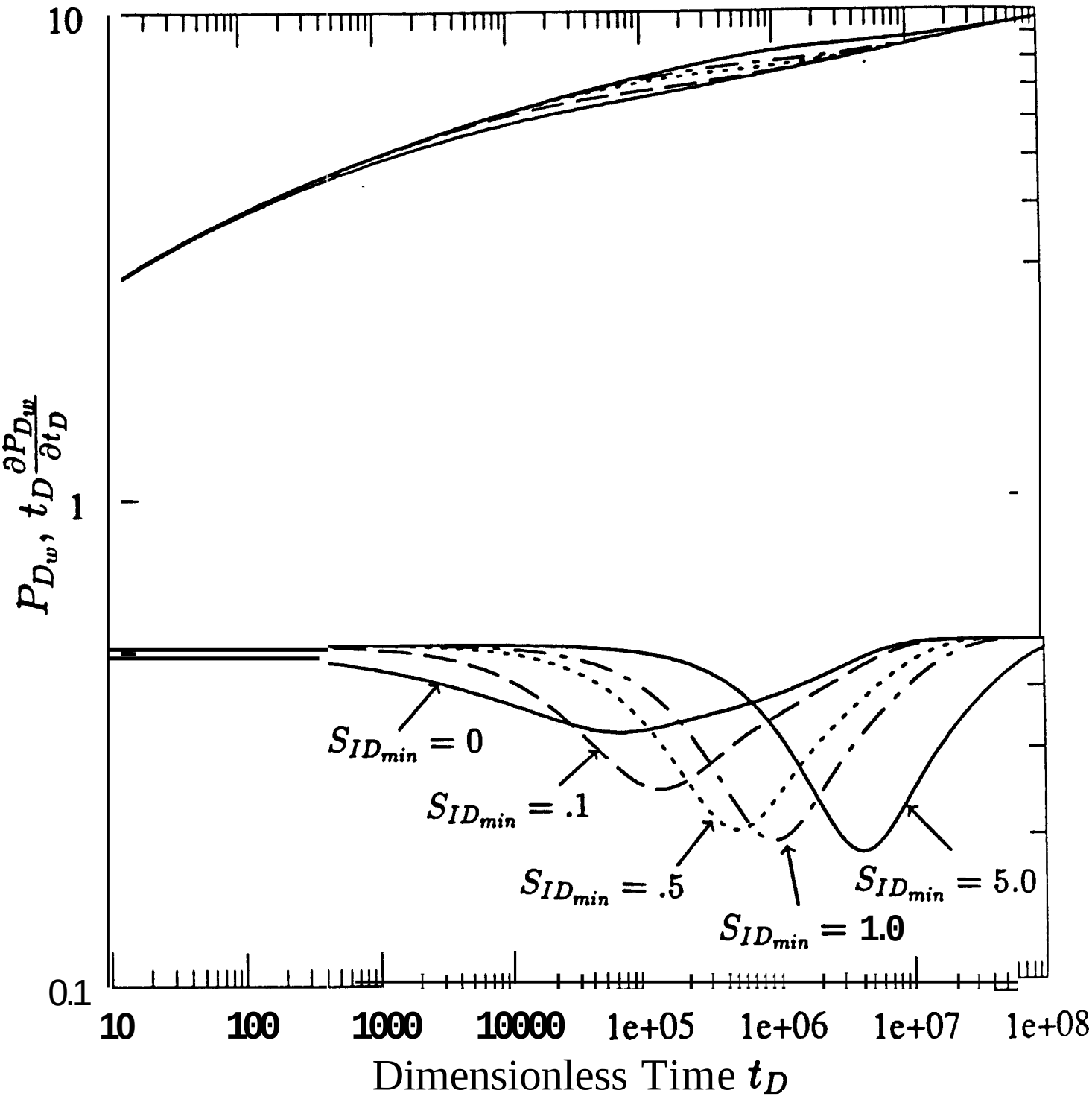

Figure 1.2.8: Rectangular PDF: Effect of Interporosity Skin, $h_{ratio} = .1, \lambda_{min} = 10^{-7}$, $\omega_m = .9$.

A type curve (Fig. 1.2.9) is prepared using the rectangular PDF for $\omega_m = 0.9$. For each value of 8, h_{ratio} is varied from zero to one. If h_{ratio} determined from the type curve is equal to one, the PDF is a Dirac delta function and the type curve is similar to that presented by *Deruyck et al* (1982).

For large values of 8, the matrix block size variability becomes increasingly important and h_{ratio} can be better estimated. Thus, if the dimensionless distance (r_D) between the active and observation wells is large, or if λ_{min} becomes large (i.e. greater fracture intensity), then matrix block size variability becomes a key parameter in interference pressure transient analysis. Conversely, for smaller values of 8, matrix block size variability (or h_{ratio}) does not affect the pressure response significantly. Also, as 8 becomes larger, the response approaches the line source solution for smaller values of $\frac{t_D}{r_D^2}$.

Conclusions

1. **A** formulation incorporating transient interporosity flow and interporosity skin is presented for fractured reservoirs with variable matrix block size. Exponential and linear probability density functions have been used to represent intensely and sparsely fractured reservoirs with varying degrees of fracture uniformity.

2. Type curves have been generated for drawdown and interference well tests based on the rectangular PDF and slab matrix block geometry. Type curves yield estimates of fracture intensity **as** well **as** fracture nonuniformity.

3. Fracture intensity determines the temporal position of the pressure response, while fracture uniformity affects the shape of the pressure response. For transient interporosity flow, uniformly fractured reservoirs exhibit asymmetric derivative profiles, whereas nonuniformly fractured reservoirs exhibit symmetric profiles.

4. The parameter h_{ratio} quantifies the degree of fracture uniformity. Uniform fracturing is indicated when h_{ratio} is near one, while nonuniform fracturing is indicated when h_{ratio} is near zero. For an extremely nonuniform fractured reservoir (h_{ratio} approaching zero), the pressure response is similar to a nonfractured homogeneous reservoir response.

5. Matrix block size variability (h_{ratio}) cannot be estimated in the presence of interporosity skin damage. The Warren and Root model overestimates matrix block size if interporosity skin is present.

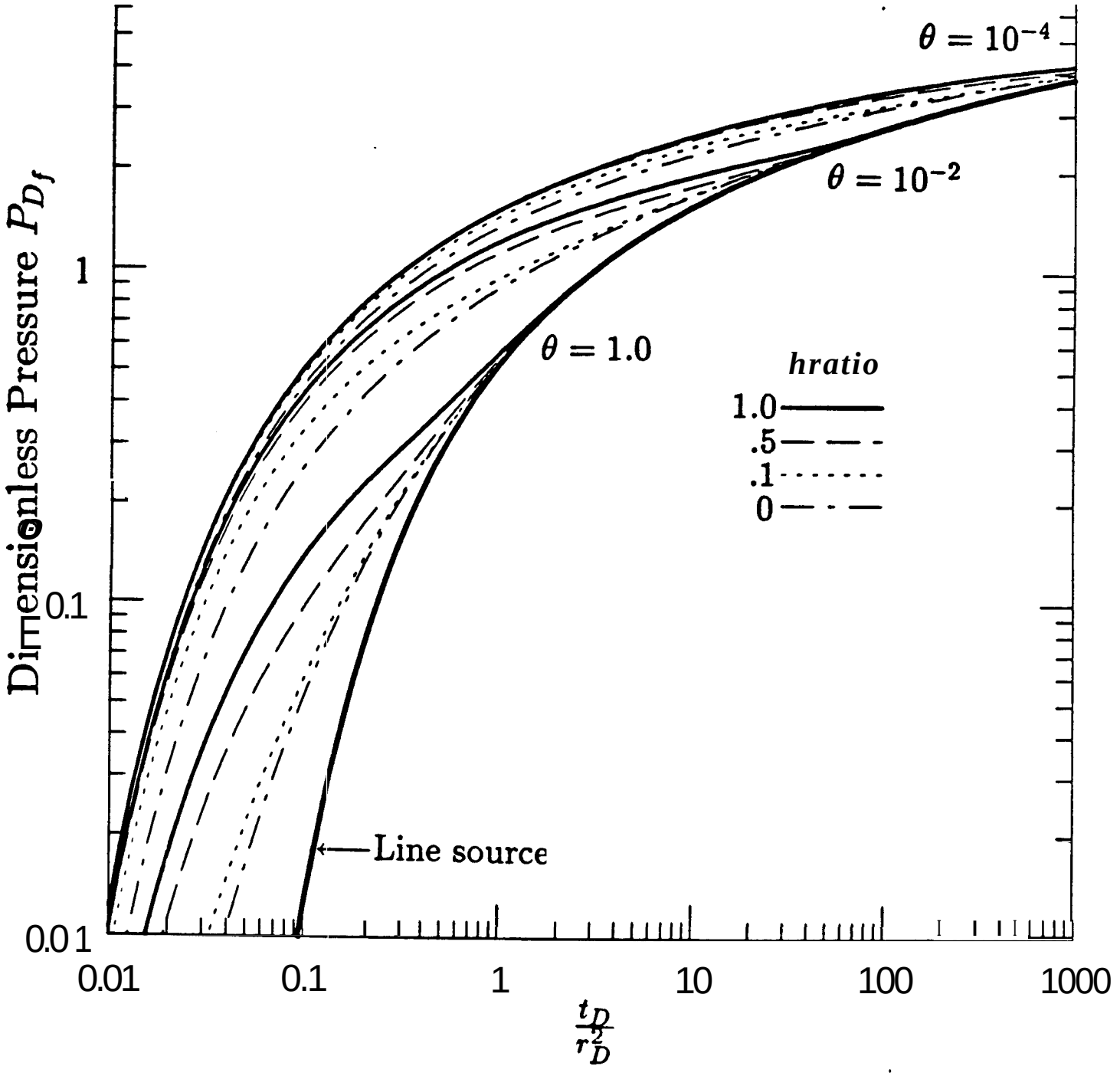

Figure 1.2.9: Rectangula PDF: Interference Type Curv for Varying h_{ratio}, θ, with $\omega_m = .9$.

Section 1.3 : Elliptical Finite Conductivity Fractures

Michael F. Riley

Movement of fluids in geothermal reservoirs takes place largely through a series of interconnected fractures. The reservoir pressure drops are due, in large part, to the fracture conductivity, i.e., how easily fluid flows in these fractures. The presence of material between the fracture walls will adversely effect their conductivity, increasing the pressure drop for a given flowrate.

The aim of the present research is to develop 'analytic' solutions for the pressure drop due to production from a single finite-conductivity fracture. It is assumed that a single fully penetrating fracture, of finite conductivity, produces from a homogeneous reservoir of infinite extent. This necessitates the solution of a two dimensional problem without the difficulty of including outer boundary effects. The novelty in the present approach is that the fracture cross- section will be modelled as a degenerate ellipse rather than a vanishingly thin rectangle. In both cases the resulting cross section is a line segment, but the equations governing the flow in the fracture are different.

The aim of this report is to show the problem as posed and solved for a rectangular fracture and to contrast it with the case of an elliptical fracture. The advantage of using elliptical coordinates will be shown to be the ease in coupling the flow in the reservoir with the flow in the fracture. This is independent of the fracture being more closely approximated by an ellipse than by a rectangle, especially in the case of hydraullically induced fractures.

Flow to a Rectangular Fracture

The classic work on finite conductivity fractures was done in a series of papers by Cinco, et al. The most important of these are ***Cinco et al.*** (1978) and *Cinco and Samaniego* (1981). The first of these references shows the derivation and solution of the problem, while the second shows the application of the solution to pressure transient testing.

The following is a modification of the derivations given in ***Cinco et al.*** (1978). Most of what follows in this section is shown in a paper by *Cinco and Meng* (1988). These modifications are made in order to better contrast the resulting equations with those derived subsequently for the elliptical case.

Figure **1.3.1** shows a schematic of Cinco's model, representing flow to a finite conductivity rectangular fracture. In order to solve this problem, two different regions are considered. The first region is the reservoir, and its properties will be denoted by the subscript, r, e.g., the reservoir peirmeability will be k_r. The equation governing the flow in the reservoir is the two dimensional diffusivity equation. The diffusivity equation in Laplace space is

$$\frac{\partial^2 \overline{p}_r}{\partial x_D^2} + \frac{\partial^2 \overline{p}_r}{\partial y_D^2} = s\overline{p}_r. \qquad \textbf{(1.3.1)}$$

Where $\overline{p}_r$ is the Laplace transform of the dimensionless reservoir pressure and s is the Laplace parameter for the dimensionless time based on reservoir properties. The independent variables, y_D and x_D have been normalized using the fracture half-length, x_f. This equation governs the flow in the reservoir and must be satisfied for **all** values of x_D and y_D, except on the fracture itself. Thus far, the only boundary condition we impose is that $\overline{p}_r$ approach zero as either y_D or x_D approach infinity. The remaining constraints are provided by coupling $\overline{p}_r$ to $\overline{p}_f$, the Laplace transform of the dimensionless fracture pressure.

If we assume that the flow in the fracture takes place under steady-state conditions, the equation for fracture flow is

$$\frac{\partial^2 \overline{p}_f}{\partial x_D^2} = -\frac{2}{F_D}\frac{\partial \overline{p}_r}{\partial y_D}_{y_D=0}. \qquad \textbf{(1.3.2)}$$

where, $F_D = k_f w_f / x_f h$

This equation governs flow in the fracture and must be satisfied everywhere on the fracture, i.e. for x_D between -1 and +1 and at y_D equal to zero. The term on the right hand side of Eq. **1.3.2** is a source term. This term appears because we are assuming the fracture can be approximated by a rectangle of zero thickness. In the usual case of composite geometries, we have an interface where we match pressures and fluxes. In our case, the 'interface' is the fracture itself. The pressures are still equated at the fracture face, but now we no longer match the fluxes. We are assuming the flow in the fracture is one-dimensional and that flow from the reservoir enters the fracture perpendicular to the fracture axis. In effect, Eq. **1.3.2** is a boundary condition for Eq. **1.3.1,** however, Eq. **1.3.2** needs two boundary conditions. The inner boundary condition, which accounts for flow to the wellbore, is

$$\bar{P}_2(x,y;s) = \frac{1}{2s}\int_{-1}^{+1} q(x',s)\, K_0(\sqrt{s}\sqrt{(x-x')^2 + y^2})\, dx'$$

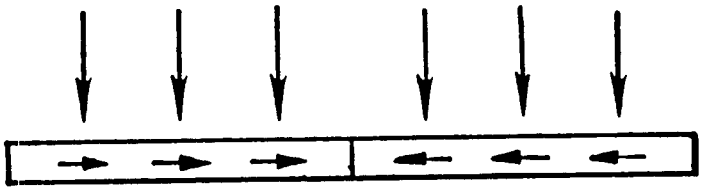

$$\left.\frac{\partial^2 \bar{P}_1}{\partial x^2} + \frac{2}{F_D}\frac{\partial \bar{P}_2}{\partial y}\right]_{y=0} = \frac{1}{\eta_D} s\bar{P}_1$$

Figure 1.3.1 : Cinco et al's Model

$$\left.\frac{\partial \bar{p}_f}{\partial x_D}\right|_{x_D=0+} = -\frac{\pi}{sF_D} \tag{1.3.3}$$

The outer boundary condition is specified as

$$\left.\frac{\partial \bar{p}_f}{\partial x_D}\right|_{x_D=+1} = 0. \tag{1.3.4}$$

These boundary conditions are only specified for the right half of the fracture. Since the problem is symmetric about the line $x_D = 0$, a corresponding set of boundary conditions are enforced on the left half of the fracture. This seems like it is overconstraining the equation, but it is not. Again, this is due to the symmetry of the problem. Another difficulty is with Eq. **1.3.4.** Ideally, we should set the two pressures equal at this point, but this will make solution of the problem more difficult. The no-flow boundary condition is much easier to handle and the effect of using this boundary condition should be minimal; especially for a low conductivity fracture. This difficulty is eliminated by using elliptical coordinates, as will be shown later. The third difficulty is with the inner boundary condition, Eq. **1.3.3.** This condition implies that we are producing to a plane of zero width rather than to a cylindrical wellbore. This difficulty is much harder to overcome, and is not taken care of by using elliptical coordinates. It should not greatly effect the ultimate solution, however, since the presence of the fracture is what profoundly affects the flowfield.

In order to solve the above equations, they are recast as integral equations using Green's functions. The Green's function form of Eq. **1.3.1** is

$$\bar{p}_r(x_D, y_D) = \int_{-1}^{+1} \bar{q}(x') K_0(\sqrt{s}((x_D - x')^2 + y_D^2))dx' \tag{1.3.5}$$

In the above equation, K_0 is a modified Bessel function.

Equation **1.3.5** represents the pressure anywhere in the reservoir in terms of the flux distribution $\bar{q}$. The flux is proportional to the normal derivative of pressure and so $\bar{q}$ is proportional to the right hand side of Eq. **1.3.2.** It is important to keep in mind that this integral formulation automatically satisfies the restriction that $\bar{p}_r$ approach zero as the distance from the fracture approaches infinity. It is also important to keep in mind that the only unknown in **Eq. 1.3.5** is $\bar{q}$. Once we know the flux distribution, we know the pressure anywhere in the reservoir.

Equation **1.3.2** can also be put in an integral form that also incorporates the two boundary conditions, Eqs. **1.3.3** and 1.3.4. In the integral form, Eq. **1.3.2** is

$$\bar{p}_f(x_D) = A(s) + \frac{(x_D-1)^2}{2\pi s F_D} + \frac{1}{2s\pi F_D}\int_{-1}^{+1}\sum_{n=1}^{\infty}\bar{q}(x')\frac{\cos(n\pi x_D)\cos(n\pi x')}{n^2}dx' \qquad (1.3.6)$$

This second integral formulation gives pressure anywhere in the fracture and includes the boundary conditions. Unfortunately, in this equation both $\bar{q}$ and $A(s)$ must be determined before the fracture pressure can be calculated. Equation **1.3.6** can be simplified somewhat but this is not necessary.

Equations **1.3.5** and **1.3.6,** along with the condition that the integral of the flux over the fracture equals $1/s$, fully specify the problem. The first step in determining pressures is to set y_D equal to zero in Eq. **1.3.1** and to equate it to Eq. **1.3.2.** This results in an integral equation for $\bar{q}$. For purposes of solution, $A(s)$ is treated as a constant, since it is independent of x_D. Once $\bar{q}$ is determined up to a multiplicative constant, A(s) is determined by the constraint on the integral of the flux. The pressures are then determined from Eq. **1.3.5** or Eq. 1.3.6. So far we have made only relatively minor simplifications, and if we could find an equation form for $\bar{q}$ and $A(s)$, we would have the analytic solution we desire. However, these equations do not appear to be solvable by any known means.

In practice, the integral equation resulting from **Eqs. 1.3.5** and **1.3.6** are solved numerically and the pressures are inverted to real space using the Stehfest algorithm. Although this is a numerical scheme, the resulting pressures seem to be very accurate. The main problem with the method is that it is time consuming and the lack of closed form representation hides the actual nature of the solution.

In order to see the behavior of the solutions, simpler approximate problems are solved and analyzed. From these, the regimes of fracture linear flow, bilinear flow and pseudolinear flow are determined. The fact that these are essentially linear flow regimes and that they were found. by solving problems where linear flow dominates brings up the question of whether they result from the assumed shape of the fracture. In other words: are these linear flow regimes a result of assuming the fracture to be rectangular? This is something we hope to check by solving the problem with an elliptical fracture.

Flow to an Elliptical Fracture

In order to overcome most of the difficulties discussed in the last section, we will now consider the problem in elliptical coordinates. The first part will show the equations ex-

pressed in elliptical coordinates and discuss the effects of changing the fracture geometry from rectangular to elliptical. The second subsection will discuss the method of solution of the equations in the new set of coordinates.

Equations for the Elliptical Fracture The transformation to elliptical coordinates is achieved by making the change of variables

$$x_D = \cos(\eta)\cosh(\xi) \tag{1.3.7}$$

$$y_D = \sin(\eta)\sinh(\xi) \tag{1.3.8}$$

The elliptical coordinate system is shown in Fig. 1.3.2. In these coordinates ξ is essentially the radial coordinate, while η plays the role of the angular coordinate. In these coordinates the diffusivity equation, Eq. 1.3.1, becomes

$$\frac{\partial^2 \overline{p}_r}{\partial \xi^2} + \frac{\partial^2 \overline{p}_r}{\partial \eta^2} = \frac{s}{2}(\cosh(2\xi) - \cos(2\eta))\overline{p}_r. \tag{1.3.9}$$

Equations 1.3.1 and 1.3.9 represent the same thing, two dimensional flow in a homogeneous reservoir -- only the form is different. The boundary conditions for the reservoir are also unchanged. We require that the pressure approach zero as ξ approaches infinity and that $\overline{p}_r$ equal $\overline{p}_f$ at $\xi = 0$. The main advantage of using elliptical coordinates is that the fracture is now located at $\xi = 0$, i.e., its position is given by only one coordinate.

The equation for flow in the fracture is found by initially considering two dimensional flow within a thin ellipse, specified by ξ_0, say. Matching conditions, i.e., equations for pressures and fluxes, are imposed on the interface separating the inner ellipse from the reservoir. Taking the limit as ξ_0 approaches zero and assuming the fracture permeability approaches infinity such that the product, $\xi_0 k_f$, is fixed, gives

$$\frac{\partial^2 \overline{p}_f}{\partial \eta^2} = -\frac{2}{F_E}\frac{\partial \overline{p}_r}{\partial \xi}_{\xi=0}. \tag{1.3.10}$$

Here we have introduced the parameter, F_E. It is defined by the ratio, $2k_f\xi_0/k_r$.

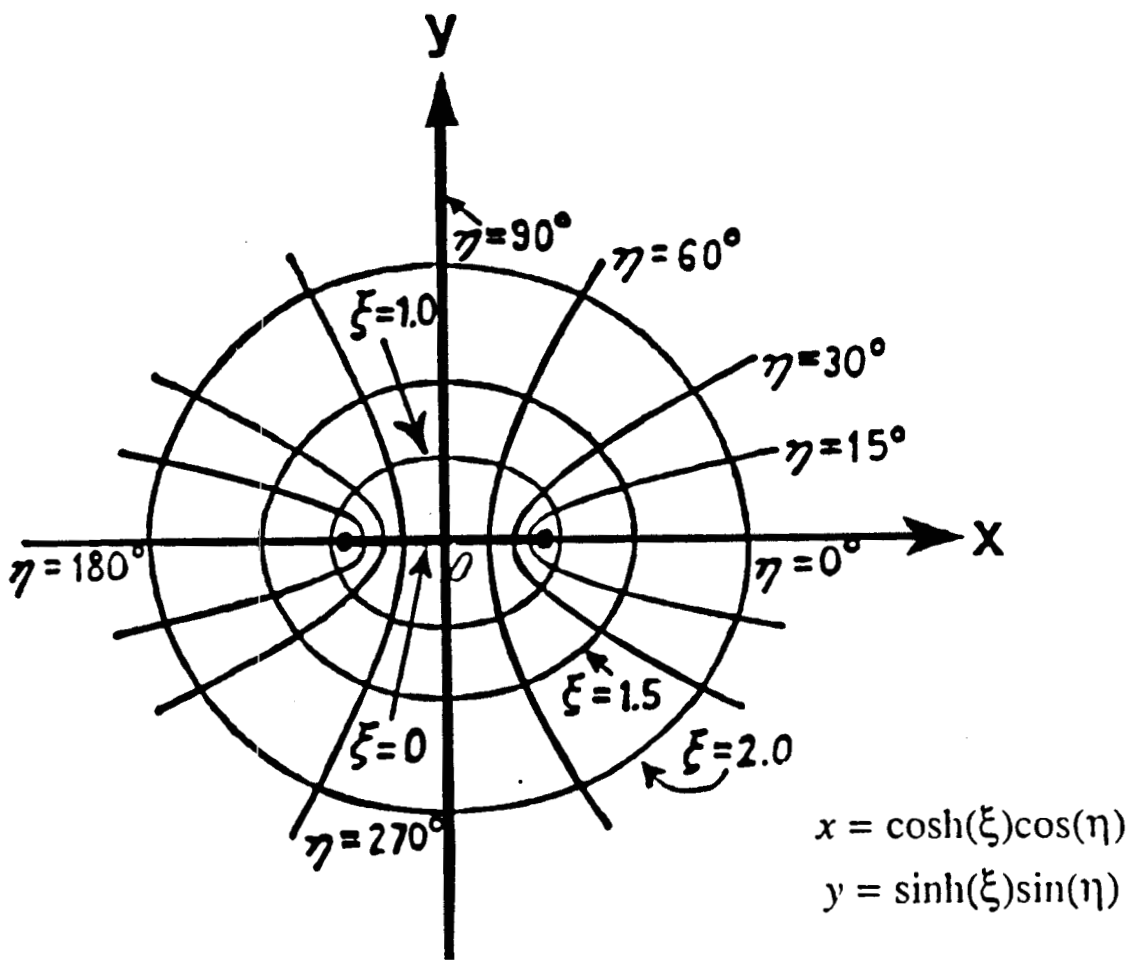

Figure 1.3.2: Elliptical Coordinate System

It is important, at this point, to consider how Eq. **1.3.10** compares with **Eq. 1.3.2.** Since a rectangle and an ellipse both degenerate to a line segment, as their width approaches zero, it seems reasonable that their respective governing equations should be the same. This is wrong. The reason it is wrong, is that they approach this limit in different ways.

As an illustration, Eq. **1.3.10,** expressed in Cartesian coordinates, becomes

$$(1-x_D^2)\frac{\partial^2 \overline{p}_f}{\partial x_D^2} - x\frac{\partial \overline{p}_f}{\partial x_D} = -\sqrt{1-x_D^2}\,\frac{2}{F_E}\frac{\partial \overline{p}_r}{\partial y_D}_{y_D=0}. \qquad \textbf{(1.3.11)}$$

This is clearly different from Eq. **1.3.2.** Near the origin, however, the difference is minor. Therefore, for cases of low conductivity, where flux is concentrated around $x_D = 0$, the rectangular and elliptical fractures should behave the same way, with F_D roughly equivalent to F_E. In the cases of moderate to high conductivity, however, the behavior may be much different. This is something we hope to check.

The boundary conditions associated with Eq. **1.3.10** are analogous to those associated with the Eq. **1.3.2.** The inner boundary condition is

$$\frac{\partial \overline{p}_f}{\partial \eta}_{\eta=\frac{\pi}{2}-} = -\frac{\pi}{F_E} \qquad \textbf{(1.3.12)}$$

and the outer boundary condition is

$$\frac{\partial \overline{p}_f}{\partial \eta}_{\eta=0} = 0. \qquad \textbf{(1.3.13)}$$

Solution Scheme for an Elliptical Fracture

Separation of variables is used to solve the above equations. The partial differential equation, Eq. **1.3.9,** is assumed to have product solutions of the form, $N(\eta)E(\xi)$. Inputting this assumed solution into the reservoir equation, and 'separating', results in a pair of ordinary differential equations; one for $N(\eta)$ and one for $E(\xi)$. The general solutions of these separated equations are found and the unsuitable solutions are discarded based on how well they match the boundary conditions. The result is that only one suitable set of product solutions remain, the eigensolutions. These eigensolutions are products of Mathieu functions and are functions of ξ, η, s and their index n. These eigensolutions are then multiplied by constants, β_{2n} say, that are functions of s and summed over their index, n.

The pressure in the reservoir, $\overline{p}_r$, is found by determining the values of these constants. They are determined by coupling the reservoir solution to the fracture solution.

The solution to the fracture problem, Eq. **1.3.10,** is approached in a similar way. Eigen-solutions are sought that satisfy the homogeneous fracture problem, i.e. the right hand side of Eq. **1.3.10** and the boundary conditions, Eqs. **1.3.12** and **1.3.13,** all equal to zero. At this point the cosine eigenfunctions are multiplied by constants, δ_{2n}, and summed over positive ***n.*** Then, the series described in the last paragraph is inserted into the right hand side of Eq. 1.3.10 and treated as a known function, i.e., as an inhomogeneity. Some fairly delicate manipulation now has to be done to allow the cosine series to satisfy the inner boundary condition. The end result of all of these manipulations is a series for the reservoir pressure in terms of β_{2n} and Mathieu functions, a series for the fracture pressure in terms of δ_{2n} and cosines and the fracture equation which contains both sets of functions and constants and couples the two solutions.

The series representing the reservoir solution is

$$\overline{p}_r(\xi,\eta) = \sum_{n=0}^{\infty} \beta_{2n} Fek_{2n}(\xi, -\frac{s}{4}) ce_{2n}(\eta, -\frac{s}{4}), \qquad \textbf{(1.3.14)}$$

where Fek_{2n} and ce_{2n} are Mathieu functions.

The series representing the fracture solution is

$$\overline{p}_f(\xi,\eta) = \sum_{n=0}^{\infty} \delta_{2n} \cos(2n\eta), \qquad \textbf{(1.3.15)}$$

So far none of the constants in the above representations are specified. They are constrained by the fracture equation obtained by inserting the two series into Eq. **1.3.10.** The result is

$$\sum_{n=0}^{\infty} (\frac{(-1)^n}{sF_E} - 4n^2\delta_{2n}) \cos(2n\eta) + \frac{1}{\pi F_E} \sum_{n=0}^{\infty} \beta_{2n} Fek'_{2n}(0, -\frac{s}{4}) ce_{2n}(\eta, -\frac{s}{4}) = 0, \qquad (1.3.16)$$

where $Fek'_{2n}(0, -\frac{s}{4})$ is the derivative of the radial Mathieu function evaluated at ξ equal to zero.

The fracture boundary conditions have been included in Eq. **1.3.16** and **so** it fully constrains the problem. The method of determining the constants is to remove one set of

constants in favor of the other. This is done by setting Eq. **1.3.14** equal to Eq. **1.3.15** and using the orthogonality of the eigenfunctions to determine a particular β **as** an infinite sum over the $\delta's$, or vice versa. The result is substituted into Eq. **1.3.16** and orthogonality of one of the eigenfunctions is used to remove one of the series.

The last few steps can be performed in a number of different ways, each resulting in a different, yet equivalent, form. Unfortunately, it does not appear that any of the formulations will allow the constants to be determined explicitly. They are determined by solving an infinite matrix equation. This is the reason for the quotation marks when refering to the solution as 'analytic'. **A** truly analytic solution would allow the calculation of the coefficients explicitly or at least in a theoretically finite number of operations.

Of course the infinite matrix equations are not solved explicitly. The matrix is truncated at some point where the coefficients asymptote to a known limiting form. The resulting coefficients are input into either Eq. **1.3.14** or Eq. **1.3.15** and the final solution is calculated by summing the series.

This concludes the theoretical consideration of the problem. Thus far in the course of this research, no attempt has been made to evaluate the matrix solutions. This is the next step. It is not known which matrix formulation will prove to be the most advantageous. Almost certainly, one formulation will work better for long times and another for short times. There is some concern, however, that no formulation will prove adequate for very early times, i.e. the bilinear **flow** period. Whether this will be the case and if we will have to resort to some sort of asymptotic method will only be determined by experience.

Section 1.4 : Pressure Oscillations in a High Rate Well in Fractured Formation

Sanjay Bhatnagar

Overview

Geothermal reservoirs are highly fractured and the effect of high flow rates can be very important in the analysis of buildup tests. The focus of this study is limited to inertial effects on the pressure response of a fractured reservoir. A model is proposed for pressure transient response in high permeability, high rate, naturally fractured reservoir. Theoretical models presently available are inadequate for handling these systems because they do not include the inertial effects of the liquid/gas in the wellbore and the fractures.

Problem Definition

Figure 1.4.1 shows a pressure buildup test performed in an oil well in Mexico. The well was shut in at the wellhead and pressure as well as the flowrate were recorded downhole. An expanded pressure and time scale in Fig. 1.4.2 shows underdamped oscillations with a time period of about 70 seconds. For high production rate in fractured reservoirs, the kinetic energy of the liquid moving in the fractures and the wellbore may be important and contribute to the early time pressure response. The relative importance of inertial effects in the wellbore and in the formation fractures is also investigated.

Saldana and Ramey (1986) considered inertial effects in the wellbore and coupled a momentum balance equation for the wellbore to the diffusivity equation in the reservoir. They presented criteria useful to evaluate the magnitude of inertial and frictional effects. *Hotzhausen* ***and*** *Gooch (1985)* observed a definite change in the period of oscillations before and after hydraulic fracturing. This suggests that the natural fractures and/or the wellbore could explain the Mexican well test data.

Solution Methodology

Two models, are considered to identify the source of oscillations. The first model considers inertia in the wellbore coupled with diffusivity equation in the reservoir while the second model considers inertial effects of the liquid in a single fracture in the reservoir. The fracture is coupled to the wellbore but does not account for inertial effects in the wellbore.

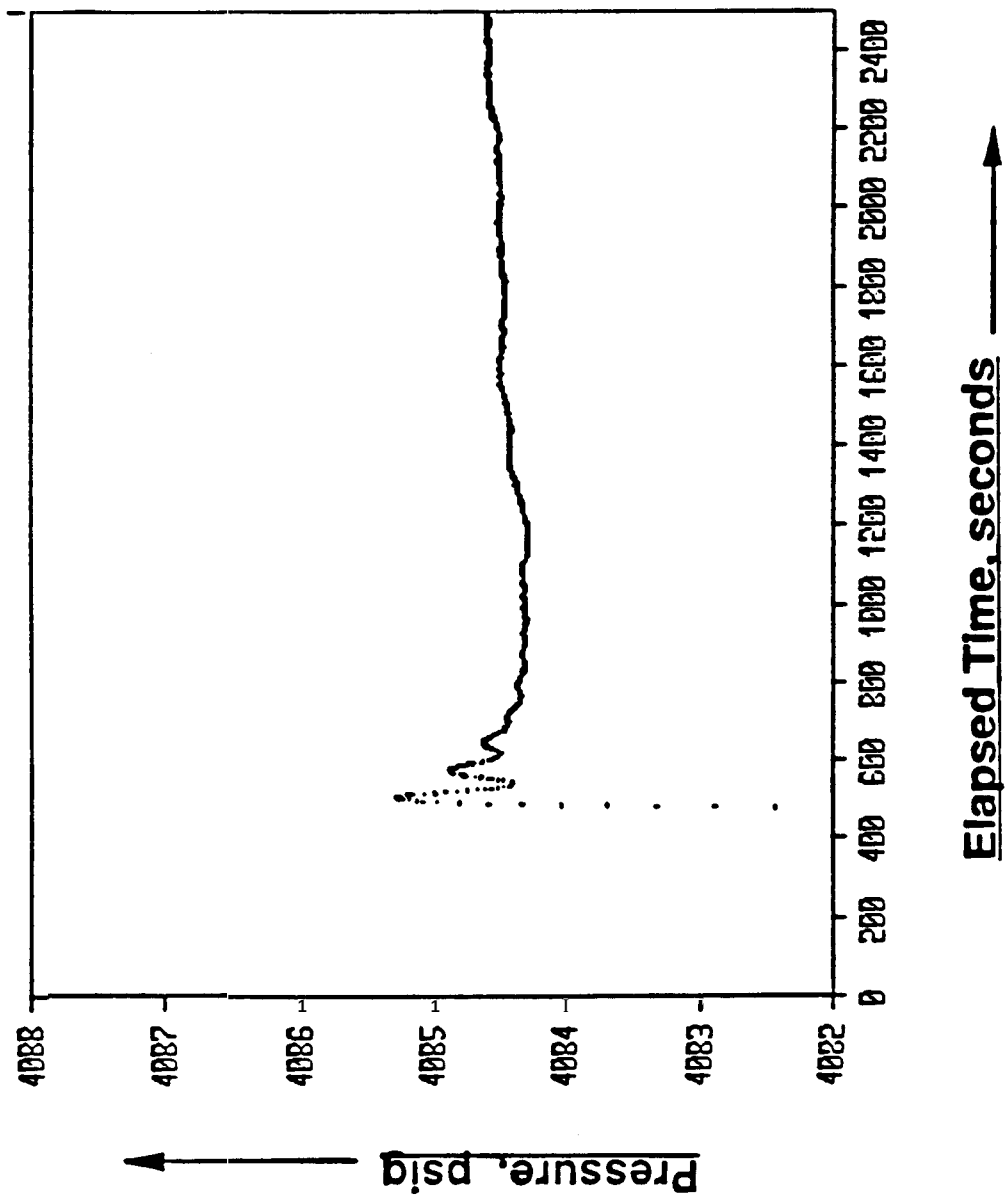

Figure 1.C.1: Mexican Pressure Buildup with an Expanded Pressure Scale

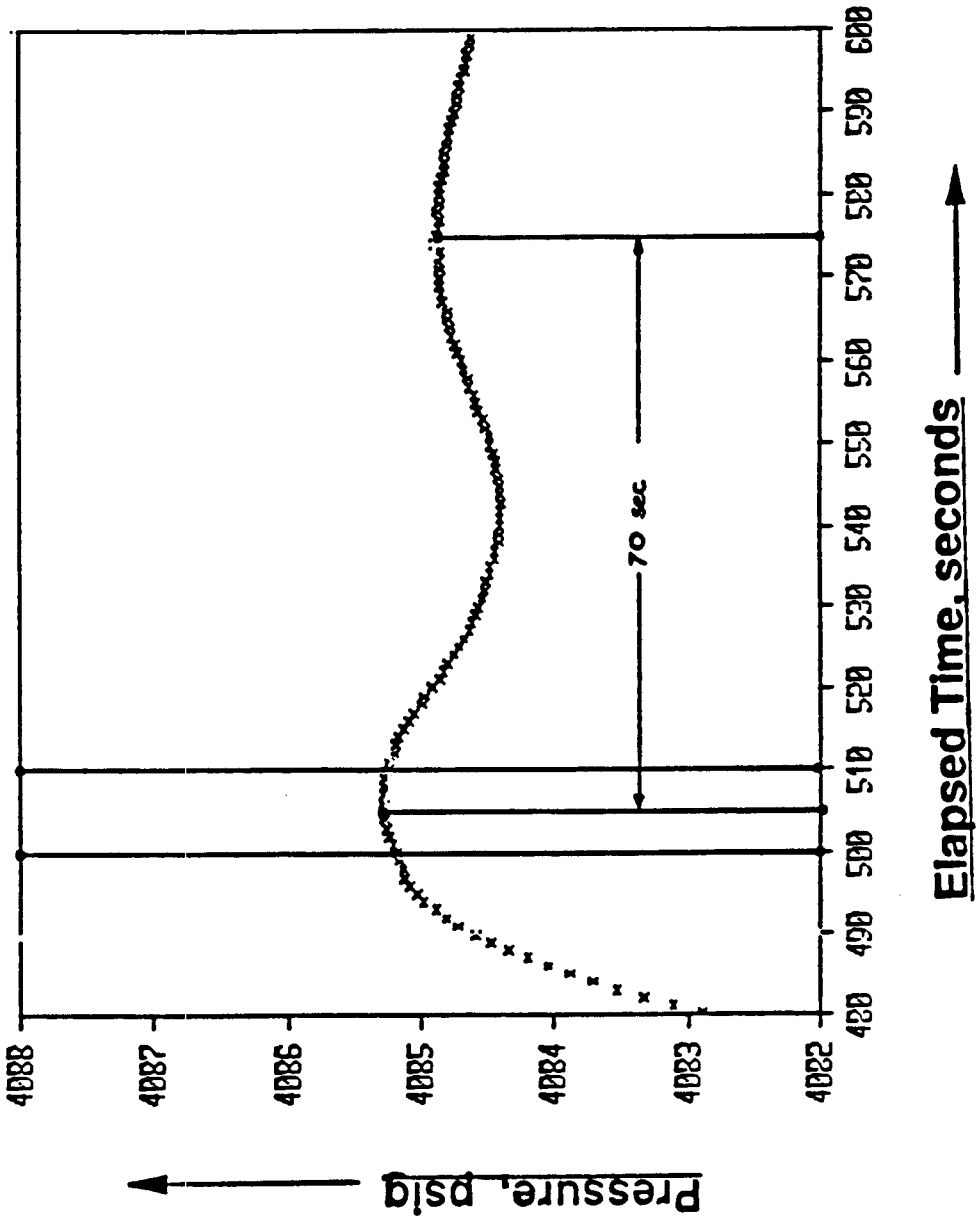

Figure 1.4.2: Pressure Buildup for Mexican Oil Well with Expanded Pressure and Time Scales

For the first model the continuity equation in the z- (vertical) direction is considered for a slightly compressible fluid. A schematic of the idealized model is shown in Fig. 1.4.3. The resulting equation is given by

$$c\frac{\partial p}{\partial t} + \frac{\partial u}{\partial z} = 0 \tag{1.4.1}$$

The equation in the wellbore is the Navier-Stokes equation. Neglecting terms which are small we obtain

$$\rho\frac{\partial u}{\partial t} + \frac{\partial p}{\partial z} = -\rho g \tag{1.4.2}$$

Detailed derivation of *Eq.* (1.4.1) and (1.4.2) is given in *Bhatnagar* (1989). Manipulation of Eqs. (1.4.1) and (1.4.2) gives

$$\frac{\partial^2 p}{\partial t^2} - \frac{1}{\rho c}\frac{\partial^2 u}{\partial z^2} = 0 \tag{1.4.3}$$

Substituting $c_s^2 = \frac{1}{\rho c}$, where c_s^2 is the wave velocity in *Eq.* (1.4.3)

$$\frac{\partial^2 p}{\partial t^2} - c_s^2\frac{\partial^2 u}{\partial z^2} = 0 \tag{1.4.4}$$

The diffusivity equation in the reservoir is given by

$$\frac{\partial^2 p}{\partial r^2} + \frac{1}{r}\frac{\partial p}{\partial r} = \frac{\phi\mu c_t}{k}\frac{\partial p}{\partial t} \tag{1.4.5}$$

The coupling conditions at the sandface are

$$\pi d^2 u|_{z=H} = -\frac{2\pi r_w kh}{\mu}\frac{\partial p}{\partial r}|_{r=r_w} \tag{1.4.6}$$

$$-c_s^2\rho\frac{\partial u}{\partial z}|_{z=H} = \frac{\partial \Delta p}{\partial t}|_{r=r_w} \tag{1.4.7}$$

The boundary and initial conditions are

$$u(z=0) = \frac{q(t)}{\pi d^2} \tag{1.4.8}$$

$$\Delta p \longrightarrow 0 \quad \text{as} \quad r \longrightarrow \infty \tag{1.4.9}$$

Solution of Eqs. (1.4.4) - (1.4.9) in Laplace space is given by

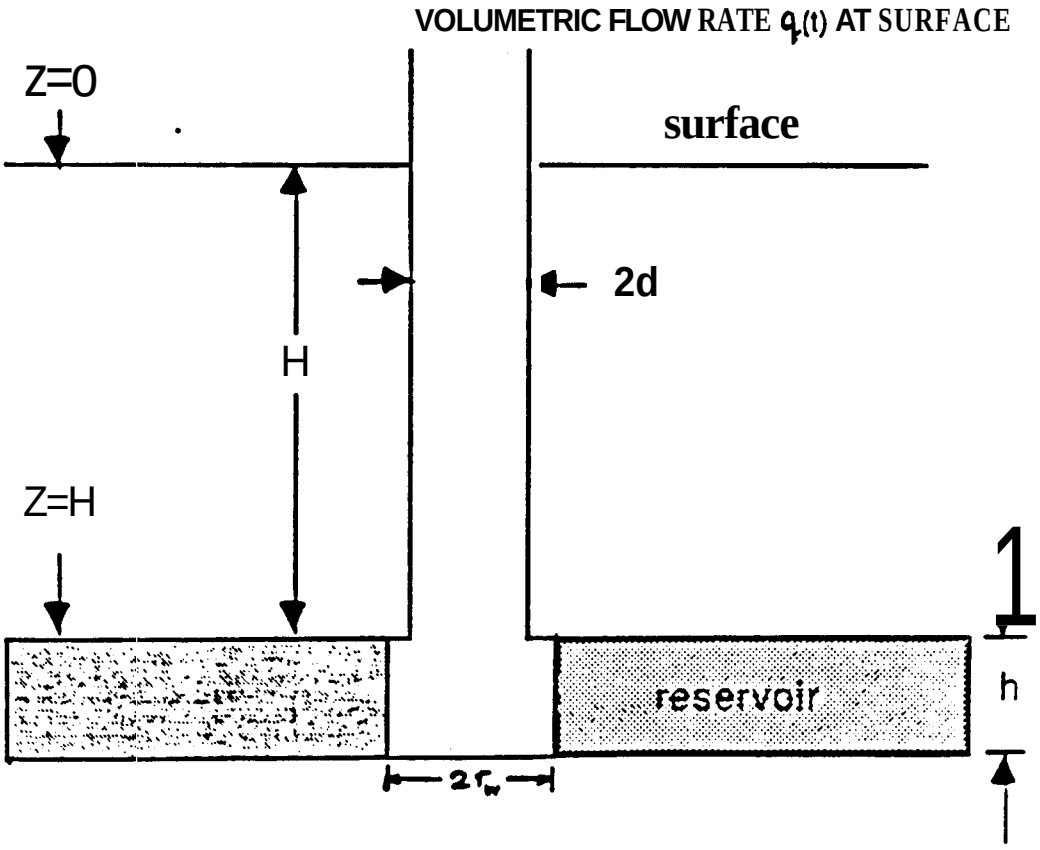

Figure 1.4.3: Schematic diagram of well and reservoir

$$\Delta\bar{p}(r_w,s) = \bar{q}(s)\lambda \frac{\dfrac{K_0(\frac{1}{\sqrt{\eta}})}{\frac{1}{\sqrt{\eta}}K_1(\frac{1}{\sqrt{\eta}})}}{\cosh(\frac{sH}{c_s}) + \dfrac{\pi d^2}{\lambda\rho c_s}\sinh(\frac{sH}{c_s})\dfrac{K_0(\frac{1}{\sqrt{\eta}})}{\frac{1}{\sqrt{\eta}}K_1(\frac{1}{\sqrt{\eta}})}} \tag{1.4.10}$$

where

$$\eta = \frac{k}{\phi\mu c_t r_w^2 s} \tag{1.4.11}$$

$$\lambda = \frac{2\pi kh}{\mu} \tag{1.4.12}$$

The flow rate ha!; to be transformed to Laplace space in the above equations. The inversion of the Laplace space solution is performed with the Crump algorithm which has excellent inversion characteristics for step inputs. This algorithm is computationally more intensive than the Stehfest algorithm. The detailed solution procedure is given in *Bhatnagar* (1989).

Results from this model indicate pressure oscillations of time period of one second approximately. This is much shorter than a period of 70 seconds observed in Mexican wells. One way to increase the time period is by the reduction of the wave velocity. This could perhaps happen if waves traveled through thin apertures (fractures) where they slow down by viscous effects. Adjusting for pressure transducer response time in the pressure signal did not match the field results.

Model 2

This model considers linear flow to a well with inertial effects in a single fracture. No inertial effects are considered in the wellbore. It is also assumed that there is instantaneous equalization of pressure between the fracture and the matrix. A schematic of the model is shown in Figure 1.4.4. The governing equations are as follows.

$$\Omega c\frac{\partial p}{\partial t} = -\frac{\partial u}{\partial x} \tag{1.4.13}$$

$$\rho\frac{\partial u}{\partial t} = -\frac{\partial p}{\partial x} + \mu\frac{\partial^2 u}{\partial z^2} \tag{1.4.14}$$

Assuming a parabolic velocity profile in the fracture with unidimensional flow we have

$$u(z) = \frac{6z}{b}\left(1 - \frac{z}{b}\right)u \tag{1.4.15}$$

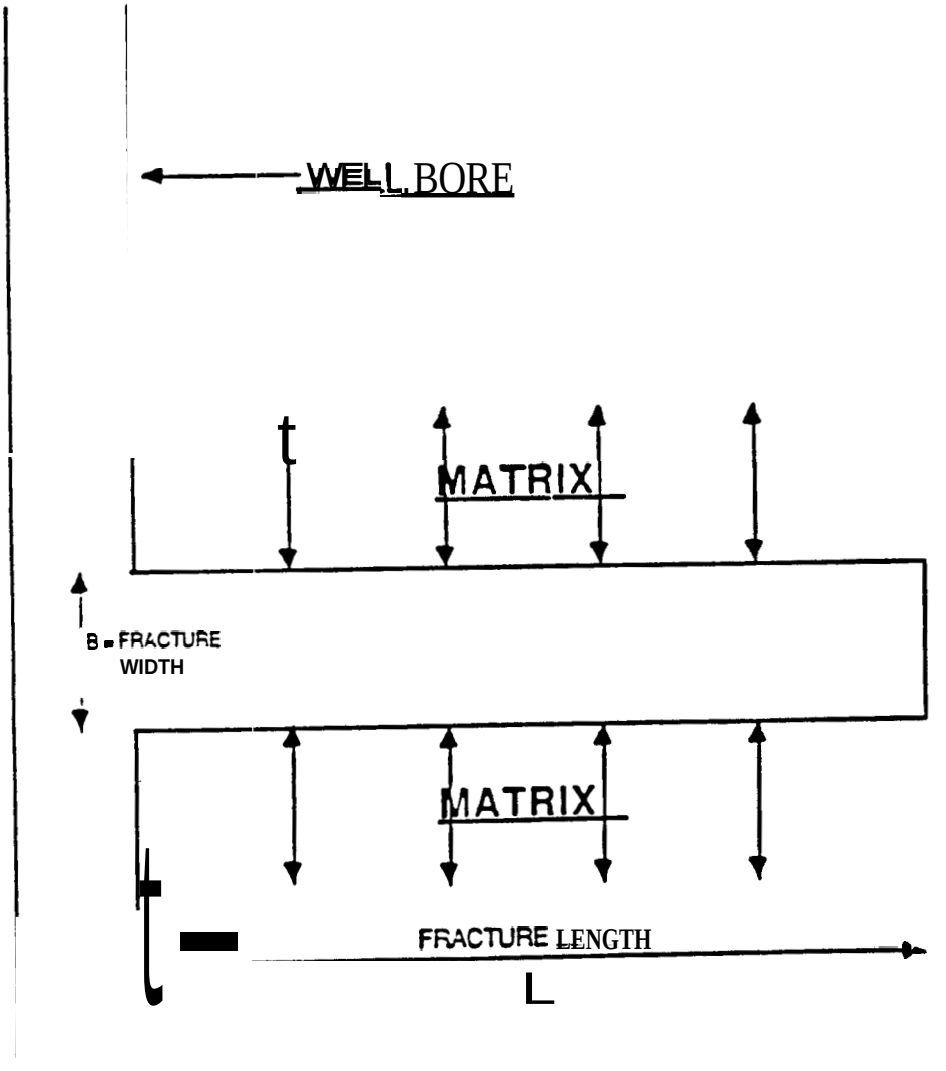

Figure 1.4.4: Schematic of a single fracture in the Linear Flow with Inertia Model

Averaging the equations in the z-direction and substituting Eq. (1.4.15) in Eq. (1.4.14) we obtain

$$\rho\frac{\partial\bar{u}}{\partial t} = -\frac{\partial\bar{p}}{\partial x} - \frac{12\mu}{b^2}\bar{u} \tag{1.4.16}$$

and

$$\Omega c\frac{\partial\bar{p}}{\partial t} = -\frac{\partial\bar{u}}{\partial y} \tag{1.4.17}$$

Manipulating Eqs. (1.4.16) and (1.4.17)

$$\frac{\partial^2\bar{u}_D}{\partial t_D^2} + \beta\frac{\partial\bar{u}_D}{\partial t_D} = \frac{\partial\bar{u}_D}{\partial x_D^2} \tag{1.4.18}$$

where

$$\beta = \frac{12\mu L}{\rho b^2 c_s} \qquad t_D = \frac{c_s}{L}t \qquad x_D = x/L \tag{1.4.19a}$$

$$u_D = \frac{u}{U} \qquad p_D = \frac{b^2\Delta p}{12\mu UL} \tag{1.4.19b}$$

Solution of the above equations with the initial and boundary conditions in Laplace space gives

$$p_D(x_D,s) = -\frac{U(s)\Gamma}{s\beta}\coth(\Gamma) \tag{1.4.20}$$

where

$$\Gamma = s^2 + \beta s \tag{1.4.21}$$

Using data from the Mexican wells gives a time period of approximately 70 seconds. Figure 1.4.5 shows the inverted solution. The oscillations are sharp which may be attributed to the choice of Cartesian formation flow geometry rather than the correct field flow geometry. Accounting for transducer time constant does not change the result because the oscillations are of a low frequency and the time constant for the transducer is an order of magnitude smaller than the period of oscillations.

This result confirms that the main features of the model match the observed pressure response for the field test. It is concluded from this work that inertia in the wellbore cannot explain the long time period of oscillations observed in the Mexican well tests. Inertial effects in a fracture in the formation may explain the period of oscillations in the field data. In view of the highly idealized nature of the fracture considered, it may not be the only explanation.

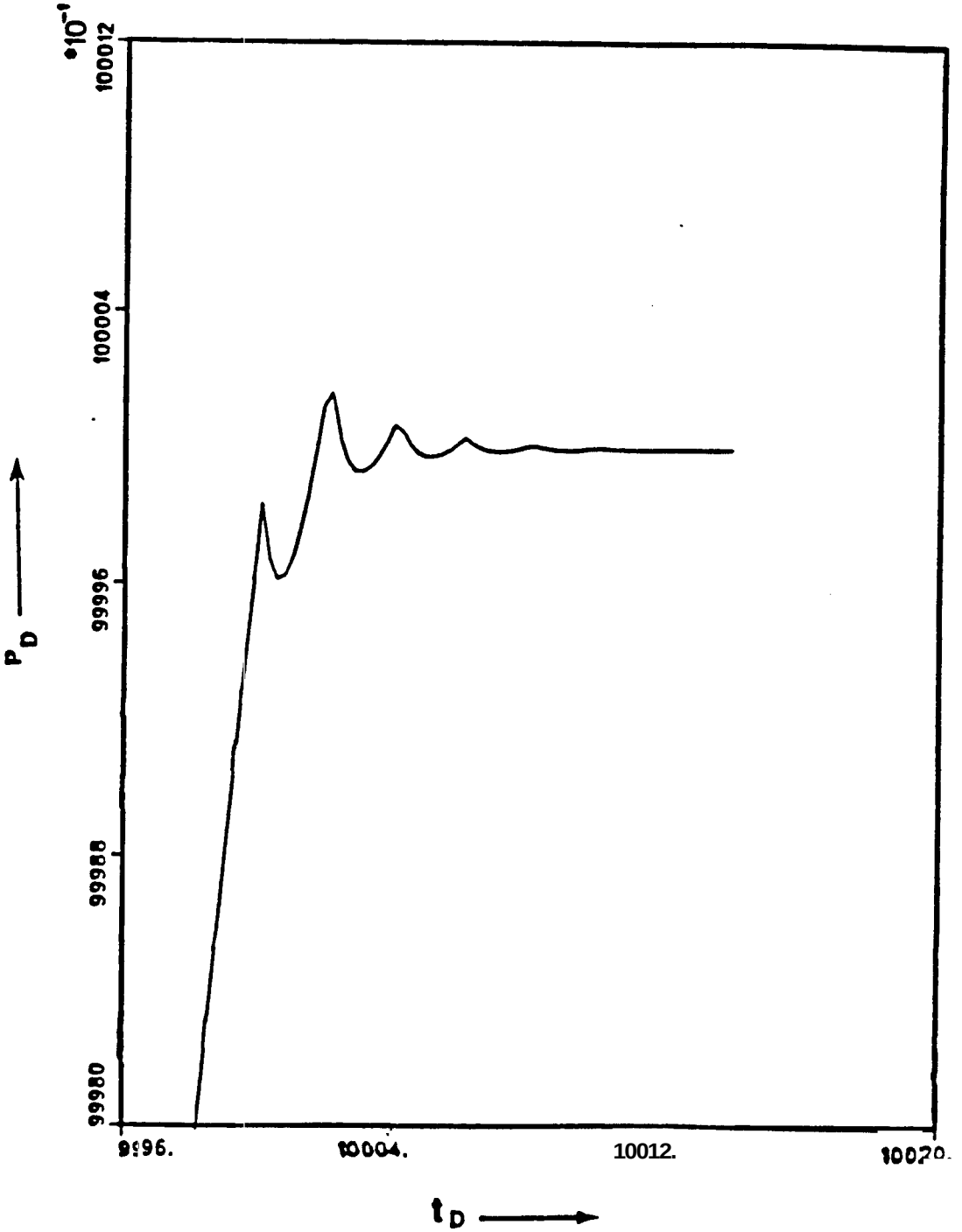

Figure 1.4.5: Dimensionless Pressure vs. Dimensionless Time for beta=1.0 and for a Transducer Time Constant of 0.5 Seconds

Section 1.5 : Well Test Analysis for Gas Wells with Storage, Damage, rnd Turbulence

Francois Groff

Overview

In spite of the numerous studies of transient real gas flow in porous media, the literature still reveals need for modem investigations of well test analysis techniques, especially when wellbore storage and non-Darcy flow are important. Build-up and drawdown tests are mainly performed on geothermal wells to determine:

[1] the flow capacity kh of the formation,

[2] the condition of the wellbore, and

[3] the average reservoir pressure.

This research is only concerned with items [1] and [2], both of which *can* be determined from the early transient period of the build-up or drawdown curves.

The purpose of this work is to enhance and upgrade an existing one-dimensional, single phase, real gas well test simulator. Wellbore storage, skin effect, non Darcy flow and pressure-sensitive formations were included in the formulation for transient gas flow in a one-dimensional radial model by *Fligelman (1981).* The Forcheimer type differential equations and the boundary conditions are approximated by finite difference equations in term of real gas potential. A similar model was developed by *Wattenbarger (1967)* for a study of the application of the real gas pseudo-pressure to short-time gas well testing. However, wellbore storage was not treated accurately.

Fluid flow rates in geothermal wells are generally quite high. Therefore high turbulence effects are very likely to be met close to the well. It should be emphasized that the non-Darcy effect which is investigated in this study is that caused by high velocity flow near the wellbore. Other possible mechanisms can also affect apparent non-Darcy flow. For example phase equilibrium phenomenori may cause a change in relative permeability.

The general idea underlying this project is mainly to provide users a user friendly computer program. Nevertheless, the following points will deserve further investigations as soon as the model is compllleted:

- Evaluation of turbulence effects during injection tests.

- Evaluation of wellbore storage effects under both build-up and drawdown tests.
- Further verifications of correlations developed by Jenkins and *Aronofsky (1954)* for ideal gas flow in a one dimensional radial reservoir.

The project is still undergoing development in the following areas :

- Testing the usability of the program for the following five configurations of well tests: (I) draw-down, (2) build-up, (3) interference, (4) injection and (5) multiple rate tests.
- Providing any combination of three different outer boundary conditions (infinite acting, no-flow, constant pressure) and two different inner boundary condition (constant rate, constant pressure) for each type of well test.
- Create access to instant graphic display of usual log-log, semi-log or Cartesian plot analysis of simulated data.

The main problems in implementing these changes are related to obtaining accurate data close to the wellbore. In addition, numerical difficulties and improving user friendliness are important considerations.

SECTION 2 : INJECTION TECHNOLOGY

Section 2.1 : Tracer and Thermal Transients During Reinjection

I. Kocabas **and R. N. Horne**

The purpose of this work is to develop a method for forecasting the thermal breakthrough time during reinjection in geothermal reservoirs. Estimation of the thermal breakthrough time must be based on both tracer and thermal data.

Tracer tests are essential to determine the degree of connectivity between the injection wells and the producing wells. To analyze the tracer return profiles quantitatively, we employed three mathematical models namely, the convection-dispersion(CD) model, matrix diffusion(MD) model, and the Avdonin(AD) model, which were developed to study tracer and heat transport in **a** single vertical fracture.

Mathematical Models

A heterogeneous system is characterized by preferential flow paths due to dead end pores aggregates, fissures fractures, layering (*Bretz and Orr*, 1985), and so on. Tracer transport in a heterogeneous porous system may be modelled in four ways ***(Bear and Berkowitz*, 1987):**

1. the very near field: tracer transport in a single well defined preferential flow path, possibly with transport into the adjacent porous matrix is considered.
2. the near field: tracer transport in a set of well defined preferential flow paths is considered.
3. the far field: tracer transport is modelled by using two superposed continua, a mobile phase composed of a network of preferential flow paths and an immobile phase representing the rest of the system.
4. the very far field: entire medium is treated as a single continuum representing characteristics of both mobile and immobile phases.

Names of these various approaches are related to the scale of heterogeneities with respect to the scale of flow.

Most of the time, groundwater field experiments have been modelled by using the very far

field approach (Pickens **and** ***Grisak,*** 1981). This is appropriate if the scale of heterogeneities is smaller than the scale of flow.

In geothermal reservoirs, extremely fast fluid movements (up **to** 100 m/hr in some instances (*Horne*, 1982a; *Horne*,1982b)) and asymmetric tracer return profiles indicate that flow takes place mainly in fractures between injection well and producing wells. Since the scale of fractures is in the order of the scale of flow, the very near field approach is appropriate to model the tracer transport.

There are three commonly used mathematical models to represent tracer transport through fractures. The first of these models, the convection-dispersion(CD) model, assumes a purely dispersive flow in the fracture. The form of the dispersion parameter depends on how the fracture is modelled.

The governing differential equation of the convection-dispersion model is given by

$$\frac{\partial C}{\partial t} + u\frac{\partial C}{\partial x} - D\frac{\partial^2 C}{\partial x^2} = 0 \qquad (2.1.1)$$

The variables, used in Eq. 2.1.1 and in **all** other equations in this report are defined in the nomenclature.

The second model is called the matrix diffusion(MD) model. It represents a system consisting of a fracture in which the tracer fluid is mobile located in a porous matrix in which the reservoir fluid is virtually immobile. The model considers the diffusion of the tracer from the fracture into the adjacent porous matrix **as** the main mechanism spreading the tracer along the transport region. It neglects longitudinal dispersion and assumes that tracer concentrations across the fracture are equalized before **any** significant effect of the convection appears.

Two coupled one-dimensional equations are used to represent tracer transport. The equations are coupled by using the continuity of the flux and concentration across the fracture-matrix interface. The equation of tracer transport in the fracture (*Neretnieks*, 1980) is

$$\frac{\partial C}{\partial t} + u\frac{\partial C}{\partial x} + q = 0 \qquad (2.1.2)$$

and the equation of transport in the matrix is

$$D_a \frac{\partial^2 C_m}{\partial y^2} = \frac{\partial C_m}{at} \tag{2.1.3}$$

The concentrations at the fracture-matrix interface are equated as

$$C = C_m \quad at \quad y = 0 \tag{2.1.4}$$

and the continuity of the flux at the interface gives q in Eq. **2.1.2** as

$$q = -\frac{2\phi D_a}{b} \frac{\partial C_m}{\partial y}\bigg|_{y=0} \tag{2.1.5}$$

Matrix diffusion model is equivalent to the ***Lauwerier*** **(1955)** model for heat transport.

The third model, called the Avdonin(AD) model, takes into account both longitudinal dispersion and diffusion into the matrix. It was developed by ***Avdonin*** **(1964)** to study the temperature distribution in an oil layer during the injection of a hot incompressible fluid. Since then the model has been widely used to study the transport of tracers. Similar to the matrix diffusion model, tracer transport in the system **is** represented by two coupled one-dimensional equations. The fracture transport equation is given by

$$\frac{\partial C}{at} + u\frac{\partial C}{\partial x} - D\frac{\partial^2 C}{\partial x^2} + q = 0 \tag{2.1.6}$$

Eq. **2.1.3,** Eq. **2.1.4** and Eq. **2.1.5** give the matrix transport equation and the equations describing the continuity of the concentration and the flux at the fracture-matrix interface.

The solutions to these models are used to analyze three types of tracer tests namely, interwell tracer tests without recirculation, interwell tracer tests with recirculation, and injection-backflow tracer tests as well as thermal injection-backflow tests.

Interwell Tracer Tests without Recirculation

A fairly complete discussion of the analysis of interwell tracer tests without recirculation can be found in the previous annual report of Stanford Geothermal Program. Also, for a detailed discussion of the results of the field experiments, refer to the dissertation by *Kocabas,* (1989).

Interwell Tracer Tests with Recirculation

The purpose of the interwell tests with recirculation is to estimate the total reservoir volume accessible to the tracer as well as the parameters affecting the tracer transport. The total reservoir volume accessible to the tracer consists of the recirculating fluid volume, which corresponds to the fracture volume, and the stationary fluid volume, which corresponds to the matrix pore volume. In general, while the recirculating fluid volume affects the breakthrough tiime, the stationary fluid volume determines the final level of concentration reached after adequate recirculations.

In the study of return profiles, it is convenient to normalize the concentration by a reference concentration, C_r, the final concentration that would be reached if all the tracer were to mixed only in the recirculating volume. The normalized concentration functions are given in Table 2.1.1. The generated return profiles indicate (see Figs. 2.1.1 to 2.1.5) as many local minima and maxima as the number of recirculations. If we try to determine the times of the local minima and maxima by equating the time derivative to zero, only the first peak time occurs in a linear equation. However, the equation of the time of the first peak allows us to make close initial estimates of the parameters.

The return profiles generated by the CD model in Fig. 2.1.1 display almost periodic patterns, and the amplitude of the peaks decreases with increasing time. The second peak occurs almost exactly at a time equal to twice the time of the first peak. *Also* the first local minimum occurs virtually at the midpoint of the first and second peaks. These features can be used to identify the number of recirculations in an experiment and to determine if a recirculation is completed or not. Therefore in cases where there is not enough data, we can look for distinguishing features such as the slope after the first peak. It should be negative until the time is close to $1.5t_p$, and then positive until the time is close to $2t_p$.

The MD model return profiles shown in Figs. 2.1.2 and 2.1.3 also have almost periodic patterns. On the other hand, their features are different from the features of the CD model profiles. First the peaks occur immediately after t_w, and the section between t_w and t_p are characterized by a steep slope. Second, the influence of time is significant in determining the shape of the return profile. For example, both a system with a small λ and large t_w and a system with a large λ and a small t_w yield similar tracer return profiles. The parameter t_w affects the injection period because the tracer reaches the observation point when $t > t_w$.

Model	IC & BC	Parameters	Solution
CD	$C(x,0) = 0$ $\lim_{x\to\infty} C(x,t) = 0$ $C(0,t) = \frac{m}{Q}\delta(t) + C(L,T)$	$\alpha_1 = \frac{1}{P_e} = \frac{D}{uL}$ $\alpha_2 = \frac{t}{t_w} = \frac{ut}{L}$	$\frac{C}{C_r} = \sum_{n=0}^{\infty} \frac{(n+1)}{2\sqrt{\pi\alpha_1\alpha_2^3}} \exp(-((n+1) - \alpha_2)^2/(4\alpha_2))$
MD	$C(x,o) = C_m(x,y,o) = 0$ $C(0,t) = \frac{m}{Q}\delta(t) + C(L,t)$ $C(x,t) = C_m(x,o,t)$ $\lim_{y\to\infty} C_m(x,y,t) = 0$	$\alpha_1 = \lambda = \frac{\phi\sqrt{D_a}}{b}$ $\alpha_2 = t_w = \frac{L}{u}$	$\frac{C}{C_r} = \alpha_2 \sum_{n=0}^{\infty} H(t-(n+1)\alpha_2) \frac{(n+1)\alpha_1\alpha_2}{\sqrt{\pi(t-(n+1)\alpha_2)^3}}$ $\exp(-((n+1)\alpha_1\alpha_2)^2/(t-(n+1)\alpha_2))$
AD	$C(x,o) = C_m(x,y,o) = 0$ $\lim_{x\to\infty} C(x,t) = 0$ $C(0,t) = \frac{m}{Q}\delta(t) + C(L,t)$ $C(x,t) = C_m(x,o,t)$ $\lim_{y\to\infty} C_m(x,y,t) = 0$	$\alpha_1 = \frac{1}{P_e} = \frac{D}{uL}$ $\alpha_2 = \frac{1}{t_w} = \frac{u}{L}$ $\alpha_3 = \lambda = \frac{\phi\sqrt{D_a}}{b}$	$\frac{\overline{C}}{C_r} = \frac{1}{\alpha_2}\left(\exp(-1/(2\alpha_1))\exp\left(\sqrt{1/(4\alpha_1^2) + (s + 2\alpha_3\sqrt{s})/(\alpha_1\alpha_2)}\right) - 1\right)^{-1}$

Table 2.1.1: Normalized Solutions to Models of Recirculating Flow

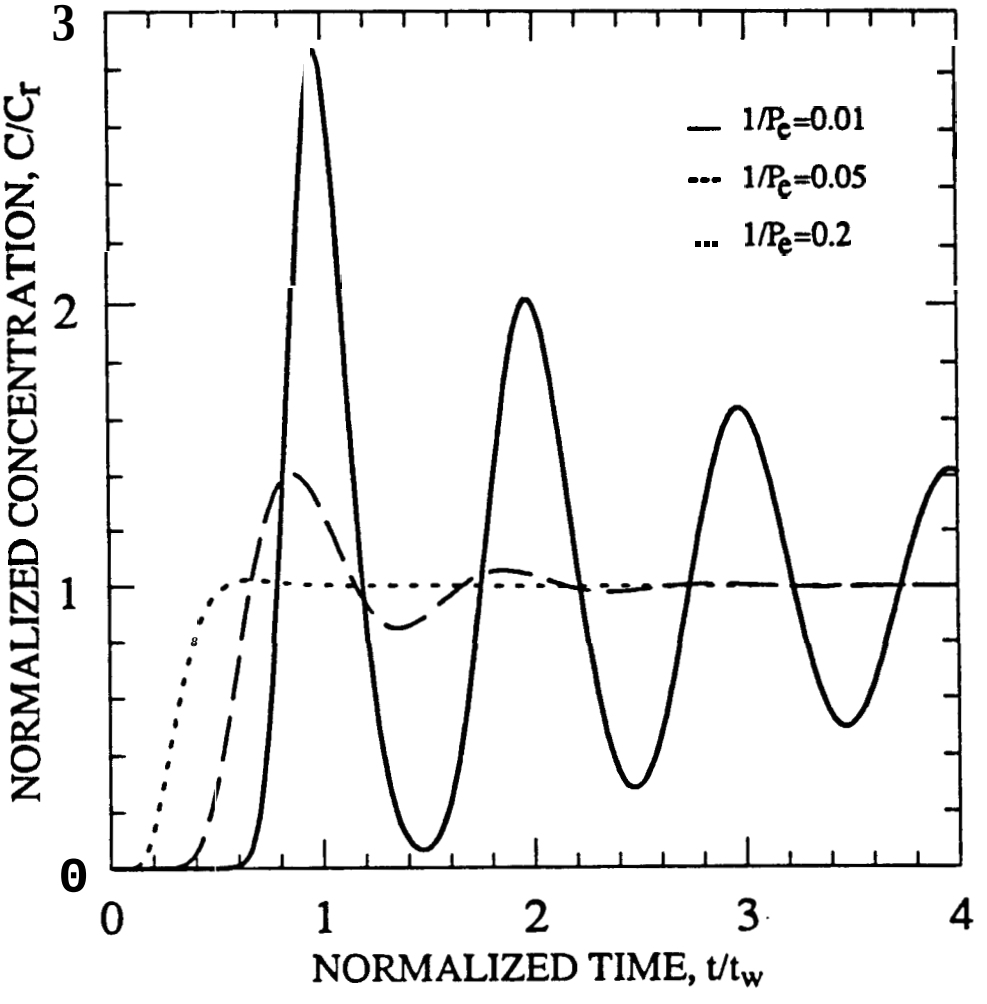

Figure 2.1.1 : Normalized Solutions to CD Model **For** Recirculating **Flow**

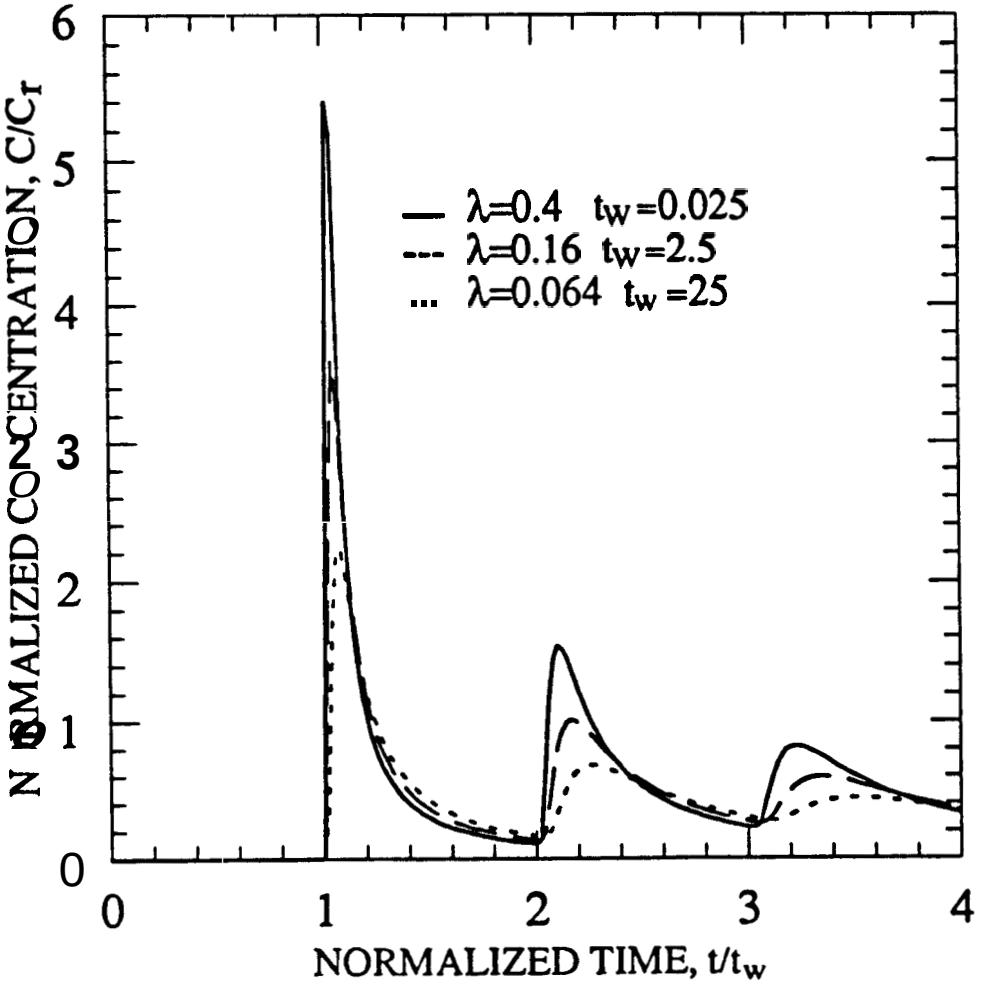

Figure 2.1.2: Normalized Solutions to the MD Model for Small Amount of Diffusion

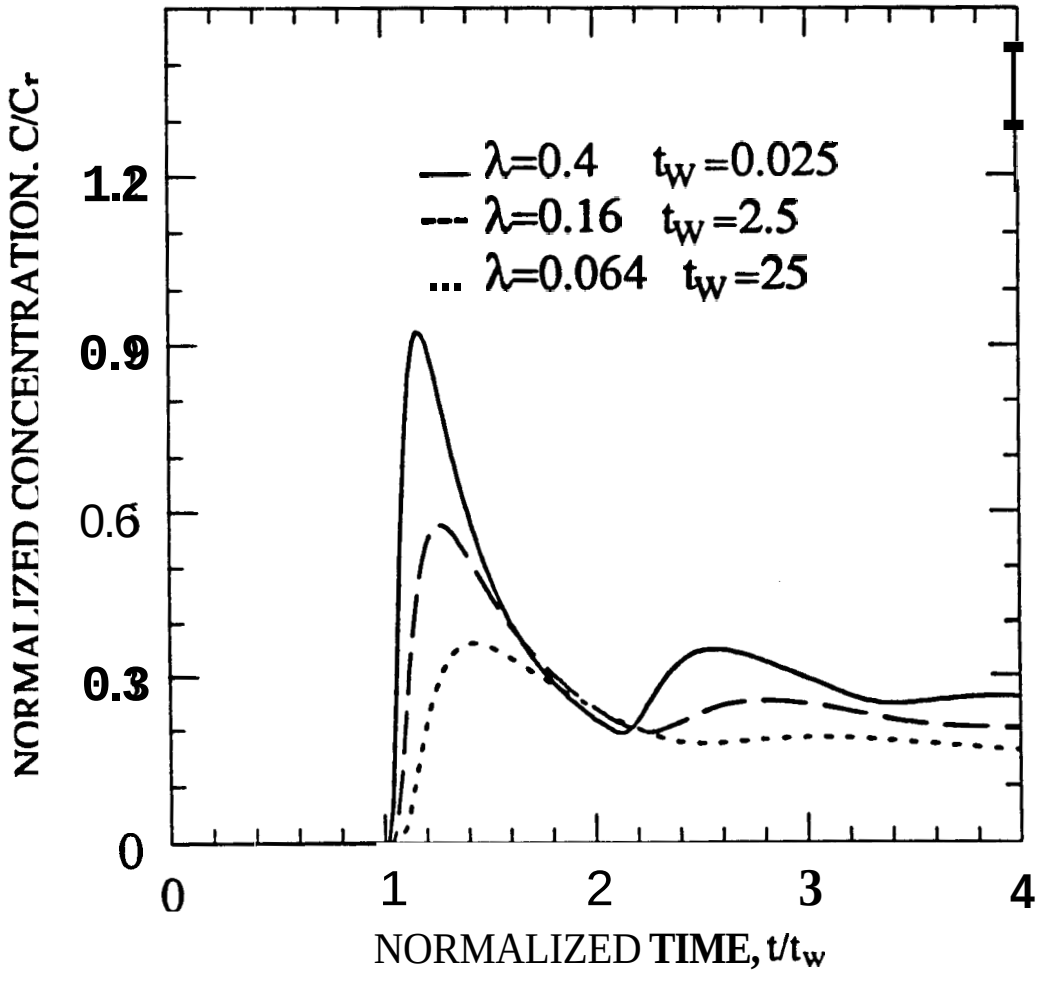

Figure 2.1.3: Normalized Solutions to the MD Model for Large Amount of Diffusion

The generated return profiles of the AD model are shown in Figs. 2.1.4 and 2.1.5. *De Smedt et al.* (1981) pointed out that for a test without recirculation the three parameters, t_w, P_e and λ are not likely to be correlated, since they affect different segments of the profiles. While t_w affects the breakthrough time, P_e affects the slope of the section between t_b and t_t, and λ affects the slope of the tail section. It is also possible to observe these distinct effects of the parameters on the return profiles of tracer tests with recirculation.

Injection-Backflow Tracer Tests

In an injection-backflow tracer test, the traced fluid is injected into the system at a well for a period of time, after which the same well is produced until the tracer is recovered. The flow conditions are assumed to be steady state and the flow due to injection to be dominant compared to the natural formation flow. The return profiles obtained during the backflow period may be analyzed to determine the dispersive flow characteristics of the flow region near the test well. The main purpose of an injection-backflow tracer test in a geothermal field is to identify high conductivity fractures intersecting the injection well. Therefore, we need to study the characteristics of return profiles of an injection-backflow test when flow takes place in a high conductivity single vertical fracture.

Injection Period Solutions Injection period solutions are the same as solutions derived for the analysis of interwell tracer tests without recirculation.

Backflow Period Solutions Since the flow directions in injection and backflow periods are opposite, the sign of the convective transport term in the transport equation of the backflow period is of opposite sign from the convective transport term in the equation of the injection period. For the convection-dispersion model, Eq. 2.1.1 is the injection period transport equation, and the backflow period transport equation is

$$\frac{\partial C}{at} - \upsilon\frac{\partial C}{\partial x} - D\frac{\partial^2 C}{\hat{d}x\hat{2}} = 0 \qquad (2.1.7)$$

The positive sign before the second term in Eq. 2.1.1 becomes negative in Eq. 2.1.7. To obtain the solution for the tracer return profiles during the backflow period, Eq. 2.1.7 must be solved subject to appropriate initial and boundary conditions. The tracer distribution at the end of the injection period is the initial tracer distribution for the backflow period. Therefore, the injection period solutions provide the initial condition of the backflow period solution.

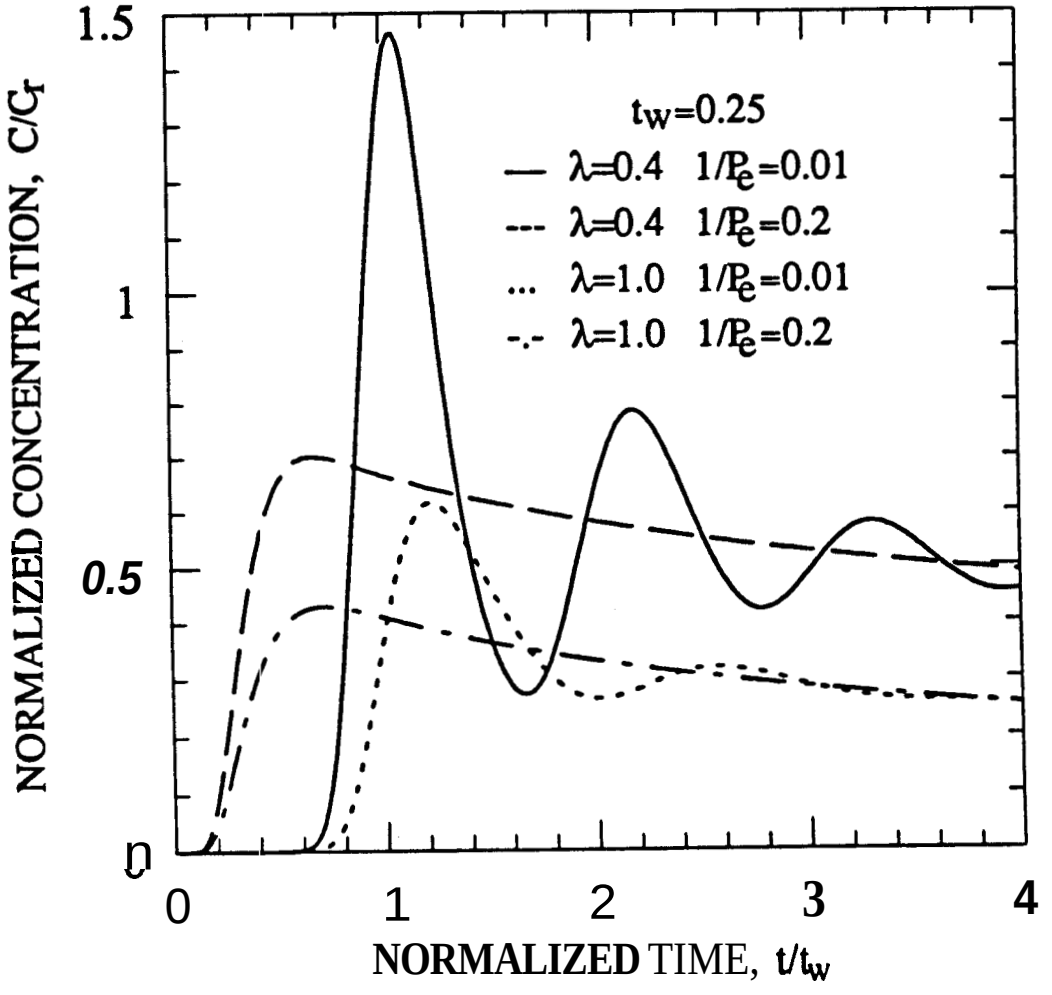

Figure 2.1.4: Normalized Solutions to the AD Model for Short Period Tests

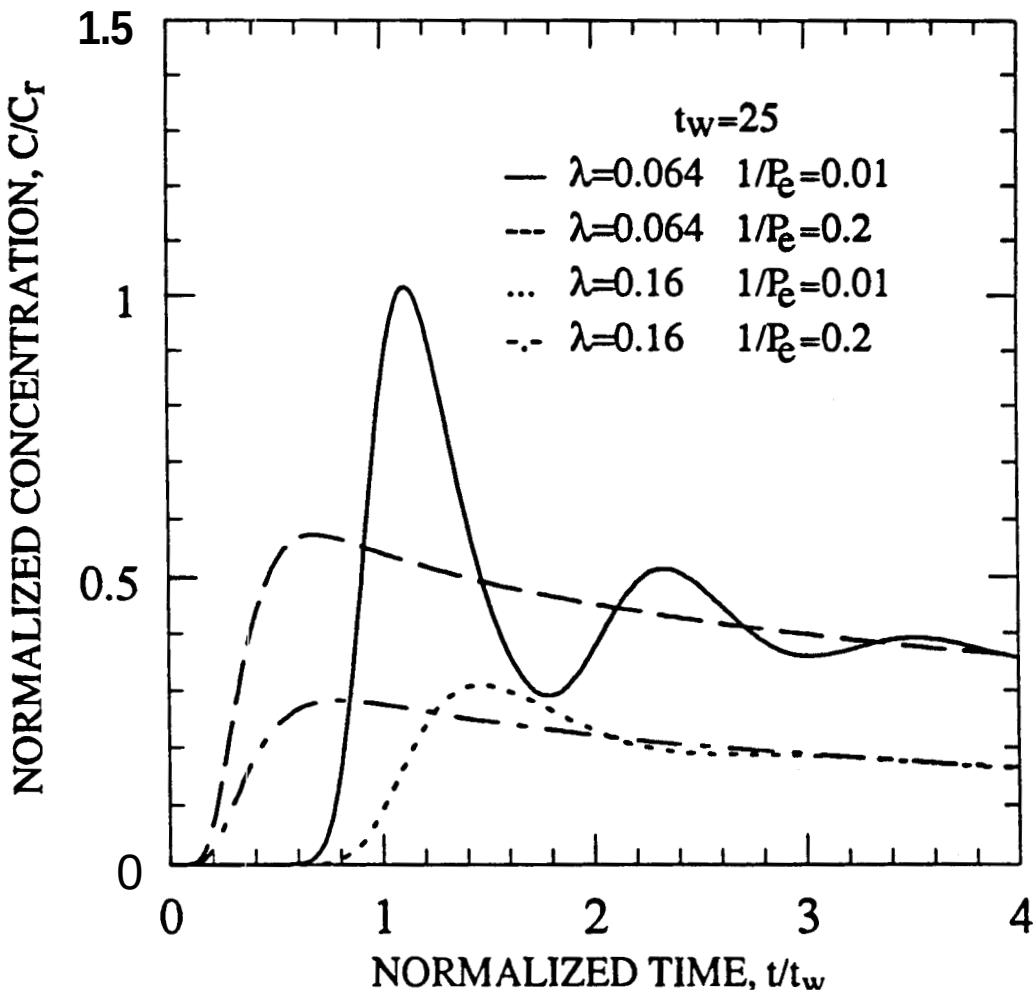

Figure 2.1.5: Normalized Solutions to the AD Model for Long Period Tests

Convection-Dispersion Model

In this study we consider four cases of injection-detection modes, namely C_{CRR}, C_{CRF}, C_{CFR} and C_{CFF}.

The solutions may be expressed in dimensionless variables as shown in Table **2.1.2.** The variable t_D is an inverse Peclet number scaled to the distance (ut_j) travelled by the convective front during the injection period. Other variables are $x_D = x/(ut_j)$ and $t_{Dp} = t/t_j$.

Numerical differences between injection-backflow solutions are similar to numerical differences between the solutions for unidirectional flow. While for small t_D differences between profiles are small (see Fig. 2.1.6), for large values of t_D differences increase (see Fig. **2.1.7).** In Fig. **2.1.6,** the C_{CRR} solution yields the highest concentration values as opposed to C_{CFF} in the case of unidirectional flow. This is because, convective and dispersive fluxes are in opposite directions.

Matrix Diffusion Model

The solutions of transport equations were obtained by using a double Laplace transformation method. The equations were transformed first with respect to the injection period time variable t_j, and then with respect to the backflow period time variable, t. Using the Laplace transformation, the difficulties caused by the effect of the step function, which is in the solutions for the injection period, have been avoided.

The Laplace space solution for equal injection and backflow rates were presented in a previous work (*Kocabas*, **1986;** *Kocabas and Horne*, **1987).** Defining a new variable, λ_D

$$\lambda_D = \lambda\sqrt{t_j} \tag{2.1.8}$$

and normalizing the time variables by t_j, Laplace space solution becomes

$$\overline{\overline{C}} = \frac{1}{s + p + 2\lambda_D(\sqrt{s} + \sqrt{p})}\left[\frac{1}{s} + \frac{2\lambda_D}{s\sqrt{p}} + \frac{2\lambda_D}{s - p}\left(\frac{1}{\sqrt{s}} - \frac{1}{\sqrt{p}}\right)\right] \tag{2.1.9}$$

In Eq. **2.1.9,** s corresponds to the variable $t_j/t_j = 1$ and **p** correspond to the variable t_{Dp}. Using the numerical inversion method, functions of functions, discussed by *Ditkin and*

$$C_{CRR}(x_D, t_{Dp}) = \tfrac{1}{2} erfc\left(\frac{x_D - 1 + t_{Dp}}{2\sqrt{t_D(1+t_{Dp})}}\right)$$

$$C_{CRF}(x_D, t_{Dp}) = \tfrac{1}{2} erfc\left(\frac{x_D - 1 + t_{Dp}}{2\sqrt{t_D(1+t_{Dp})}}\right) - \tfrac{1}{2}\frac{\sqrt{t_D}}{\sqrt{\pi(1+t_{Dp})}} \exp\frac{-(x_D - 1 + t_{Dp})^2}{4t_D(1+t_{Dp})}$$

$$C_{CFR}(x_D, t_{Dp}) = \int_{-\infty}^{\infty} f(x'_D) \frac{1}{2\sqrt{\pi t_D t_{Dp}}} \exp\frac{-(x_D + t_{Dp} - x'_D)^2}{4t_D t_{Dp}} dx'_D$$

$$f(x'_D) = \tfrac{1}{2} erfc\left(\frac{|x'_D| - 1}{2\sqrt{t_D}}\right) - \tfrac{1}{2} \exp\frac{|x'_D|}{t_D} erfc\left(\frac{|x'_D| + 1}{2\sqrt{t_D}}\right)$$

$$\left[1 + \frac{(|x'_D| + 1)}{t_D}\right] + \frac{1}{\sqrt{\pi t_D}} \exp\frac{-(|x'_D| - 1)^2}{(4t_D)}$$

$$C_{CFF}(x_D, t_{Dp}) = \int_{-\infty}^{\infty} f(x'_D) \frac{1}{2\sqrt{\pi t_D t_{Dp}}} \exp\frac{-(x_D + t_{Dp} - x'_D)^2}{4t_D t_{Dp}} dx'_D$$

$$f(x'_D) = \tfrac{1}{2} erfc\left(\frac{x'_D - 1}{2\sqrt{t_D}}\right) - \tfrac{1}{2} \exp\frac{x'_D}{t_D} erfc\left(\frac{x'_D + 1}{2\sqrt{t_D}}\right)$$

$$\left[3 + \frac{2(x'_D + 1)}{t_D}\right] + \frac{2}{\sqrt{\pi t_D}} \exp\frac{-(x'_D - 1)^2}{(4t_D)} \qquad x \geq 0$$

$$f(x'_D) = \tfrac{1}{2} erfc\left(\frac{|x'_D| - 1}{2\sqrt{t_D}}\right) + \tfrac{1}{2} \exp\frac{|x'_D|}{t_D} erfc\left(\frac{|x'_D| + 1}{2\sqrt{t_D}}\right) \qquad x \leq 0$$

Table 2.1.2: Dimensionless Backflow Period Solutions

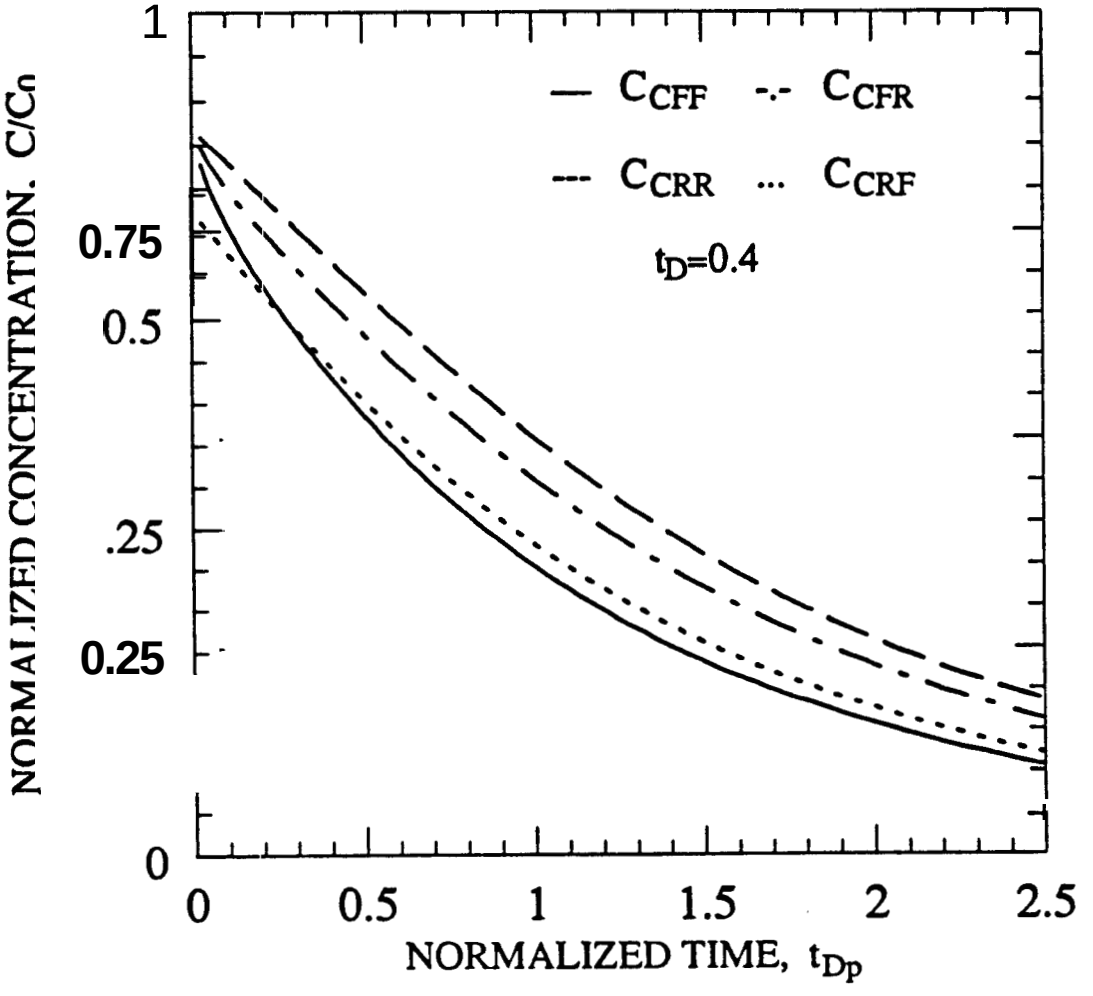

Figure 2.1.6: Solutions for Different Injection and Detection Modes-Medium t_D

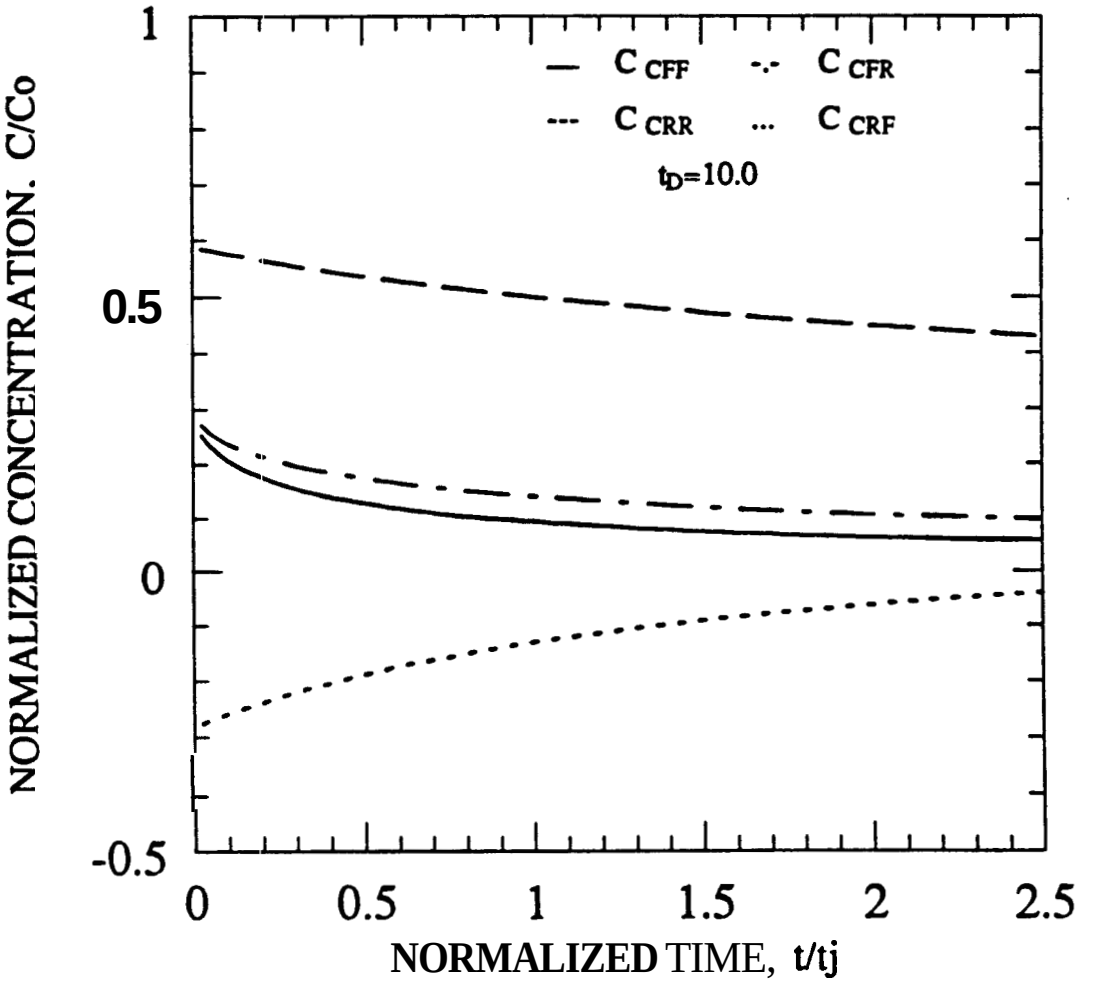

Figure 2.1.7: Solutions for Different Injection and Detection Modes-Large t_D

Prudnikov (1962), and the inversion formula given by *Voelker and* **Doetsch** (1950), the real space function of Eq. **2.1.9** is

$$
\begin{aligned}
C_f = \int_0^{min(1,t_{Dp})} \Bigg\{ & erfc\left(\frac{\lambda_D\theta}{\sqrt{1-\theta}}\right) \frac{\lambda_D\theta}{\sqrt{\pi(1-\theta)^3}} \exp\left(-\frac{\lambda_D^2\theta^2}{t_{Dp}-\theta}\right) + \\
& 2\lambda_D\, erfc\left(\frac{\lambda_D\theta}{\sqrt{1-\theta}}\right) + \frac{1}{\sqrt{\pi(1-\theta)}} \exp\left(-\frac{\lambda_D^2\theta^2}{t_{Dp}-\theta}\right) \Bigg\} d\theta \\
+ 2\lambda_D \int_0^1 d\eta \int_0^{min(1-\eta,t_{Dp}+\eta)} \Bigg\{ & \frac{1}{\sqrt{\pi(1-\eta-\theta)}} \exp\left(-\frac{\lambda_D^2\theta^2}{1-\eta-\theta}\right) \\
& \frac{\lambda_D\theta}{\sqrt{\pi(t_{Dp}+\eta-\theta)^3}} \exp\left(-\frac{\lambda_D^2\theta^2}{t_{Dp}+\eta-\theta}\right) \Bigg\} d\theta \\
- 2\lambda_D \int_0^1 d\eta \int_0^{min(1-\eta,t_{Dp}+\eta)} \Bigg\{ & \frac{\lambda_D\theta}{\sqrt{\pi(1-\eta-\theta)^3}} \exp\left(-\frac{\lambda_D^2\theta^2}{1-\eta-\theta}\right) \\
& \frac{1}{\sqrt{\pi(t_{Dp}+\eta-\theta)}} \exp\left(-\frac{\lambda_D^2\theta^2}{t_{Dp}+\eta-\theta}\right) \Bigg\} d\theta \qquad \textbf{(2.1.10)}
\end{aligned}
$$

Eq. **2.1.10** was evaluated numerically for several values of λ_D, and Eq. **2.1.9** was inverted numerically by using a double numerical inversion technique based on the **Stehfest** (1970) algorithm.

Figs. 2.1.8 to **2.1.10** show the results of numerical integration of the solution **as** well as the numerically inverted Laplace space solution. From these figures, the profiles computed by both methods preserve a material balance. The material balance can be checked by drawing a vertical line at $t_{Dp} = 1$, and determining whether the areas above the curve before the line and under the curve after the line are equal **or** not. For small values of λ_D, the curves for the two methods differ considerably. For large values of λ_D, the profiles become smooth, and both methods produce the same result.

Thermal Injection-Backflow Tests

A thermal injection-backflow test may be the best way to estimate the thermal characteristics of a system to avoid high cost or extremely long test period of thermal interference tests. The heat and the tracer transport mechanisms in porous media are nearly identical in form. The transport of both heat and tracer may be modelled by the same differential

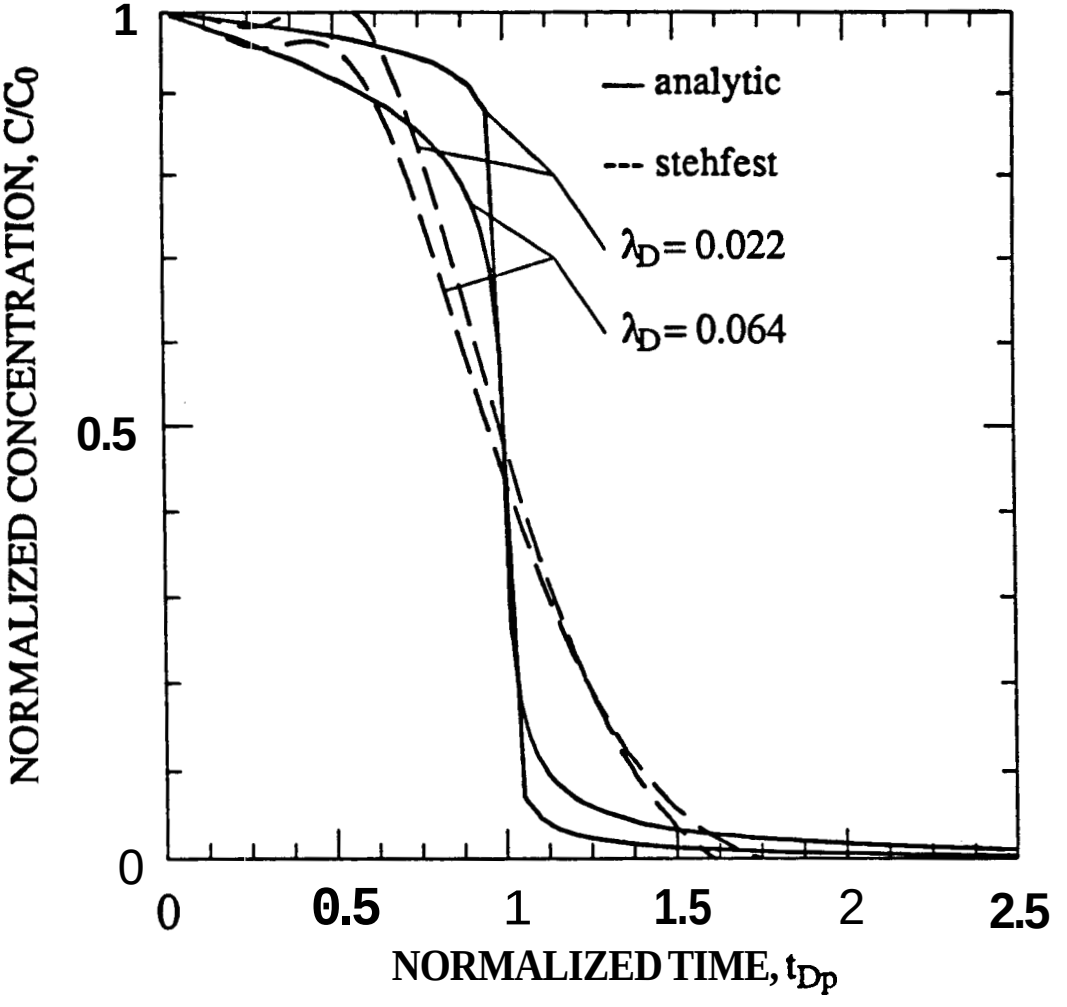

Figure 2.1.8: Solutions to MD Model for Small λ_D

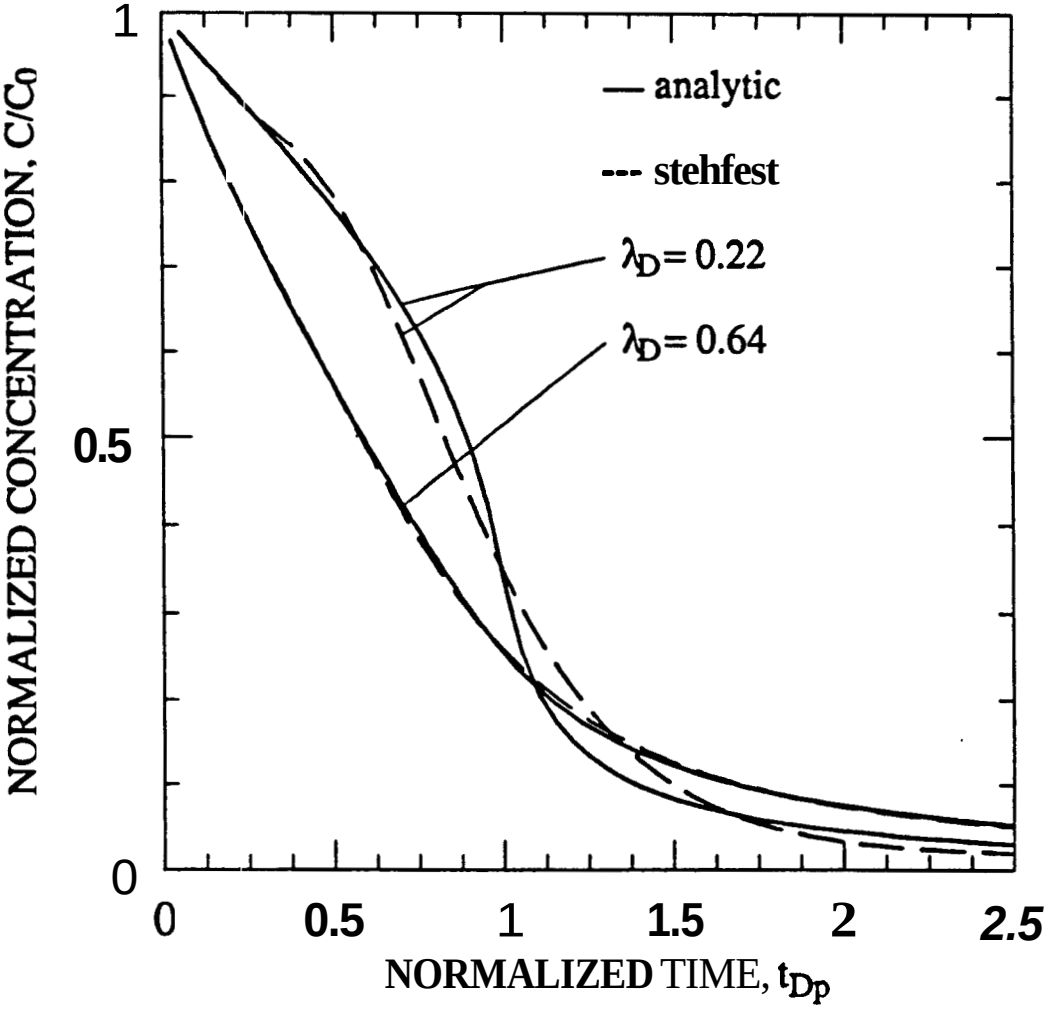

Figure 2.1.9: Solutions to MD Model for Medium λ_D

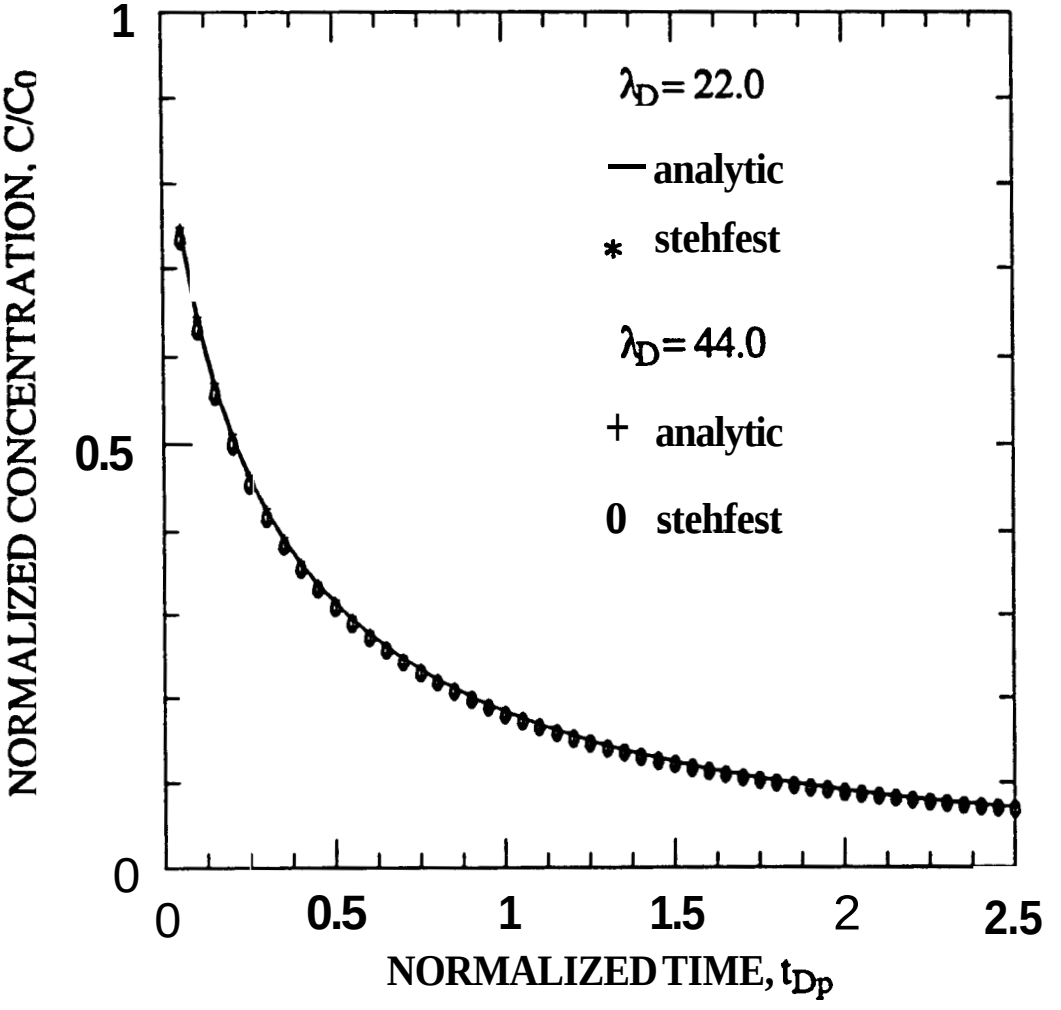

Figure 2.. 1.10: Solutions to MD Model for Large λ_D

equations. Therefore, the solution to the MD model, which was developed for the analysis of injection-backflow tracer tests is used to interpret temperature return profiles from thermal injection-backflow tests. In this case, the dependent variable of the system is temperature, and the parameter of the model, λ_D, for flow in a porous stream tube, is

$$\lambda_D = \frac{\sqrt{k_m \rho_m c_m}}{\phi_f b \rho_w c_w} \sqrt{t_j} \qquad (2.1.11)$$

In heat transport problems, a dimensionless temperature variable is

$$T_D = \frac{T - T_o}{T_{in} - T_o} \qquad (2.1.12)$$

The thermal breakthrough time, if equal the breakthrough time of $T_D = 0.75$, is *(Pruess and Bodvarsson, 1984)*

$$t_t = \frac{\rho_1 c_1}{\rho_w c_w} \frac{t_w}{\phi_f} + \frac{\lambda_D^2}{t_j} \frac{t_w^2}{0.8134^2} \qquad (2.1.13)$$

The contribution of the first group of terms in **Eq. 2.1.13** is small compared to the contribution of the second group of terms, because the lateral heat conduction is the main mechanism retarding propagation of the thermal front. In other words, it is the parameter $\lambda = \lambda_D / \sqrt{(t_j)}$ which determines the thermal breakthrough time.

Using the values given in Table **2.1.3** for the rock and fluid properties *(Reynolds and Perkins, 1977)* and for $t_j = 1\,hr$ and $t_w = 50\ hrs$, corresponding breakthrough times were calculated and are given in Table **2.1.4.**

While the effect of temperature on some of the rock and the fluid properties such as $\rho_w c_w$ and $\rho_r c_r$ are not important, others such as k_w and b, may be affected by temperature. In Table **2.1.3** the properties of water were evaluated at $176°C$, and the reservoir rock was assumed to be granitic. It is reported *(Reynolds and Perkins, 1977)* that k_r of granite may have values ranging from **1.73** to **3.98.** If k, is taken to be **1.73,** then for $\phi_f b = 1\,mm$, the corresponding breakthrough time in Table **2.1.4** would have decreased from **633** to **398** 'years. This demands an accurate determination of the thermal conductivity of the rock. An in-situ determination of thermal conductivity, and other parameters as well, may be achieved by using thermal injection-backflow tests.

ϕ	k_w $W/m°C$	ρ_w kg/m^3	c_w $kJ/kg°C$ $kJ/kg°C$	k_r $W/m°C$	ρ_r kg/m^3	c_r $kJ/kg°C$	hts	t_w hts
0.05	0.677	890	4.371 4.371	2.655	2640	0.82	1	50

Table 2.1.3:Thermal Properties of the System

$\phi_f b\,(mm)$	0.5	1	2	5	10	50
$\lambda_D/\sqrt{t_j}$	76.6	38.3	19.2	7.6	3.8	0.76
$t_t\,(years)$	2531	633	159	25	6	0.25

Table 2.1.4 :Estimated Thermal Breakthrough Times

Eq. 2.1.13 requires two important parameters, namely, water transit time t_w and λ which is a measure of thermal interaction between fracture and matrix. The parameter t_w is estimated from interwell tracer tests and λ is estimated from thermal injection-backflow tests.

Conclusions

Any method of estimating the thermal breakthrough time must be based on both tracer and thermal data. This work involved quantitative interpretation techniques of tracer tests and thermal injection-backflow tests, and development of a new method to estimate thermal breakthrough times.

Depending on the scale of heterogeneities relative to the scale of flow, one of the four approaches namely, the very near field, the near field, the far field and the very far field may be used to model tracer and heat transport through fractures. In geothermal reservoirs, extremely fast fluid movements and asymmetric tracer return profiles of interwell tracer tests indicate that the scale of fractures is in the order of the scale of flow. Therefore, tracer return profiles should be interpreted by using the very near field approach. Based on this approach, quantitative interpretation techniques of interwell tracer tests with and without recirculation, and injection-backflow tests are presented.

Tracer return profiles are matched with the solutions of three mathematical models(CD,MD and AD) developed to study tracer transport through a single vertical fracture. Matching tracer return profiles with solutions of mathematical models provides estimates of three parameters:

- t_w a measure of flow speed,
- D, a measure of dispersive characteristics,
- λ, a measure of fracture-matrix interaction.

Estimating the thermal breakthrough time may be based solely on tracer data. The two parameters D, and λ can be used to estimate the fracture aperture b, the most important parameter controlling the propagation of thermal front. However, estimating b from D requires that $P_e \simeq 500 - 1000$. **For** most of the tracer return profiles $P_e \ll 500$. Estimating b from λ is also questionable, since D_a and **4** are usually unknown.

Alternatively, estimation of the thermal breakthrough time may be based solely on thermal interference tests. Thermal interference tests are infeasible, because durations of

these tests are similar to thermal breakthrough times. Small scale thermal interference tests are **also** unattractive mainly because of high cost.

Finally, a new method of forecasting thermal breakthrough times is developed by using interwell tracer tests and thermal injection-backflow tests. If the **Lauwerier (1955)** model, which is equivalent to the MD model for tracer transport, is used to represent heat transport in the system, the thermal breakthrough time is given by Eq. **2.1.13.** Eq. **2.1.13** requires two important parameters namely, water transit time t_w and λ which is a measure of thermal interaction between fracture and matrix. The parameter t_w is estimated from interwell tracer tests and λ is estimated from thermal injection-backflow tests.

In conclusion, the new method requires the following steps to estimate the thermal breakthrough time during reinjection:

1. estimate the water transit time t_w from interwell tracer tests,
2. estimate the parameter λ_D from thermal injection-backflow tests,
3. substitute values of t_w and λ_D into Eq. **2.1.13** to evaluate the thermal breakthrough time.

This new technique does not have the disadvantages of previously suggested methods namely, ambiguity of estimates from non-thermal methods and high cost and long periods of thermal interference tests.

Section 2.2 : Optimal Selection of Flow Rates at Palinpinon Geothermal Field Based on Tracer Return Dat4

Ma. Elena **G.** Urbino

Overview

The Palinpinon Geothermal Field is one of the two producing rteamfields currently operated by the Philippine National Oil Company (PNOC). The requirements of the commercial plant, known as Palinpinon 1, are met by 21 production wells, 10 reinjection wells and 1 condensate reinjection well. The need for reinjection of liquid waste effluent has been primarily dictated by environmental constraints which prohibit full disposal into the river systems that are used for rice field irrigation. In addition to this, the other benefits of injection, such as maintaining reservoir pressures and increasing thermal recovery from rocks have been recognized.

Although injection wells had been drilled on the periphery of the field, preferably at the identified outflows, initial chemical monitoring of the produced fluids have shown increases in well fluid chloride measurements. These have been interpreted as evidence of the return of reinjected fluids to the production sector. The premature thermal breakthrough of cooler injected fluids at producing wells could cut short the economic life of the field. Hence, guidelines for the safe and efficient management of the Palinpinon reservoir have been established. These include the requirements of 1) minimizing fluid residence times in the surface and downhole piping while operating reinjection wells at or near, maximum capacity, 2) minimizing steam wastages brought about by varying steam demand and supply, and, 3) adopting a production and reinjection well utilization scheme, under any given load demand, such that the rate and magnitude of reinjection fluid returns could be minimized, if not avoided.

The first of these requirements is the answer to the problem of silica deposition which occurs on injection of a fluid that is supersaturated with respect to amorphous silica. The second requirement which is economical in nature, has been satisfied by prioritizing high enthalpy production wells for peak steam requirements and choosing injection wells with additional capacity. The decisions on well utilization (the third requirement) to achieve optimum well configurations have been arrived at, on a relative-basis, by the confluence of production and reinjection fluid chemistry, downhole measurements of pressure and temperature, interference testing, tracer tests, and the interpreted field model. It is to this requirement that the rtudy is directed.

Problem Formulation and Approach

This study aims to provide answers to two questions. First, given an existing configuration of production and reinjection wells, as well as operating requirements in the Palinpinon Geothermal Field, is it possible to choose in a systematic fashion, an optimum number and

configuration of production and reinjection wells such that the likelihood of premature thermal breakthrough is minimized? Second, in the absence of tracer return data, are there other measurable field parameters that can be used to make this optimization possible? In essence, this study is a continuation of the work by James Lovekin (May 1987) on optimization of geothermal injection scheduling.

In his study, the geothermal reservoir is idealized as a network of direct connections or arcs between every pair of wells. Each arc has an associated breakthrough index, b_{ij}, which is the product of injection rate, q_{ri} and an arc cost, c_{ij} which is an expression of thermal breakthrough. The arc cost is composed of weighting factors which have been culled from tracer tests, field geometry, and operational constraints. The sum of b_{ij} -values for all arcs constitute the fieldwide breakthrough index, B. The problem, then, becomes one of minimizing B subject to injection capacities and requirements. With this formulation, algorithms from the field of Operations Research were used to solve the optimization of geothermal injection.

This method and the general approach shall be retained and validated using the Palinpinon 1 tracer return data. Other measurable parameters shall be tested against the results from these wells with tracer return data in the hope of obtaining other weighting factors to be used in the arc cost so that further optimization can be pursued.

Progress and Remaining Work

Prior to defining this problem, a literature search on tracer testing was conducted to narrow down possible topics for study. Methods of solving linear programming problems, particularly the Phase 1 –Phase 2 method were studied since the algorithm from the IMSL routine uses this method to solve optimization of linear programming problems. Sample problems were applied to test these routines. Field data on tracer testing, chemical monitoring, downhole pressure and temperature testing, were gathered.

Presently, other algorithms from Lovekin's work, such as those for solving non-linear problems, are being studied and/or modified to accomodate the appropriate changes envisioned. It is hoped that the new IMSL routine on optimization can be used.

SECTION 3.1: HEAT EXTRACTION PROJECT

Progress Report on Heat Extraction Research

Paul Kruger

Introduction

The primary objective of the SGP Heat Extraction Project is to provide a means for estimating thermal behavior of geothermal fluids reinjected into fractured hydrothermal reservoirs under sustained production. The methods are based on estimated thermal properties of the reservoir components, reservoir management planning of production and reinjection, and the mixing of reservoir fluids: geothermal resource fluid cooled by drawdown and infiltrating ground water, and reinjected recharge heated by sweep flow through the reservoir formation. Several reports and publications, listed in Appendix A, describe the development of the anadytical methods which were part of five Engineer and PhD dissertations, and the results from many applications of the methods to achieve the project objectives.

During FY89, the Heat Extraction Project carried out several thermal cooldown applications in geothermal fields in a number of countries. Heat sweep joint studies are underway for reinjection evaluation at the Los Azufres, Los Humeros, and La Primavera fields in Mexico under the DOE-CFE Geothermal Agreement. The location of these three geothermal fields in relation to Mexico City was shown in the *FY89 Annual Report* (1989). The timing of these studies is especially important because the development at each of these fields is at the stage when decisions must be made on the selection of brine disposal wells at each of the production zones.

Also during the year, initial estimates of thermal effects by heat sweep for the Rosemanoes Hot Dry Rock experiment were made as a joint study with the Camborne School of Mines to match the observed cooldown over the life of the long-term test. Excellent match agreement of the cooldown data is expected to provide values for key reservoir parameters.

A broad cooperative program was initiated with the Leningrad Mining Institute in Leningrad, USSR on the development of hot water supply recirculation systems to be developed in the USSR, the first of which is scheduled for the Zakarpate Oblast in western Ukraine in 1990. During the invited two-month visit to the Leningrad Mining Institute in the spring of 1989, a paper was prepared on the joint efforts on the Zakarpate field and presented *(Dyadkin and Kruger,* 1989) at the Camborne School of Mines International Conference on Hot, Dry Rock Resources, in Cornwall, England, June, 1989. Cooperative efforts were also carried out for the initial tracer test at the Mutnovsky Geothermal Field in Kamchatka, far eastern USSR. During FY89, a joint study on the comparison of thermal decline during the tracer flow test was prepared *(Kiryukhin and Kruger,* 1990) for the Fifteenth SGP Geothermal Workshop in January, 1990.

A main effort of the Heat Extraction Project is the early evaluation of thermal drawdown by small wellhead electrical generating units on potentially large geothermal resources. Such evaluations are of use in the planning of large central power plant units. The long-term

cooperative studies at Los Azufres, are now included under the DOE-CFE Geothermal Agreement. An evaluation of the effects of the first five years of operation of the CFE 5-MW wellhead generators on the reservoirs of the thermally different Maritaro and Tejamaniles zones of the large Los Azufres geothermal field was made.

During FY89, two visits to Mexico were made to advance the joint study of the chemical reservoir startup of the 5-MW portable generators in the three two-phase zones (Maritaro, El Chino, and Tejamaniles) of the Los Azufres field. The study should assist in determining the extent of thermal drawdown over the lifetime of the local reservoir units and in evaluating changes in thermodynamic properties of the reservoir and long-term production characteristics. A separate joint study with M. Gallardo is underway to evaluate the reliability of the very large chemical database with respect to the location of the liquid leg sampling site. A joint paper (*Kruger and Galardo*, 1990) is being prepared for the 1990 GRC meeting.

The laboratory experiments in the SGP physical reservoir model were completed by PhD candidate Steven Lam to examine the effects of thermal stress by reinjection cooling on the thermal conductivity of reservoir fractured rock blocks. The SGP Physical Reservoir Model completed its useful life during FY89 and is in the process of decommissioning. The data acquired by Research Asst. Lam is in the process of analysis and comparison with theoretical predictions for completion of his PhD dissertation in June, 1990.

Development of the 1-D Heat Sweep Model

The 1-D Heat Sweep Model was developed under the Heat Extraction Project as a tool for early analysis of the thermal effects of reinjected cooled brines as recharge into geothermal reservoirs under steady production. Evaluation is required for prudent reservoir management in selection and operation of recharge wells. The potential benefit is secondary heat recovery (in addition to the primary benefits of waste brine disposal and reservoir pressure maintenance) and the potential risk is premature thermal breakthrough of the cooled reinjection liquid. The original 1-D Linear Heat Sweep model, was described in the User's Manual prepared by *Hunsbedt et al.* (1984). The physical basis for heat transfer from fractured rock to reinjected fluid in hydrothermal reservoirs has been described in earlier project reports. The model was simplified in terms of the Number of Heat Transfer Units, which expresses the ratio of the residence time of the reinjected sweep fluid to the time constant of the fractured rock. A large number of heat transfer units implies a reservoir that is heat transfer rate limited, whereas a low number indicates a reservoir that is fluid flow limited.

The 1-D Linear Heat Sweep Model was improved by Graduate Student Stephen Lam as part of his PhD thesis to allow for other types of injected recharge flow and for mixing of injected fluid with reservoir fluid near a production well. The model was able to handle reinjection flow in linear or radial geometry between either single or lines of injection and production wells. Either heat sweep alone or mixing sweep flow with percolation recharge from above and/or hot water flow from the reservoir resource below declining in temperature at a constant exponential cooldown rate could be considered. Other improvements included

evaluation of several Laplace transform inversion methods to optimize the accuracy of the output cooldown curves and compilation of the heat sweep source code as a microcomputer version for use in field applications.

In FY88, the 1-D Heat Sweep Model was improved to include doublet flow from a pair of injection-production wells. The doublet flow geometry is useful in new geothermal zones where only exploratory production wells are available and flow boundaries, such as faults, are not identified. The difficulty encountered in using doublet flow geometry in a one-dimensional model is its intrinsic two-dimensional behavior. The approach taken was to accomplish reduction in dimensionality by division of the total flow field into a number of linear channels, and integration of the one-dimensional linear heat sweeps over the domain of the two-dimensional flow. For a sufficiently large number of flow channels (e.g., $N > 50$), the crescent flow channels between streamlines can be expressed as equivalent rectangles having the same heat transfer surface and mean fluid velocity. With the mean channel length and mean fluid velocity in each channel, the heat transfer between fluid and reservoir rock is modeled as a 1-D linear heat sweep in each channel. Summing of the N channel data in an array of residence time intervals provides the time dependent cooldown curve for the total flow at a production well. If the reinjection rate is only part of the production rate, mixing of the sweep fluid with reservoir resource fluid at the appropriate cooldown rate is also modeled.

The first application of the 1-D Doublet Heat Sweep Model was made for the El Chino zone of the Los Azufres geothermal field. This zone is between the steam reservoir in the Tejamaniles (south) zone and the two-phase reservoir in the Maritaro (north) zone. One production well (Az-9) and one potential reinjection well (Az-3) have been drilled in this zone. CFE has decided to locate one of the four new 5-MW wellhead units at well Az-9 and reinject at Az-3. The application of the 1-D Doublet Heat Sweep Model allows a comparison of the linear and radial models for flow bounded by the El Chino and Laguna faults. The results of this study were presented by ***Lam and Kruger*** (1987).

During FY89, work continued on development of the doublet flow model for non-uniform temperature distribution in the production zone of the reservoir. For a uniform initial reservoir temperature, the heat content available above a useful abandonment temperature increases rapidly with increasing crescent number. The result is a very long cooldown time to the abandonment temperature relative to results obtained with a uniform temperature in the bounded flow geometry inherent in the linear and radial flow models. An improvement in the 1-D Doublet Heat Sweep Model was achieved by limiting the formation volume of the reservoir at mean initial temperature to a defined geometry. Unfortunately, little temperature distribution data exist in the new geothermal fields covered under the current joint projects. During, FY89, efforts were continued to acquire temperature data, and an initial temperature cross section was prepared by the CFE staff at the La Primavera field. To obtain early insight on the effect of bounded temperature distribution on doublet recharge return flow geometry, an exercise was carried out for several potential initial temperature distributions at the La Primavera field and the El Chino zone of the Los Azufres field. The output temperature was evaluated as a function of crescent number, where crescent number

25 corresponded to one well-axis radius, crescent number 31 corresponded to the 170 C abandonment temperature at the La Primavera field, and crescent number 50 corresponded to the furthermost crescent in the external temperature regime of 145 C. The results of the study were illustrated in the ***FY88 Annual Report*** (1989), and presented at the Fourteenth Annual Stanford. Geothermal Workshop, (***Lam and Kruger,*** 1989).

DOE-CFE; Heat Sweep Project

The l-D Heat Sweep Model has been used in cooperation with CFE in Mexico since its first use in matching the observed cooldown along the western border of the Cerro Prieto I upper reservoir ***(Kruger et al.,*** 1985). A review of the several SGP-CFE joint studies in heat sweep analysis at the four Mexican geothermal fields was presented at the first CFE Symposium on Geothermal Reservoir Engineering ***(Kruger,*** 1988). A list of the joint studies under the cooperative arrangements is given in Table 3.1.1.

During FY89, two reunions were held with the senior staffs of the respective fields to review the results from prior visits, evaluate the current output data, and incorporate the most recent production, chemical, and reservoir data and changes in plans for the development of the field. A major advantage that has already resulted from the joint application of the Heat Sweep Model has been the preparation of field generated reservoir and production conditions **as** Input Data for the simulations runs. In most cases, the compilation of the required reservoir, structural, and thermal data for the study has required cooperative estimation among the senior staff of each field. Results of the joint studies completed before the DOE- CFE tasks were underway have been published in several Symposia.

Heat sweep studies underway during FY89 at the three Mexican fields include Los Humeros and **La,** Primavera under the SGP geothermal agreement, and the 10 case studies for the three zones of the Los Azufres field under the DOE-CFE geothermal agreement. Progress, including presentation of results, was achieved for each field.

A. Los Humeros

Joint project HSP5, ***(Kruger et al.,*** 1987) was completed. The project examined the potential for reinjection recharge flow from recharge well **H5** individually to the two production wells **H7** and H1. The radial flow geometry used for these two well pairs was shown in the prior Annual Report. The results of the study were prepared **as** a technical article (in Spanish) ***(Arugon and Kruger,*** 1987). The joint study was re-focused on reinjection heat sweep for the four new portable wellhead units expected in 1989-90. The wells being considered for these units are listed in 3.Table 3.1.2. The results of the study was presented at the 1989 GRC Symposium ***(Kruger et al.,*** 1989).

B. Los Azufres

Studies under the DOE-CFE Geothermal Agreement were completed for the several **well** pairs listed in Table 3.1.1, including thermal breakthrough estimates at the new well pairs in both the Tejarnaniles and Maritaro zones. The results were reported at the Final Symposium ***(Kruger et al.,*** 1989). During FY89, cooldown studies were revised to reflect the change

in philosophy of CFE to change to plastic (polyethylene) surface tubing, which costs less but has a lower maximum allowable fluid temperature for the recharge lines. CFE is evaluating the option of using the nearby Laguna Verde lake for cooling and silica deposition before reinjection. Therefore, the studies, revised to reflect the specific objectives outlined in the original DOE-CFE Task 5.1 joint study for heat sweep analysis in the Los Azufres field, should be useful in determining the optimum reinjection time and temperature. During the site visits in FY89, review of the new objectives for heat sweep analyses were discussed and compilation of the input data sets was initiated under the Renewed 5-year DOE-CFE Geothermal Agreement. Continuation of these joint studies is expected by the pertinent CFE co-investigators when the reorganization of CFE Gerencia is completed.

C. La Primavera

Heat sweep studies for the La Primavera field in FY88 were centered on the plans for the first 5-MW portable wellhead unit planned to be installed at well PR9 with reinjection into existing well PR.2. The joint studies for this unit were presented at the SGP 12th annual Workshop ***(Kruger et al.***, 1987). During FY89, the joint project was adjusted to examine the effects of a second 5-MW unit to be installed concurrently with Unit 1. Steam for the two wells are expected to be supplied from three existing production wells, PR9, PR1, and PR8. During FY89, CFE suspended plans to develop the La Primavera field pending clarification of environmental and other local problems. The joint study is scheduled to proceed only in project preparation until CFE plans are changed.

DOE-CFE: Los Azufres Well Startup Project

A. Startup Analysis of the First Seven Years of Production in the Maritaro Zone Reservoir

The response of the Los Azufres geothermal field to the onset of continuous production from the original five wells to supply the five 5-MW wellhead units has been examined in previous annual reports. Publications were prepared after 2, 2.5, 4, and 5 years of operation. The final report under the original DOE-CFE Agreement is published **(Kruger *and Arugon,*** 1989). The accumulation of the many production, chemical, and reservoir data has allowed a detailed examination of the effects of the cumulative production on the thermal drawdown of the reservoir. An important aspect of this analysis is the thermal history of the produced water, especially in the two-phase Maritaro zone, where geothermometer temperature data allows the estimation of reservoir specific volumes for the chemical components.

During FY89, the major effort on this joint study was the compilation and analysis of the additional cumulative data from the now seven years of continuous operation and initiation of new startup analysis at the new wells in the El Chino and Tejamaniles zones. In continuation of the joint study on thermal drawdown effects, the general objective remains to observe the thermodynamic changes in the reservoir and to evaluate the extent of changes observable by operation of small wellhead units in potentially large geothermal fields. Data for all years of production are accumulated in the form of chemical data for Na, K, Ca, Cl, and SiO2. Production data include wellhead pressure P(wh), separator pres-

sure P(sep), liquid flowrate Q(l), vapor flowrate Q(v), noncondensable gas flowrate Q(g), and wellhead enthalpy (H). From these data, calculated mean values are compiled for the Na-K-Ca and Si02 geothermometers and with the wellhead enthalpy the reservoir specific volumes are being estimated. Analysis of the relationship between wellhead concentration and reservoir specific volume and the extent of hemispherical thermal drawdown for production wells acting as just-penetrating into a fully-fractured geothermal resource is continuing.

B. Planning for the Renewed DOE-CFE Geothermal Agreement

During the two visits in FY89, plans were made with the operating staff of the three neo-volcanic geothermal fields to develop start-up analysis programs for reservoir management objectives. The joint proposals generated for each field under the DOE-CFE renewed Geothermal Agreement was reviewed. The title of each joint study is Chemical Reservoir Engineering at the respective field and the co-principle investigators are expected to be as listed below:

1. Los Humeros: P. Kruger (SGP) R. Molinar (CFE Gerencia) M. Medina and J. Lopez (Los Humeros)

2. Los Azufres: P. Kruger (SGP) R. Molinar (CFE Gerencia) M. Gallardo, and C. Miranda (LAz)

3. La Primavera P. Kruger (SGP) R. Molinar (CFE Gerencia) R. Maciel, C. Lucio, and S. Villa (La Pr)

The general objectives of the two new fields, Los Humeros and La Primavera are to define an adequate brine sampling program and to initiate an evaluation of observable changes in chemical and physical parameters under steady production and to interpret the changes by statistical and flow models based on geothermometer and enthalpy analyses. The existing joint program at Los Azufres was amended to continue the startup analysis of the original wellhead unit wells and to add new startup analysis of the wells that will be receiving the new units expected in 1990.

A joint study was initiated in FY88 to examine the problems associated with the collection of brine samples at the discharge weir following pressure reduction and cooling at the silencer. The preparation of brine for reinjection in this manner results in four potential problems in measuring chemical concentrations and brine flow rates: (1) reduction in pressure (2) reduction in brine temperature **(3)** loss of water due to flashing in the silencer **(4)** introduction of atmospheric oxygen. An experimental program was designed to examine the extent of these potential sources of error. The results will be published as a joint study by P. Kruger (SGP) and M. Gallardo (LAz): "Comparison of Sampling Locations for Chemical Analysis at the Los Azufres Geothermal Field" for publication and presentation at the 1990 GRC Annual Symposium, and by Gallardo and Kruger: "Comparacion de Sitios de Mostrear para Analisis Chimica en el Campo de Los Azufres" in the CFE Journal, Geotermia, 1990.

Other Joint Studies

A. Heat Sweep Joint Study with CSM, England

In June, 1989, during a visit to Cornwall to present a paper from the Leningrad Mining Institute, a joint effort was initiated with D. Nicol on examination of the cooldown observed during, the current long-term experiment at the Rosemanoes Hot,Dry Rock Experiment reservoir. All of the temperature, production, and other data were provided in disk form and preliminary analysis of the cooldown has been completed. It was possible to obtain an excellent match of the observed cooldown by estimation of two key parameters, (1) the reservoir dimensions, which determine the mean residence time of the circulating fluid, and (2) the mean fracture spacing, which determines the rock thermal time constant for providing the heat content to the circulating fluid. In the SGP 1-D Heat Sweep Model, the primary parameter, the Number of Heat Transfer Units, is the ratio of these two times. The present match is expected to be further refined with evaluation of the reservoir volume estimated by seismic monitoring techniques.

B. Heat Sweep Joint Study with LMI, Leningrad, USSR

During the Fulbright Lectureship visit to the Stanford Geothermal Program in the Spring Quarter of 1987, Prof. Yuri D. Dyadkin of the Leningrad Mining Institute offered the PE269 course in Geothermal Technology in which he reviewed the plans for geothermal energy development in the USSR. He published an article in the May, 1987 issue of the Geothermal Resources Council Bulletin *(Dyadkin,* 1987) describing the initiation of two closed geothermal circulation systems in petrogeothermal areas as part of the USSR national program to provide hot water supplies to remote towns and villages. As a result of these exercises, a joint analysis was undertaken to examine the lifetime of hydrofractured reservoirs in providing large flowrates of 100+ C artificially circulated water to an abandonment temperature of 90-100 C with recharge water of 30 C. The case study for the hot water supply was a comparison of the calculations made with the LMI heat extraction model developed from basic principles of heat transfer from oblate slabs of parallel hydrofractured rock using heat transfer coefficients derived from simulations and regression analysis of Soviet oil and gas well experience and the SGP 1-D heat sweep model using the same input data. The results were presented by ***Dyadkin and Kruger*** (1987). The agreement between the two models was satisfactory.

During FY89, communications continued with the Leningrad Mining Institute for the execution of a cooperative agreement with the Stanford Geothermal Program for joint efforts in low- temperature petrothermal resources noted by USSR authors to be abundant throughout the Soviet Union. A visit by the principal investigator of the Heat Extraction Project for two months was carried out from April to June, 1989. A formal Geothermal Agreement is being executed between Stanford University and the Leningrad Mining Institute. Four technical joint projects are contemplated under this Agreement. One of the projects is the experimental hydrofractured reservoir at the Russkie Komarovtsy field in the Zakarpate Oblast of the Ukraine SSR. A joint paper on these studies was presented at the

Camborne School of Mines 1989 International Symposium on Hot, **Dry** Rock Technology ***(Dyadkin and Kruger,*** 1989).

Also during this visit to **LMI,** a joint study was initiated with **A.** Kiryukhin of the Institute of Volcanology in Kamchatka to combine heat sweep analysis with a fluorescein tracer test to be run in late 1989. The experiment was carried out August- September, 1989, and the results were shipped to Stanford to be included in a preliminary report (***Kiryukhin and Kruger,*** 1990) at the **SGP** Annual Workshop, January, 1990. A more detailed report is expected to be prepared for the **GRC** Symposium, August, 1990.

C. Heat Sweep Joint Study with **LANL,** New Mexico

A similar comparative study was initiated during FY87 with B. Robinson of **LANL** to compare simple models for estimating cooldown history in the Fenton Hill hydrofractured Hot,Dry Rock reservoir for the phase **2** experiment of thermal drawdown. The **LANL** model is based on a convolution of observed tracer response curves for a network of flow paths connected in parallel with a consistent set of fracture apertures and flowrates chosen for the measured tracer residence time distribution. Heat transfer within each path is calculated with a model similar to the SGP **l-D** Heat Sweep Model. The overall production fluid temperature is the mixed outlet temperature from the individual paths. **A** joint paper describing the analysis of the predicted heat transfer behavior in the current Phase II HDR reservoir at Fenton Hill by both models was presented ***(Robinson and Kruger*** ,188). Currently, additional heat sweep analysis is underway to incorporate the reservoir volume estimated by **M.** Fehler **(LANL)** based on **his** microseismic response measurements.

Thermal Stress Analysis

The study of thermal stress effects on fractured rock thermal conductivity was continued during FY88. The thermal stress experiments, by Research Asst. Steven Lam, conducted in the large SGP physical reservoir model with a fractured rock loading of two cylindrical granite blocks were completed in FY87. The objective of these experiments was to determine the extent of changes in thermal conductivity of fractured reservoir rocks due to reinjection of cooled geothermal brines with subsequent sweep induced thermal stress cracking over the useful lifetime of the reservoir. The experiments consisted of thermally stressing the system (rocks, water, and pressure vessel) over three cycles of heatup, several intermittent partial cooldowns of the system, and a cold-water heat sweep, and at the end, a final long-term cooldown to room temperature. In each cycle, the heatup process was carried out very slowly and stops were made at various system temperatures to conduct thermal conductivity measurements using radial temperature gradients generated in the rock core with core axial heaters. Core cooldown tests were conducted at several system temperatures before the heat sweep process was initiated at an initial temperature of 232 C. After the three heat sweep cycles, the final system cooldown was initiated from a temperature of 221 C to **20** C.

The extensive physical measurement system of the SGP reservoir model was used to acquire recorded temperature data for each of the three thermal cycles, consisting of: (1) transient rock temperatures when the core axial heaters were turned on at the several

system temperature levels; (2) steady-state rock temperatures with the axial heaters on and the cores ai; thermal equilibrium with the total system at each temperature level; (3) transient natural cooldown temperatures initiated intermittently during the system heatup process; and (4) transient cooldown temperatures during cold-water heat sweep cooling. System temperatures were also recorded for the complete system cooldown test. These temperature data are needed to derive rock thermal conductivity values for the pre- and post-sweep states and as a function of the number of sweeps.

The temperature data have been compiled and organized in FY88 for analysis with both steady and transient thermal models of the cylindrical rock blocks. Several thermal models are being used to interpret the experimental data from the three thermal stressing cycles and the final long-term natural cooldown test (LTCT).

Section 3.2 : Appendix A

Heat Extraction Project Reports and Publications

Aragon, A. and Kruger P., Uso del Modelo de Barrido Termico en el Campo Geotermico de Los Humeros, Puebla, Geotermia 3, No.3, 263-273 (1987).

Dyadkin, Y. and Kruger P., Estimates of Thermal Cooldown in Fractured Petrogeothermal Resources, Transactions, Geothermal Resources Council, October, 1987.

Dyadkin, Yu. and Kruger P., Heat Extraction from Low- Temperature Fractured Petrothermal Resources, Proceedings, International Conference on HDR Geothermal Energy, Cornwall, England, June, 1989.

Hunsbedt, A., Iregui R., Kruger P., and London A.L., Energy Recovery from Fracture-Simulated Geothermal Reservoirs, Proceedings, ASME/AIChE Heat Transfer Conference, Paper 79-HT-92, 1979.

Hunsbedt, A., Lam S., and Kruger P., User's Manual for the 1D Linear Heat Sweep Model, Stanford University Technical Report No. SGP-TR-75, April, 1984.

Hunsbedt, A., Lam S., Kruger P., and Pruess K., Heat Extraction Modeling of the Stanford Reservoir Model, Proceedings, 8th Workshop on Geothermal Reservoir Engineering, Stanford University Technical Report No. SGP-TR-60, 255-260, December, 1982.

Kiryukhin, A. and Kruger P., Preliminary Analysis of Tracer Response and Thermal Cooldown Estimates for the Mutnovsky Geothermal Field in Kamchatka, USSR, Abstract submitted to 15th SGP Workshop in Geothermal Engineering, Jan, 1990.

Kruger, P., Experimental Studies on Heat Extraction from Fractured Geothermal Reservoirs, in S. Nemat-Nasser, H. Abe, and S. Hirakawa, eds, Hydraulic Fracturing and Geothermal Energy, 373-397 (M. Nijhoff, The Hague, 1983).

Kruger, P., Application of the SGP 1-D Linear Heat Sweep Model, Proceedings, 7th New Zealand 'Geothermal Workshop, 45-48, November, 1985.

Kruger, P., The Role of Heat Sweep in Reinjection of Cooled Geothermal Fluids, Geotermia 4, No.1, 247-253, (1988).

Kruger, P. and Aragon A., Heat Sweep Analysis of Reinjection Recharge at the Los Azufres Geothermal Field, Proceedings, Final Symposium, DOE-CFE Geothermal Agreement, April, 1989.

Kruger, P., Aragon A, Maciel R., Lucio C., and Villa, S. Preproduction Simulation of Thermal Decline at the La Primavera First 5-MW Wellhead Units, Transactions, Geothermal Resources Council, 12, 475-480, (1988).

Kruger, P., Aragon A., Maciel R., Lucio C., and Villa, S. Simulacion de la Declinacion Termico Antes de la Produccion con Unidades de 5MWe en el Campo Geotermico de La Primavera, Jalisco, Geotermia 4, No.3, 195-210, (1988).

Kruger, P., Lam S., Hunsbedt A., Esquer C., Marquez, R. Hernandez L., and Cobo, J., Analysis of Recharge Cooldown at the Western Boundary of Cerro Prieto I Geothermal Field, Proceedings, 10th Workshop on Geothermal Reservoir Engineering, Stanford University Technical Report No. SGP-TR-84, 73-78, January, 1985.

Kruger, P., Lam S., Molinar R., and Aragon, A., Heat Sweep Analysis of Thermal Breakthrough at Los Humeros and La Primavera Fields, Mexico, Proceedings, 12th Workshop on Geothermal Reservoir Engineering, Stanford University Technical Report No. SGP-TR-109, 97-102, January, 1987.

Kruger, P., Medina, M. and Aragon, A. Preproduction Analysis of Thermal Breakthrough by Reinjection at the Los Humeros First 5-MWe Units, Transactions, Geothermal Resources Council 12, October, 1989.

Kruger, P., Ortiz, J., Miranda, C. and Gallardo, M., Response of the Los Azufres Geothermal Field to Four Years of 25 MW Wellhead Generation, Proceedings, 12th Workshop on Geothermal Reservoir Engineering, Stanford University Technical Report No. SGP-TR-109, 181-1.87, January, 1987.

Kruger, P., Sanchez, P. and Ortiz, J. Startup Analysis of Wellhead Unit Production Wells, Proceedings, Final Symposium, DOE-CFE Geothermal Agreement, April, 1989.

Kruger, P., Semprini, L., Verma, S., Barragan, R., Molinar, R., Aragon, A., Ortiz, J., Miranda, C., Garfias, A., and Gallardo, M., Initial Chemical and Reservoir Conditions at Los Azufres Wellhead Power Plant Startup, Proceedings, 10th Workshop on Geothermal Reservoir Engineering, Stanford University Technical Report No. SGP-TR-84, 219-226,

January, 1985.

Kruger, P., Semprini, L., Nieva, D., Verma, S., Barragon, R., Molinar, R., Aragon, A., Ortiz, J., Miranda, C., Garfias, **A.,** and Gallardo, M., Analysis of Reservoir Conditions during Production Startup at the Los Azufres Geothermal Field, Transactions, Geothermal Resources Council 9, 527-532, August, 1985.

Kuo, M.C.T., Kruger, P., and Brigham, W.E., Shape-Factor Correlations for Transient Heat Conduction from Irregular-Shaped Rock Fragments to Surrounding Fluid, Proceedings, AIChE-ASME Heat Transfer Conference, Paper 77-HT-54, 1977.

Lam, S.T., The Effect of Heat-Sweep Induced Thermal Stress on Reservoir Rock Thermal Conductivity, Ph.D. Thesis, Stanford University, 1989 (in preparation).

Lam, S., Hunsbedt, A., Kruger, P., and Pruess, K., Analysis of the Stanford Geothermal Reservoir Model Experiment Using the LBL Reservoir Simulator, Geothermics 17, 595-605 (1988).

Lam, S. and Kruger, P., 1-D Doublet Heat Sweep Model, Proceedings, 9th New Zealand Geothermal Workshop, November, 1988.

Maciel, R., Kruger, P., Aragon, A., Lucio, C., and Villa, S. Estudio del Declinamiento Termico en el Yacimiento del Campo Geotermico de La Primavera, Usando Datos de Preproduction, Proceedings, IX convention of the Mexican Geological Society, Mexico City, October, 1988.

Molinar, R., Aragon, A., Kruger, P., and Lam, S., One-Dimensional Heat Sweep and Fluid Mixing at the Los Azufres Geothermal Field, Proceedings, 8th New Zealand Geothermal Workshop, November, 1986.

Robinson, **B.A.** and Kruger, P., A Comparison of Two Heat Transfer Models for Estimating Thermal Drawdown in Hot Dry Rock Reservoirs, Proceedings, 13th SGP Geothermal Workshop, TR-113, 113-120, 1988.

Table 3.1.1

SGP–CFE COOPERATIVE HEAT SWEEP STUDIES

Study No.	Project Zone	Injection Wells	Production Wells	Status*
CPI	Cerro Prieto I	influx	western line	P
LAz1	w. Tejamaniles	Az-31	Az–26	P,+
LAz2	e. Tejamaniles	Az–8	Az–2	R
LAz3a,b	Maritaro	Az–15	eastern line	P
LAz4	Tejamaniles	(4)	Central (15)	U
LHu1	1st Wellhead	H–5	H-1, H–7	P
LaP1	1st Wellhead	PR–2	PR–9	P
LAz5b	n. Tejamaniles	Az-1	Az–22	P,+
LAz6b	Maritaro	Az–15	Az–4	P
LAz7	El Chino	Az–3	Az-9	P,+
LHu2	2nd Wellhead	H–4	H-16	P
LaP2	2nd Wellhead	PR-2	PR-1,8,9	P
LAz8a	Maritaro Unit7	Az–15	Az–4	P,+
LAz8b	Maritaro Unit7	Az–40	Az-4	P,+
LAz9a	Maritaro Unit8	Az–15	Az–51	PI+
LAz9b	Maritaro Unit8	Az–40	Az-51	PI+
LAz10	Maritaro Unit9	Az–52	Az–42	PI+
LAz11a	Maritaro Unit10	Az–15	Az–43	PI+
LAz11b	Maritaro Unit10	Az–40	Az–43	P,+

*Status: P=published; R=reported to CFE; U=underway;
+ = studies included under the First DOE–CFE Geothermal Agreement (1986–89).

Table 3.1.2

Wells for the First Wellhead Units at Los Humeros

5MW Unit	Production Wells	Injection Well
1	H9	H5
2	H16 (+H17)	H5
3	H7 (+H8)	H5
4	H12 (+H6)	H2

NOMENCLATURE

A	= Area of the problem domain
A_i	= Area of the region i
C	= Wellbore storage, resident concentration variable of fracture transport equations
C_r	= A reference concentration (concentration that would be obtained if all the injected tracer were to mix in the recirculating fluid volume)
D	= Longitudinal dispersion coefficient
D_a	= Apparent diffusion coefficient (diffusion coefficient in a porous matrix in this study)
F_s	= Storativity ratio, $\frac{\phi c_{t_1}}{\phi c_{t_2}}$
$G(x, y, \xi, \zeta; s)$	= Free Space Green's Function, Laplace Space
G_j	= Right hand side vector
H	= Length of the wellbore
H_ij	= Coefficient matrix
$K_0(x)$	= Modified Bessel function, second kind, order zero
$K_1(x)$	= Modified Bessel function, second kind, order one
L	= Length of the fracture
M	= Mobility ratio, $\frac{(k/\mu)_1}{(k/\mu)_2}$
P(h)	= Block size distribution function
P_e	= Peclet number
Q	= Flow rate of a well
Q(h)	= Flow contribution from matrix size h
R	= Distance to the discontinuity (phase front) or external boundary
S	= Wellbore skin factor
T	= Temperature of the fracture
T_{in}	= Temperature of the injected fluid
T_0	= Initial temperature of the system
U	= Velocity in the fracture at the wellbore
a	= Exponential PDF constant
a_{ij}	= Coefficient matrix for pressure
b	= Intercept of linear PDF, Fracture aperture
b_{ij}	= Coefficient matrix for fluxes
c	= Single phase fluid compressibility
c_s	= Wave speed in fluid
c_t	= Total compressibility
c_m	= Specific heat of the immobile(matrix) phase
c_r	= Specific heat of the reservoir rock
c_w	= Specific heat of water
c_1	= Specific heat of the mobile(fracture) phase

$f(s)$ = Laplace space function
g = Gravitational constant
h = Formation thickness, Matrix block size characteristic length (Volume/Surface Area)
h_{ratio} = Ratio of h_{min} to h_{max}
h_s = Interporosity damaged zone thickness
k = Permeability
k_{xx}, k_{yy} = Principal directions of permeability
k_s = Interporosity damaged zone permeability
k_m = Thermal conductivity of the immobile(matrix) phase
k_r = Thermal conductivity of the reservoir rock
k_w = Thermal conductivity of water
m = Slope of linear PDF
n = Outward pointing normal to a line segment
n_w = Number of wells in the problem domain
p = Pressure, Laplace space variable (corresponding to the backflow time variable)
q = A source/sink in the system (amount of tracer generated/lost per unit volume of the system per unit time)
r = Radial coordinate
s = Laplace transform parameter
t = Time
t_b = Tracer breakthrough time
t_D = Inverse Peclet number scaled to the distance travelled by the convective front during the injection period
t_{Dp} = Dimensionless backflow time variable
t_j = Injection period
t_p = Peak arrival time of a tracer slug
t_t = Thermal (temperature) breakthrough time
t_w = Water transit time (breakthrough time of the convective front)
u = Velocity in the x-direction
u_j = Solution vector
x, y = Variables in Cartesian coordinate system
Ω = Ratio of reservoir to fracture volume
Γ = Boundary of the solution region
α, β, γ = constants
α_i = i^{th} nonlinear parameter of a regression function
β_i = i^{th} linear parameter of a regression function
γ = 1.781, exponential of Euler's constant
$\delta(x - xi)$ = Dirac-delta function, singular at $x = \xi$
δ_{ij} = Kronecker delta, 0 if i != j, and 1 if i = j
θ = Angle subtended between two adjacent elements

ξ, ζ = Local coordinate system based on the fictitious source point
η = Diffusivity = k_x over $\phi\mu c$
ϵ = Belongs to, or is an element of
μ = Viscosity
ρ = Density
ρ_m = Density of immobile(matrix) phase
ρ_r = Reservoir rock density
ρ_f = Density of mobile(fracture) phase
λ = Dimensionless interporosity flow coefficient
τ = Dimensionless matrix response time coefficient,
= Tranducer time constant
ϕ = Porosity
ω = Dimensionless storativity ratio
η = Integration variable of the solution to the MD model for injection-backflow tests

Subscripts

D = Dimensionless
I = Interporosity
eD = Dimensionless, based on external boundary area
DA = Non-Dimensionalized with respect to area
f = Fracture
i = Initial
m = Matrix
min = Minimum
max = Maximum
t = Partial derivative with respect to t (also Total)
w = Wellbore
wf = Wellbore flowing
x, y = Partial derivative with respect to x or y
1, 2, 3 = Sections of the boundary
i, *j*, *j* t 1 = Nodal locations on the boundary

REFERENCES

Ambastha, A.K.,: "Pressure Transient Analysis for Composite Systems," **Ph.D Thesis,** Stanford University, Oct. 1988, pp. 190.

Aragon, A. and Kruger **P.,: Uso** del Modelo de Barrido Termico en el Campo Geotermico de **Los** Humeros, Puebla, ***Geotermia 3,*** *No.3*, 263-273, 1987.

Aronofsky, J.S., and Jenkins, R.,: "A Simplified Analysis of Unsteady Radial **Gas** Flow,: ***Trans.*** AIME, ***201,*** *149*, 1954.

Avdonin, N. A.: "Some Formulas for Calculating the Temperature Field of a Stratum Subject to Thermal Injection," ***Nefti Gaz,*** 1964, ***3,*** 37-41.

Bear, J. and Berkowitz, B: "Groundwater Flow and Pollution in Fractured Aquifers," ***Developments*** **in** ***Hydraulic*** **Engineering,** Vol. *4* ,P. Novak (Editor), Elsevier, London, 1987, 175-235.

Belani, A.K. and Jalali-Yazdi, **Y.:** "Estimation of Matrix Block Size Distribution in Naturally Fractured Reservoirs," SPE 18171, presented at the 63rd **Annual** Technical Conference, Houston, **TX,** Oct. 1988.

Bhatnagar, **S.,:** "Pressure Oscillations Caused by Momentum **on** Shut **In** of a High Rate Well in a Fractured Formation," ***M.S. Report*** Stanford University, June 1989.

Braester, C.: "Influence of Block Size **on** the Transition Curve for **a** Drawdown Test in a Naturally Fractured Reservoir," Soc. Pet. Eng. J., 498-504, 1984.

Bretz, R. **E.**anti Orr, F. M. Jr.: "Comparison of Analytical and Explicit Finite Difference Solutions of the Convection- Dispersion Equation," PRRC report 85-6, 1985, New Mexico petroleum Recovery Research Center.

Britto, P.R., and Grader, A.S.: "The Effects of Size, Shape, and Orientation of an Impermeable Region on Transient Pressure Testing," ***SPE*** **Form.** ***Eval.,*** Sept. 1988, pp. 595-606.

Carslaw, H.S., Jaegar, J.C.,: "Conduction of Heat in Solids", Clarendon Press, **Oxford,** second ed., 1959.

Cinco, H., Samaniego, **F.,** and Dominguez, N.: "Transient Pressure Behavior for **a** Well with a Finite-Conductivity Vertical Fracture", ***Soc.*** **Pel. Eng. J. Aug.** 1978,253-264.

Cinco, **H.,** Samanicgo, F.: "Transient Pressure Analysis for Fractured **Wells',** J. *Pet.* ***Tech.,*** Sept. 1981, 1749-1766.

Cinco, H., et al: "The Pressure Transient Behavior for Naturally Fractured Reservoirs with Multiple Block Size," SPE 14168, presented at the 60th Annual Technical Conference, Las Vegas, NV, Sept. 1985.

Cinco, H., Meng, F.V.,: "Pressure Transient Analysis of Wells with Finite Conductivity Vertical Fractures in Double Porosity Reservoirs", paper SPE 18172 presented at the 1988 SPE Annual Technical Conference and Exhibition, Dallas, October 2-5.

Deruyck, B.G., et al: "Interpretation of Interference Tests in Reservoirs with Double Porosity Behavior-Theory and Field Examples," SPE 11025, presented at the 57th Annual Technical Conference, New Orleans, LA, Sept. 1982.

De Smedt, F., Wierenga, P. J. and Van der Beken, A.: ***Theoretical* and *Experimental* Study of Solute Movement through Porous Media with Mobile and Immobile Water,** Vrije Universtait Brussel, Brussel, 1981.

Ditkin, V.A. and Prudnikov, A. P.: **Operntional Calculus in** Two **variables,** Int. Ser. Pure Appl. Math.., Pergamon Press, London, 1962, 46-47.

Dyadkin, Yu.,,: "Engineering Problems and Possible Stages of Geothermal Resource Development in the Soviet Union", Geothermal Resources Council Bulletin, 3-8, May, 1987.

Dyadkin, Yu. and Kruger P.,: "Estimates of Thermal Cooldown in Fractured Petrogeothermal Resources", Transactions, Geothermal Resources Council, October, 1987.

Dyadkin, Yu. and Kruger P.,: "Heat Extraction from Low- Temperature Fractured Petrothermal Resources", Proceedings, International Conference on HDR Geothermal Energy, Cornwall, England, June, 1989.

Fligelman, H.,: "Drawdown and Interference Test Analysis for Gas Wells with Wellbore Storage, Damage, and non Laminar Flow Effects", *Ph.D.* **Dissertation,** Stanford University, 1981.

Holthausen, G.R., and Gooch, R.P.: "Impedance of Hydraulic Fractures," *SPE 13892,* presented at the Low Permeability Gas Reservoir Symposium, Colorado, 1965.

Horne, R. N.: "Geothermal Reinjection Experience in Japan," **J. Pet.** Tech., March 1982a, 495-503.

Horne, R. N.: "Effects of Water Injection into Fractured Geothermal Reservoirs : A Summary of Experience Worldwide," **Geothermal Resources Council,** Davis, 1982, Special Report 12, 47-63.

Hunsbedt, A., Lam S., and Kruger P.,: "User's Manual for the 1D Linear Heat Sweep Model", Stanford University Technical Report No. SGP-TR-75, August, 1964.

Johns, R.T.: Comparison of Pressure Transient Response in Intensely and Sparsely Fractured Reservoirs, M.S. Report, Stanford University, 1989.

Johns, R.T. and Jalali-Yazdi, Y.: "Comparison of Pressure Transient Response in Intensely and Sparsely Fractured Reservoirs," SPE 18800, presented at the California Regional Meeting, Bakersfield, CA, April 1989.

Kikani, J. and Horne, R.N.,: "Pressure Transient Analysis of Arbitrary Shaped Reservoirs with the Boundary Element Method," paper SPE 18159 presented at the 1988 Annual Technical Conference and Exhibition, Houston, Oct. 2-5, 1988a.

Kikani, J., and Horne, R.N.,: "A Convolution Boundary Element Method for Unsteady State Groundwater Flow in Homogeneous Aquifers," Proc. XIII Geothermal Res. Eng. Workshop, Stanford U., Stanford, Jan. 19-21, 1988b.

Kikani, J. and Horne, R.N.,: "Application of Boundary Element Method to Reservoir Engineering Problems,", **The Journal of *Petroleum* Science and Engineering,** Pub : Elsevier Science, Nov. 1989.

Kikani, J.,: "Use of Boundary Element Method for Streamline Generation and Pressure Transient Testing:' ***Ph.D*** **Dissertation,** Stanford University, Sept. 1989.

Kiryukhin, A. and Kruger P.,: "Preliminary Analysis of Tracer Response and Thermal Cooldown Estimates for the Mutnovsky Geothermal Field in Kamchatka, USSR", Abstract submitted to 15th SGP Workshop in Geothermal Engineering, Jan, 1990.

Kocabas, I. and Home, R. N.,: "Analysis of Injection-Backflow Tracer Tests in Fractured Geothermal Reservoirs," Proceedings, Thirteenth Workshop on Geothermal Engineering, Stanford U., Stanford, Jan. 1987.

Kocabas, I.,: "'Analysis of Injection-backflow Tracer Tests" Stanford Geothermal Program, SGP-TR-96, Stanford, 1986.

Kocabas, I. : "Analysis of Tracer and Thermal Transients During Reinjection," *Ph.D.* **Dissertation,** Stanford University, **Oct.** 1989.

Kruger, P.,: "Heat Extraction Project: Geothermal Reservoir Engineering Research at Stanford", Fourth Annual Report, SGP-TR-121, Stanford University, January, 1989.

Kruger, P.,: "The Role of Heat Sweep in Reinjection of Cooled Geothermal Fluids", **Geotermia *4*, *No.1*, 247-253,** (1988).

Kruger, P. and Aragon A.,: "Heat Sweep Analysis of Reinjection Recharge at the Los Azufres Geothermal Field, Proceedings," Final Symposium, DOE-CFE Geothermal Agreement, April, 1989.

Kruger, P. and Gallardo M.,: "Comparison of Sampling Locations for Chemical Analysis at the Los Azufres Geothermal Field", Abstract prepared for the 1990 GRC Meeting, August, 1990.

Kruger, P., Lam P., Hunsbedt A., Esquer C., Marquez, R. Hernandez C. , and Cobo J.,: "Analysis of Recharge Cooldown at the Western Boundary of Cerro Prieto I Geothermal Field, Proceedings", 10th Workshop on Geothermal Reservoir Engineering, Stanford University Technical Report No. SGP-TR-84, 73-78, January, 1985.

Kruger, P., Lam S., Molinar R. , and Aragon A.,: "Heat Sweep Analysis of Thermal Breakthrough at Los Humeros and La Primavera Fields, Mexico", Proceedings, 12th Workshop on Geothermal Reservoir Engineering, Stanford University Technical Report No. SGP-TR-109, 97-102, January, 1987.

Kruger, P., Medina M., and Aragon A.,: "Preproduction Analysis of Thermal Breakthrough by Reinjection at the Los Humeros First 5-MWe Units", Transactions, Geothermal Resources Council 12, October, 1989.

Kruger, P., Sanchez P., and Ortiz J.,: "Startup Analysis of Wellhead Unit Production Wells", Proceedings, Final Symposium, DOE-CFE Geothermal Agreement, April, 1989.

Lam, S. and Kruger P.,: "1-D Doublet Heat Sweep Model", Proc. 9th New Zealand Geothermal Workshop, November, 1987.

Lam, S. and Kruger P.,: "Doublet Heat Sweep Model with Bounded Initial Temperature Distribution, Proceedings, 14th SGP Geothermal Workshop, TR-120, January, 1989.

Lauwerier, H. A.: "The Transport of Heat in an Oil Layer Caused by the Injection of Hot Fluid," *Appl. Sci. Res.,* 1955, **5,** 2-3, 145-150.

Liggett, J.A., and Liu, P.L-F.,: The Boundary Integral Equation Method for Porous Media Flow, George Allen and Unwin, London, 1983.

Masukawa, J., and Horne, R.N.,: "Application of the Boundary Integral Method to Immiscible Displacement Problems," *SPE* Res. Eng., Aug. 1988 1069-77.

Moench, A.F.: "Double-Porosity Models for a Fissured Groundwater Reservoir with Fracture Skin," J. Water Resources, 1984 20 7, 831-846.

Najurieta, H.L.: "A Theory for Pressure Transient Analysis in Naturally Fractured Reservoirs," J. Pet. Tech., 1241-1250, July 1980.

Neretnieks, I.: "Diffusion in the Rock Matrix. An Important Factor in Radionuclide Retardation?" *J. Geophys. Res.,* 1980, 85, B8, 4379-4397.

Numbere, D.T.,, and Tiab, D.: "An Improved Streamline-Generating Technique That Uses the Boundary (Integral) Element Method" SPE Res. Eng. Aug. 1988 1061-68.

Pina, H.L.G.,: "Time Dependent Potential Problems," in Boundary Element Methods in Computer Aided Engineering, Ed. Brebbia, C.A., Martinus Nijhoff Publishers, Dodrecht, 1984.

Pickens, J. F. and Grisak, G. E.: "Scale-Dependent Dispersion in a Stratified Granular Aquifer," Water Resour. Res., 1981 17 4, 1191-1211.

Pollard, D.D. and Aydin, A.: "Progress in Understanding Jointing Over the Past Century," Geol. Soc. Amer. Bull.-Centennial Vol., March 1988.

Pruess, K. and Bodvarsson, G. S.: "Thermal Effects of Reinjection in Geothermal Reservoirs With Major 'Vertical Fractures," J. Pet. Tech., September 1984, 1567-1578.

Reynolds, W. C. and Perkins, H. C.: Engineering Thermodynamics 2nd ed., McGraw-Hill, New York, 1977.

Robinson, B.A. and Kruger P.,: "A Comparison of Two Heat Transfer Models for Estimating Thermal Drawdown in Hot Dry Rock Reservoirs", Proceedings, 13th SGP Geothermal Workshop TR-113, 113-120, 1988.

Sageev, A., and Horne, R.N.: "Pressure Transient Analysis of Reservoirs with Linear or Internal Circular Boundaries," Paper SPE 12076 presented at the 58th Annual Mtg. in San Francisco, Sept. 5-8, 1983.

Saldana, M.A., and Ramey, H.J.Jr.,: "Slug Test and Drill Stem Test Flow Phenomena Including Wellbore Inertial and Frictional Effect," SPE 15118, presented at the California Regional Meeting,,Oakland, 1986.

Schapery, A.: "Approximate Methods of Transform Inversion for Viscoelastic Stress Analysis," Technical Report, 4th U.S. National Congress Appl. Math., 1961.

Segall, P.: The Development of Joints and Faults, PhD dissertation, Stanford University, July 1981.

Stehfest, H.,: "Algorithm 368, Numerical Inversion of Laplace Transforms [D5]," Communications of ACM, Jan, 1970, vol. 13, No. 1, 47-49.

Teng, E.: "Transient Pressure Analysis in Composite Reservoirs with Rectangular Discontinuities," M.S. Report, Stanford University, Sept. 1984, pp. 153.

Voelker, D. and Doetsch, G.: Die Zwiedimensionale Laplace-Transformation Birkhauser, Basel Switzerland, 1950, 186-187.

Warren, J.E. and Root, P.J.: "The Behavior of Naturally Fractured Reservoirs," Soc. Pet. Eng. J., 245-55, Sept. 1963.

Wattenbarger, R.A.,: "Effects of Turbulence, Wellbore Damage, Wellbore Storage, and Vertical Fractures on Gas Well Testing," *Ph.D. Dissertation*, Stanford University, 1967.

PUBLICATIONS FY89

Dyadkin, Yu. and Kruger P.,: "Heat Extraction from Low- Temperature Fractured Petrothermal Resources", Proceedings, International Conference on HDR Geothermal Energy, Cornwall, England, June, 1989.

Fligelman, H., Cinco-Ley, H., Ramey, H.J.Jr., Braester, C., and Couri, F.,: "Pressure-Drawdown Test Analysis of a Gas Well - Application of New Correlations", SPE *Formation* **Evaluation,** Sept. 1.989.

Horne, R.N., and Sanchez-U, P.,: "Use of Computers in Well Test Analysis", Proceedings 14th Annual Stanford Geothermal Workshop, Stanford, Jan. 1989.

Horne, R.N., and Puente, H.,: "Tracer Testing at Los Azufres", Proceedings 14*th* Annual Stanford Geothermal Workshop, Stanford, Jan. 1989.

Johns, R.T., and Jalali-Yazdi, Y.,: "Comparison of Pressure Transient Response in Intensely and Sparsely Fractured Reservoirs", Proceedings 14*th* Annual Stanford Geothermal Workshop, Stanford, Jan. 1989.

Kikani, J., and Horne, R.N.,: "Modeling Pressure Transient Behavior of Sectionally Heterogeneous Reservoirs by the Boundary Element Method", SPE 1778, presented at the 1989 Annual Technical Conference and Exhibition, San Antonio, TX, Oct. 1-3.

Kikani, J., and Horne, R.N.,: "Application of Boundary Element Method to Reservoir Engineering Problems", *Journal* of **Petroleum Science and Technology, Pub:** *Elsevier* **Science,** Nov. 1989.

Kruger, P. and Aragon A.,: "Heat Sweep Analysis of Reinjection Recharge at the Los Azufres Geothermal Field, Proceedings," Final Symposium, DOE-CFE Geothermal Agreement, April, 1989.

Kruger, P., Medina M., and Aragon A.,: "Preproduction Analysis of Thermal Breakthrough by Reinjection at the Los Humeros First 5-MWe Units", Transactions, Geothermal Resources Council 12, October, 1989.

Kruger, P., Sanchez P., and Ortiz J.,: "Startup Analysis of Wellhead Unit Production Wells", Proceedings, Final Symposium, DOE-CFE Geothermal Agreement, April, 1989.

Lam, S., and Kruger, P.,: "Doublet Heat Sweep Model with Bounded Initial Temperature Distribution", Proceedings 14*th* Annual Stanford Geothermal Workshop, Stanford, Jan. 1989.